MSE Spectroscopy in CHS Heliotron/Torsatron

Sadatsugu Takayama

DOCTOR OF SCIENCE

Department of Fusion Science
School of Mathematical and Physical Science
The Graduate University for Advance Studies

1998

Keyword:

motional Stark effect (MSE), local magnetic field line pitch angle measurement
ferroelectric liquid crystal (FLC), DigDagCCD

Abstracts

The spectroscopic measurement using the motional Stark effect (MSE) has been recognized to be a useful tool to measure the direction of the magnetic field inside the plasma. The MSE arises from the Lorentz Electric Field, $\boldsymbol{E}=\boldsymbol{v}\times\boldsymbol{B}$, in the atom's rest frame, which is induced when the neutral beam, having the velocity $\boldsymbol{v}$, crosses the magnetic field $\boldsymbol{B}$. The spectrum with the motional Stark splitting in the H_α emission consists of 15 components. The spectra which are circularly polarized perpendicular to the Lorentz field are called as σ (0σ, $+1\sigma$, and -1σ lines) components, while the spectra which are linearly polarized parallel to the Lorentz field, namely perpendicular to the magnetic field are called as π ($\pm 2\pi$, $\pm 3\pi$, and $\pm 4\pi$ lines) components. Four kinds of spectra with the polarization angle of 0, 45, 90 and 135 degrees are measured to derive the polarization angle of the circularly polarized σ component, and eliminate the overlap between π components and σ components those are perpendicular to each other. The diagnostic neutral beam (DNB) is injected almost perpendicularly to magnetic field line into the Compact Helical System (CHS) heliotron/torsatron device in order to maximize the Lorentz field, namely Stark shift. The line broadening due to a beam divergence angle results in overlapping between the adjacent lines. Therefore, the smaller beam divergence angle is desirable in DNB for the MSE measurement. The beam divergence angle of DNB is 0.65 degrees, and it gives enough separation between the measured σ and π components in MSE spectroscopy. Although the one-third energy (E/3) component has the smaller motional Stark splitting than the full energy component, the intensity of E/3 component is larger than that of full energy component. Therefore, the one-third energy component is used to derive the pitch angle in CHS.

The new polarization sensitive spectroscopy, which consists of a polarizer and a ferroelectric liquid crystal (FLC) cell, has been developed to measure the polarization angle with good accuracy. The FLC cell functions as a switchable half-wave retarder, in which polarization angle of the light is rotated by 90 degrees. By using the FLC, the polarization angle can be measured with the error bar of less than ± 1 degrees.

Because the FLC has fast response, the spectra with the polarizer angle of 0 and 90 degrees or -45 and 45 degrees can be measured with the fast modulation of 50 Hz. New CCD detector, where the charge of each pixel is shifted up and down (Dig Dag) synchronized with the two sets of FLC modulation, has been developed for MSE measurements.

The pitch angle of the magnetic field line is derived from the polarization angle of measured the σ and π components H_α line with the polarization sensitive spectroscopy. The radial profile of a pitch angle of a local magnetic field is measured for the plasma with the magnetic field of 0.88 T and the magnetic axis of 92.1 cm in CHS. The spectra of the σ and π component of the H_α line with the motional Stark effect are measured with the polarization sensitive spectroscopy. The major radius, where the local pitch angle is zero, shifts outboard from that calculated with coil current alone (no plasma) by 28 ± 16 mm. This shift is consistent to that predicted by the effect of finite beta due to bulk plasma and fast ions of heating neutral beam.

Acknowledgements

The author wishes to express special thanks go to Dr. Katsumi Ida, and Dr. Shin-ichiro Kado, their thesis adviser, for his continuous encouragements, valuable discussions, and a great deal of advice and assistance in preparing this manuscript.

The author acknowledges the experimental supports and suggestions by Prof. Keisuke Matsuoka, Prof. Shoichi Okamura, Dr. Masaki Osakabe, and all members in CHS group. The author wishes to thank Mr. Satoru Hattori for his help in DNB operation. The author thanks Mr. Mamoru Kojima and Mr. Chihiro Takahashi for their supports to data acquisition.

The author thanks the member of Research and Development division, especially Dr. Mitsutaka Isobe, Dr. Shin Nishimura, Dr. Akihide Fujisawa, Dr. Keiichi Hirano, Dr. Masayoshi Tanaka, Dr. Mamiko Sasao, Dr. Hiroyuki Sakaue for the useful discussions on this work and their continuous encouragement.

The author wish to thank Dr. Joong-san Koog, Dr. Hajime Sakakita in NIFS for heartful kindness and their help.

The author would like to thank many people of prefectural government of Gifu for giving him the chance to study in National Institute for Fusion Science (NIFS) and their continuous encouragement.

Finally, the author wishes to express sincere gratitude to his parents, and brothers for supporting and encouraging.

Table of CONTENTS

Abstracts

Acknowledgments

Table of CONTENTS

Chapter 1 Introduction 1

1.1 Overview 1

1.2 Compact Helical System (CHS) 2

Chapter 2 Diagnostic System for MSE Spectroscopy 7

2.1 Principle of MSE Spectroscopy 7

2.2 Calculation Code of MSE Spectra 11

2.3 Necessity of DNB for MSE Spectroscopy 14

2.4 Schematic View of Experimental Arrangement 17

Chapter 3 Performance of Diagnostic Neutral Beam (DNB) 21

3.1 Measurement of DNB Performance 21

3.2 Estimation of Beam Divergence 21

3.3 Optimization of Operation for MSE Spectroscopy 28

Chapter 4 Performance of Polarization Sensitive Spectroscopy 41

4.1 Performance of the DigDagCCD 41

4.1.1 Design of DigDagCCD 41

4.1.2 Estimation of Performance for DigDagCCD 43
4.1.3 MSE Spectra by using Dig Dag Scheme on CCD 47
4.2 Performance of Ferroelectric Liquid Crystal 50
4.3 Spectrometer 59

Chapter 5 Experimental Results of MSE Spectroscopy 64
5.1 Measurements of MSE Spectra 64
5.2 Estimation of Pitch Angle from MSE Spectra 70
5.2.1 Intensity Difference of MSE Spectra 70
5.2.2 Radial Profile of Pitch Angle 72

Chapter 6 Discussion and Summary 80

Appendix A Principle of FLC 82
B Dispersion of Spectrometer 84

Chapter 1
Introduction

1.1 Overview

In the heliotron/torsatron devices, the pitch angle of the vacuum magnetic field is determined by external coil currents. However, the bootstrap current and the Pfirsch-Schluter current change the poloidal magnetic field in the plasma as the plasma pressure increases. In the plasma of Compact Helical System (CHS), the Shafranov shift is observed to be 40% of a plasma minor radius when the volume averaged equilibrium beta value increases up to 2.1%[1-2]. In this plasma, the pitch angle of the local magnetic field and the magnetic shear are significantly modified with the shift of the magnetic axis, and the plasma stability is quite different from that in low beta plasmas. Measuring the radial profile of the pitch angle of the magnetic field and the shift of the magnetic axis are important to understand the plasma stability and the confinement.

The Stark effect arises from the Lorentz Electric Field, $\boldsymbol{E}=\boldsymbol{v}\times\boldsymbol{B}$, which is induced when the neutral beam, having the velocity $\boldsymbol{v}$, crosses the magnetic field $\boldsymbol{B}$, is called a motional Stark effect (MSE). The direction of the magnetic field inside the plasma has been measured with the MSE spectroscopy in tokamaks[3-9]. Recently, the MSE diagnostics are applied to measure the radial electric field profile inside the plasma in TFTR[10] as well as the safety factor profiles q(r) and the current profiles in TFTR, DIII-D, and JT-60U[11-14]. The pitch angle of the local magnetic field can be measured from the spectrum of the σ component circularly polarized perpendicular to the Lorentz electric field, or the π component linearly polarized parallel to the Lorentz electric field. The polarization angle of the linearly polarized π component can be measured by using the two linear polarizer. On the contrary, the σ component is circularly polarized and the observed spectra of the σ component is elliptically polarized. The polarization

angle of elliptical component is measured by using a photoelastic modulator (PEM). So far, in PBX-M[4,6] and DIII-D[5], the pitch angle of the local magnetic field is measured from the spectra of the σ component by using the PEM and the interference filter. In JET[7,8] and JIPP T-IIU[9], the pitch angle is derived from the spectra of the π component by using the linear polarizer and the spectrometer. The problem of the measurement by using the PEM is the offset of the polarization angle by the magnetic field due to the Faraday rotation effect [5]. Therefore, it is necessary to calibrate the offset of the polarization angle by injecting the neutral beam to gas target with the magnetic field. On the other hand, the difference in transmission ratio of each fiber arrays or polarizer produces the offset of the polarization angle in the MSE diagnostic which uses the linear polarizer.

The new polarization sensitive spectroscopy using the ferroelectric liquid crystal (FLC) cell, has been developed to solve the offset of the polarization angle due to the magnetic field [15]. The FLC cell, which functions as half-wave retarder whose optic axis is controlled by an electrically applied voltage, can rotate the direction of the polarization angle by 90 degrees. By using the FLC, the polarization angle can be measured with only one linear polarizer.

1.2 Compact Helical System (CHS)

CHS is the heliotron/torsatron type device which has the poloidal mode number of 2 and the toroidal mode number of 8[16-18]. The major radius is 1 m and the averaged minor radius is 0.2 m. The main purpose of CHS research is examining the plasma confinement in the helical device with the low aspect ratio of 5. The magnetic field strength in CHS is from 0.6 T to 1.8 T and the magnetic axis of the vacuum magnetic surface can be shifted from 0.8 m to 1.1 m by changing the vertical magnetic field strength. The CHS device has two neutral beam injectors (NBI) : heating power of 1.1MW and 0.8MW, and it has two

electron cyclotron heating (ECH) gyrotrons : 53 GHz and 106 GHz. The electron temperature and the density profiles are measured with YAG Thomson scattering[19], and the ion temperature profile is measured with the charge exchange spectroscopy[20,21].

The magnetic field line in CHS has the complicated feature. Figure 1.1 shows the magnetic field line in CHS when the magnetic axis is 92.1 cm. The direction of the poloidal magnetic field on the mid-plane reverses its sign every 22.5 degrees. As the major radius becomes larger, the poloidal magnetic field on the mid-plane (B_z) at the horizontally elongated cross section increases, while the poloidal magnetic field at the vertically elongated cross section decreases. The magnetic axis is shifted outward by decreasing the vertical magnetic field strength, while it is shifted inward by increasing the vertical magnetic field strength. When the magnetic axis is 92.1 cm, there is only 2 mm difference between the position of the B_z=0 at the horizontally elongated cross section and the vertically elongated one. In this configuration, the magnetic field on the magnetic axis has very small helical ripples (zero ripple configuration).

When the magnetic axis is shifted inward (89.9 cm), the pitch angle on the magnetic axis at the horizontally elongated cross section is negative, while it is positive at the vertically elongated one. The position of zero pitch angle is almost unshifted from R=94.5 cm. When the magnetic axis is shifted outward (101.6 cm), the position of zero pitch angle shifts outward by 4 cm at the horizontally elongated cross section, while it shift inward by 3 cm at the vertically elongated cross section. The position of zero pitch angle moves less than the shift of the magnetic axis. The position of zero pitch angle at the horizontally elongated cross section shifts the same direction as the magnetic axis, while it shifts in the direction opposite to the magnetic axis at the vertically elongated cross section. Thus, the structure of magnetic field in CHS is complex and the measurement of the magnetic

field line is considered to be very important.

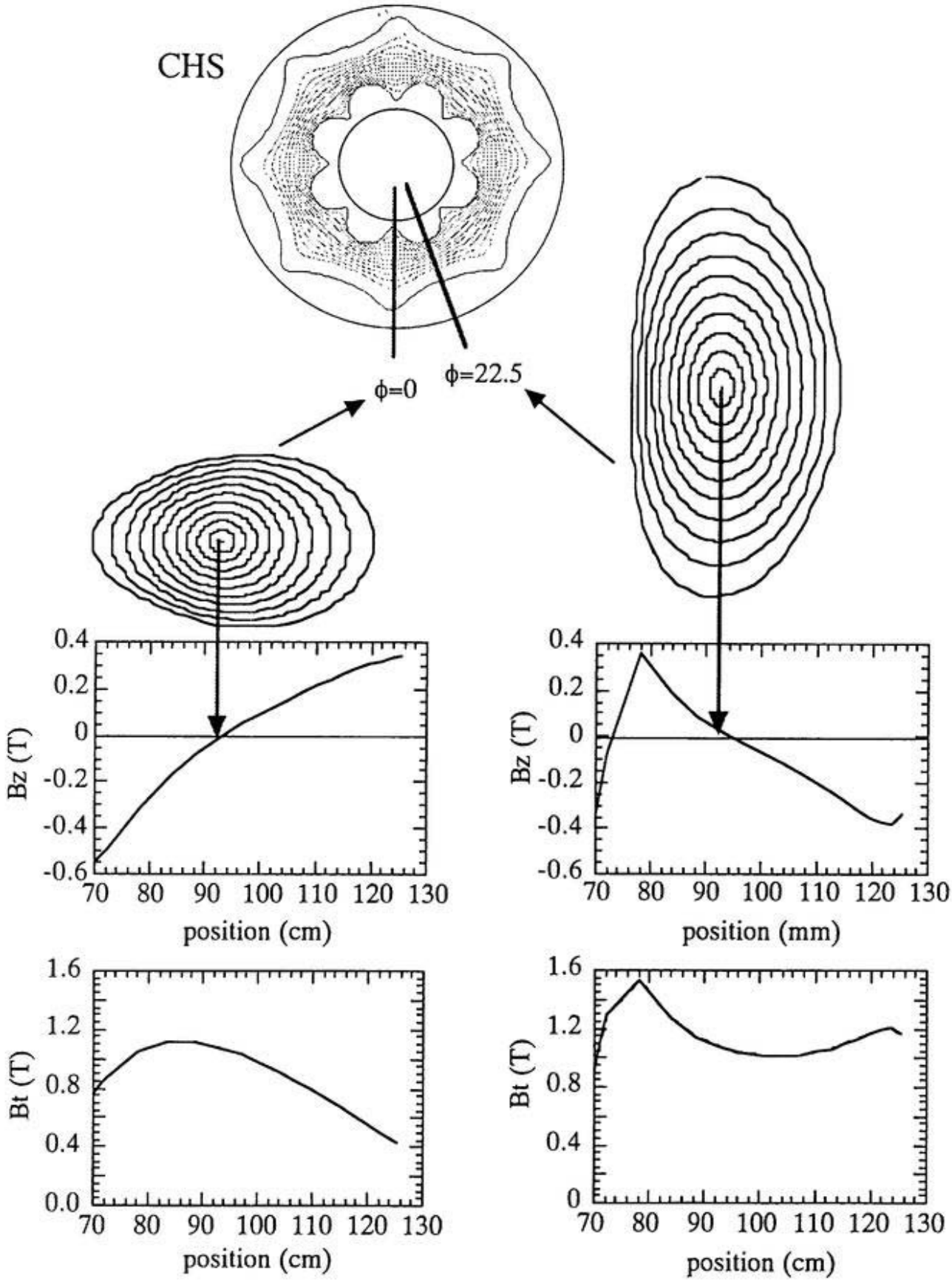

Fig. 1.1 Magnetic field of CHS at Rax=92.1 cm.

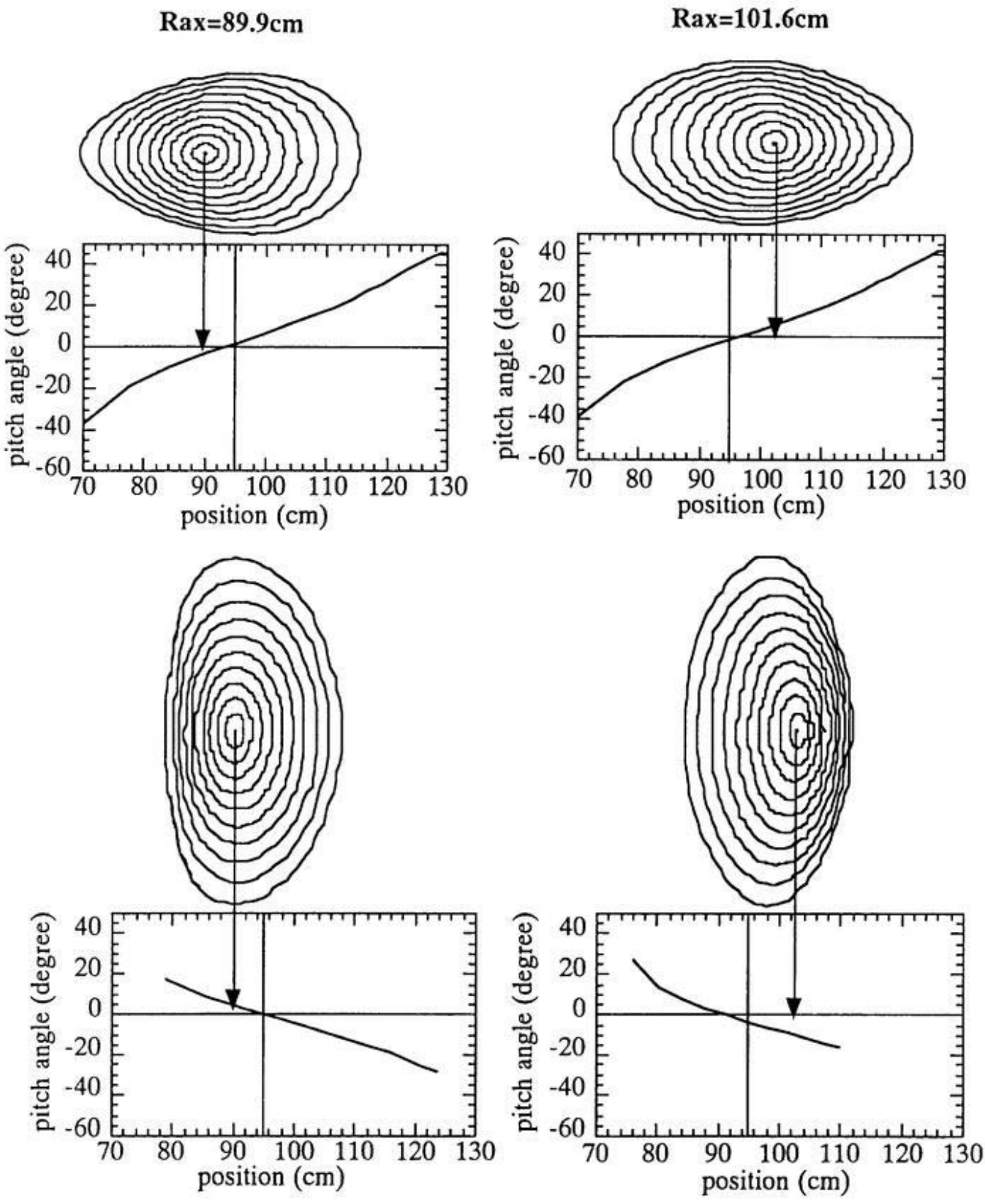

Fig. 1.2 Magnetic field of horizontally elongated cross section and vertically elongated cross section in CHS.

Chapter 2
Diagnostic System for MSE Spectroscopy

2.1 Principle of MSE Spectroscopy

The neutral beam injected in the plasma is excited to the n=3 state from the n=1 state due to the collision between the neutral beam and the particle in the plasma. By the radiative transition from the n=3 state to the n=2 state, H_α spectra emits. The energy level ,E (cm-1), with the electric field ,F (V/cm), is given by

$$E = \left[-\frac{1.097 \times 10^5}{n^2} + \frac{F}{15620} n(n_1 - n_2) \right], \qquad (2\text{-}1)$$

where n is the principal quantum number. The first term represents the energy level without electric field , while the second one represents the splitting of energy levels due to the Stark effect. The n=2 energy level splits into three, while the n=3 energy level splits into five as shown in Figure 2.1. The MSE spectrum in the H_α emission consists of 15 components, and they are separated to the σ components ($\Delta m_1 = \pm 1$) and the π components ($\Delta m_1 = 0$) due to the Stark effect.

As shown in Figure 2.2, the σ component (0σ, $+1\sigma$, and -1σ lines) is circularly polarized perpendicular to the Lorentz electric field, and the $+\pi$ ($+2\pi$, $+3\pi$, and $+4\pi$ lines) component and the $-\pi$ (-2π, -3π, and -4π lines) component are linearly polarized parallel to the Lorentz field, namely perpendicular to the magnetic field. As shown in Figure 2.2, when the H_α emission is observed with the "viewing angle", β, which is between the beam path and the line of sight, the Doppler shift is given by $(v_j/c)\lambda_0 \cos\beta$, where v_j is the beam velocity and c is the velocity of the light. The wavelength shift due to the motional Stark splitting is given by

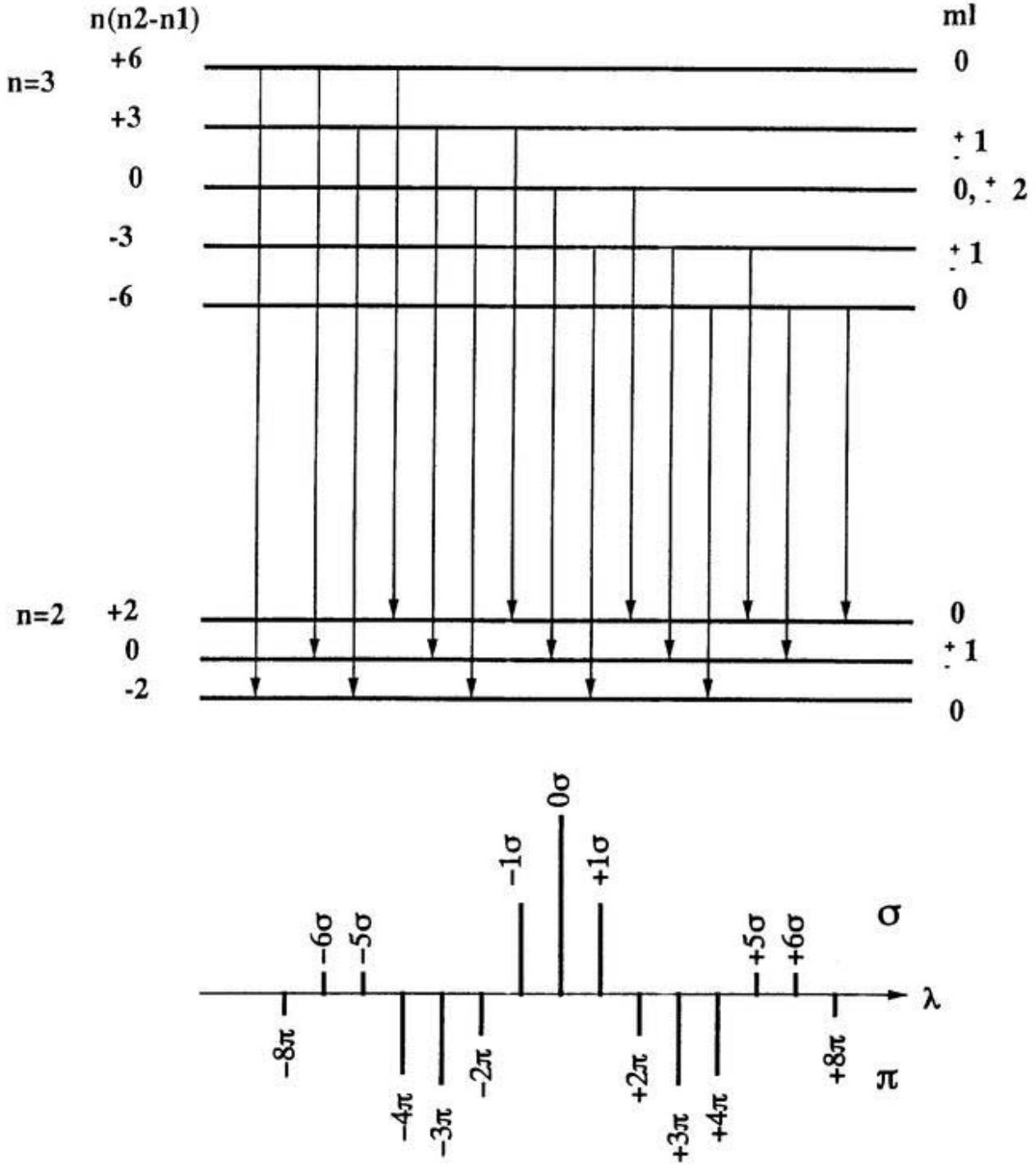

Fig. 2.1 Hα lines with Stark effect

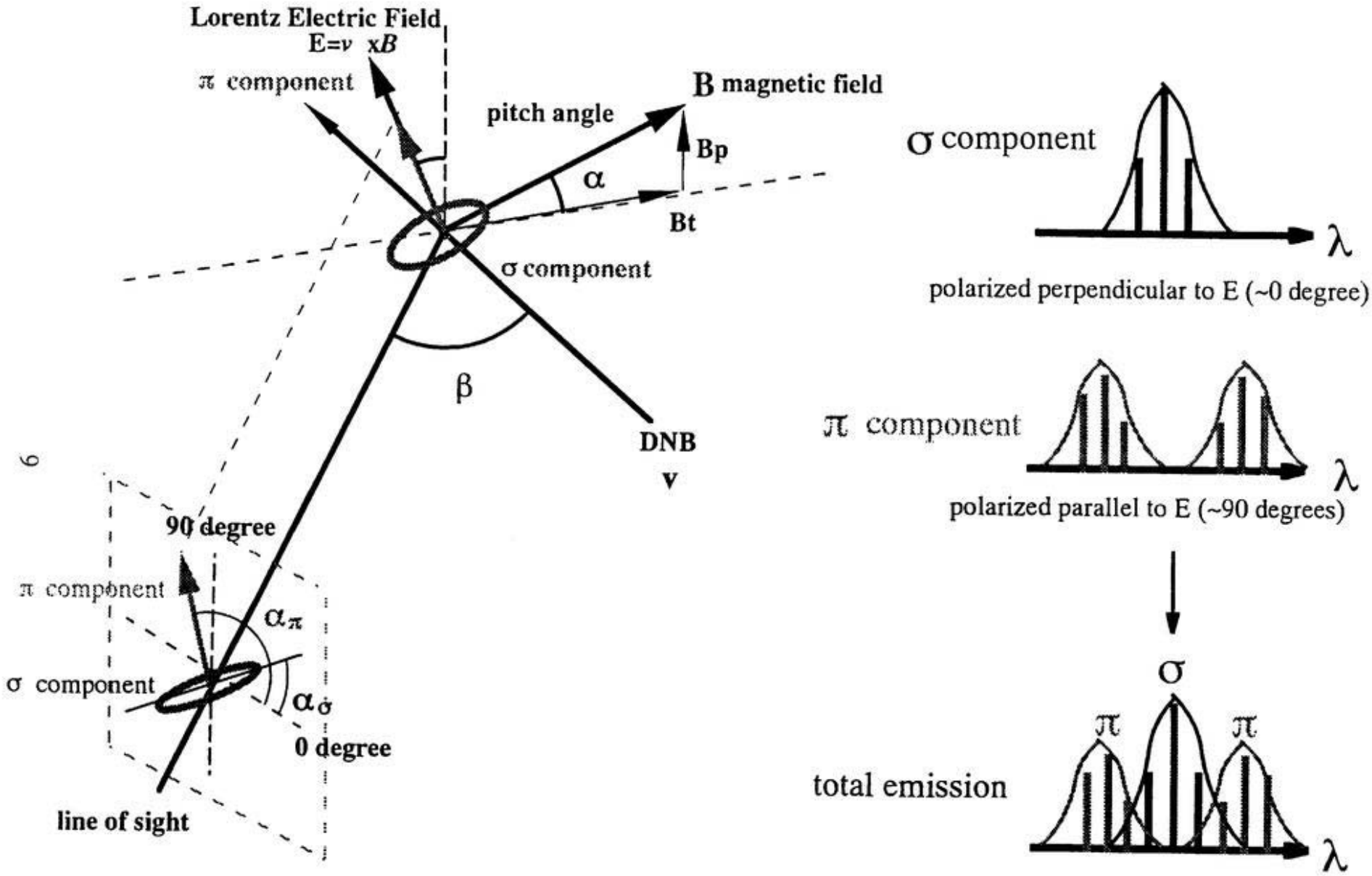

Fig. 2.2 Principle of MSE spectroscopy

$a_i v_j \lambda_0^2 B\sin\varphi$, where λ_0 is the wavelength of H_α, φ is the angle between the beam path and the magnetic field line, a_i is the coefficient of the wavelength shift due to the Stark split, i is the number of the Stark split, and j is the number of the beam components. The wavelength of the observing light is given by

$$\lambda_{ij} = \lambda_0 \left(1 + \frac{v_j}{c}\cos\beta\right)\left(1 + a_i v_j \lambda_0 B\sin\varphi\right). \qquad (2\text{-}2)$$

The spectral intensity through the optics transmitting at ϕ degree with respect to the mid-plane at the wavelength λ is given by

$$I(\phi,\lambda) = I_{\pi l}(\lambda)\cos^2(\alpha_\pi - \phi) + I_{\sigma l}(\lambda)\cos^2(\alpha_\sigma - \phi) + \frac{1}{2} I_{\sigma c}(\lambda) \ . \qquad (2\text{-}3)$$

Where α_π and α_σ are the polarization angles of the π and the σ components, respectively, $I_{\pi l}(\lambda)$ and $I_{\sigma l}(\lambda)$ are intensity of the linearly polarized π and the σ components, respectively, while $I_{\sigma c}(\lambda)$ expresses the circularly polarization of the σ component. When the pitch angle is zero, the σ component is transmitted through the linear polarizer with the transmission axis of 0 degree, while the $+\pi$ and the $-\pi$ components are transmitted through the linear polarizer with transmission axis of 90 degrees. When there is only one linearly polarized component, the polarization angle is given by the spectra of two directions (ϕ=0,90 or ϕ=45,-45). However, the spectra with the motional Stark splitting have the circularly polarized σ component and the overlap of line broadening of the σ and the π components. The circularly polarized σ component and the overlap of linearly polarized σ component and the π component can be eliminated by measuring the four spectra of 0, 45, 90, and 135 degrees polarization angle. The spectral intensity of the four polarization directions for ϕ=0, 45, 90, and −45 are given by

$$I_0(\lambda) = \frac{1}{2} I_{oc}(\lambda) + I_{ol}(\lambda) + \left\{ I_{\pi l}(\lambda) - I_{ol}(\lambda) \right\} \sin^2(\alpha_\sigma) \qquad (2\text{-}4)$$

$$I_{45}(\lambda) = \frac{1}{2} I_{oc}(\lambda) + I_{ol}(\lambda) + \left\{ I_{\pi l}(\lambda) - I_{ol}(\lambda) \right\} \sin^2(\alpha_\sigma - 45) \qquad (2\text{-}5)$$

$$I_{90}(\lambda) = \frac{1}{2} I_{oc}(\lambda) + I_{ol}(\lambda) + \left\{ I_{\pi l}(\lambda) - I_{ol}(\lambda) \right\} \cos^2(\alpha_\sigma) \qquad (2\text{-}6)$$

$$I_{-45}(\lambda) = \frac{1}{2} I_{oc}(\lambda) + I_{ol}(\lambda) + \left\{ I_{\pi l}(\lambda) - I_{ol}(\lambda) \right\} \cos^2(\alpha_\sigma - 45). \qquad (2\text{-}7)$$

The polarization angle of the σ component, α_σ, is given by

$$\tan(2\alpha_\sigma) = \tan(180 - 2\alpha_\pi) = \frac{I(-45,\lambda) - I(45,\lambda)}{I(90,\lambda) - I(0,\lambda)}, \qquad (2\text{-}8)$$

using the four sets of intensity, $I(\phi,\lambda)$, with different ϕ [=0, 45, 90, 135]. The pitch angle, α, defined as $\tan^{-1}(B_p/B_t)$ (B_p : the poloidal magnetic field, B_t : the toroidal magnetic field), is derived from the polarization angle, α_σ, or, α_π, as

$$\tan\alpha = \tan\alpha_\sigma / \cos\beta = \cot\alpha_\pi / \cos\beta, \qquad (2\text{-}9)$$

where β is the "viewing angle".

2.2 Calculation Code of MSE Spectra

The intensity of the spectra with the Doppler shift and the wavelength shift due to the motional Stark splitting are given by Equation (2-1). There are various causes to produce the line broadening of each splitting line. Because the line broadening causes overlapping between the adjacent lines, it should be smaller than the motional Stark splitting. The main reasons of the line broadening are the beam divergence angle, the beam steering angle, and the instrumental width of the spectrometer. Therefore, the code has been developed to calculate the line

broadening due to the beam divergence and the instrumental width of the spectrometer.

The line broadening produced by the Stark effect and the Doppler shift due to the beam divergence angle, θ_b, is roughly given by $\theta_b a_i v_j \lambda_0^2 B\sin\varphi$ and $\theta_b(V/c)\lambda_0\cos\beta$, respectively. In this code, by taking into account the beam divergence angle more precisely, the beam intensity is given by $\exp(-\theta^2/\theta_b^2)$. The intensity is calculated at the various position, k, along the line of sight as shown in Figure 2.3. The spectra is calculated on each region separated to K point. The Stark shift and the Doppler shift inward are larger than one outward, respectively, because of the stronger magnetic field strength and the larger viewing angle between the line of sight and the beam line. Moreover, the motional Stark shift is in the same direction as the Doppler shift in the $+\pi$ component, while it is in the direction opposite to the Doppler shift in the $-\pi$ component. Instrumental function of the spectrometer is given by the Gausian profile with the instrumental width, dw. In the code, the intensity of the spectra with these line broadening is given by

$$I_{ijk} = \exp(\theta_k^2/\theta_b^2) \times \exp\left\{-\frac{(\lambda-\lambda_{ijk})^2}{dw^2}\right\}, \qquad (2\text{-}10)$$

where θ_k is the beam divergence angle at the position k. Here λ_{jik} and $I(\phi,\alpha)$ are given by

$$\lambda_{ijk}(\beta,\varphi) = \frac{\lambda_0}{c} v_j \cos\beta_k + a_i \lambda_0^2 B_k \sin\varphi_k, \qquad (2\text{-}11)$$

$$I(\phi,\alpha) = \sum_{i=1}^{9}\sum_{j=1}^{3}\sum_{k=1}^{K}\left\{I_{\pi l}(\lambda)\cos^2(\alpha_\sigma + 90 - \phi) + I_{\sigma l}(\lambda)\cos^2(\alpha_\sigma - \phi) + \frac{1}{2} I_{\sigma c}(\lambda)\right\}, \qquad (2\text{-}12)$$

where

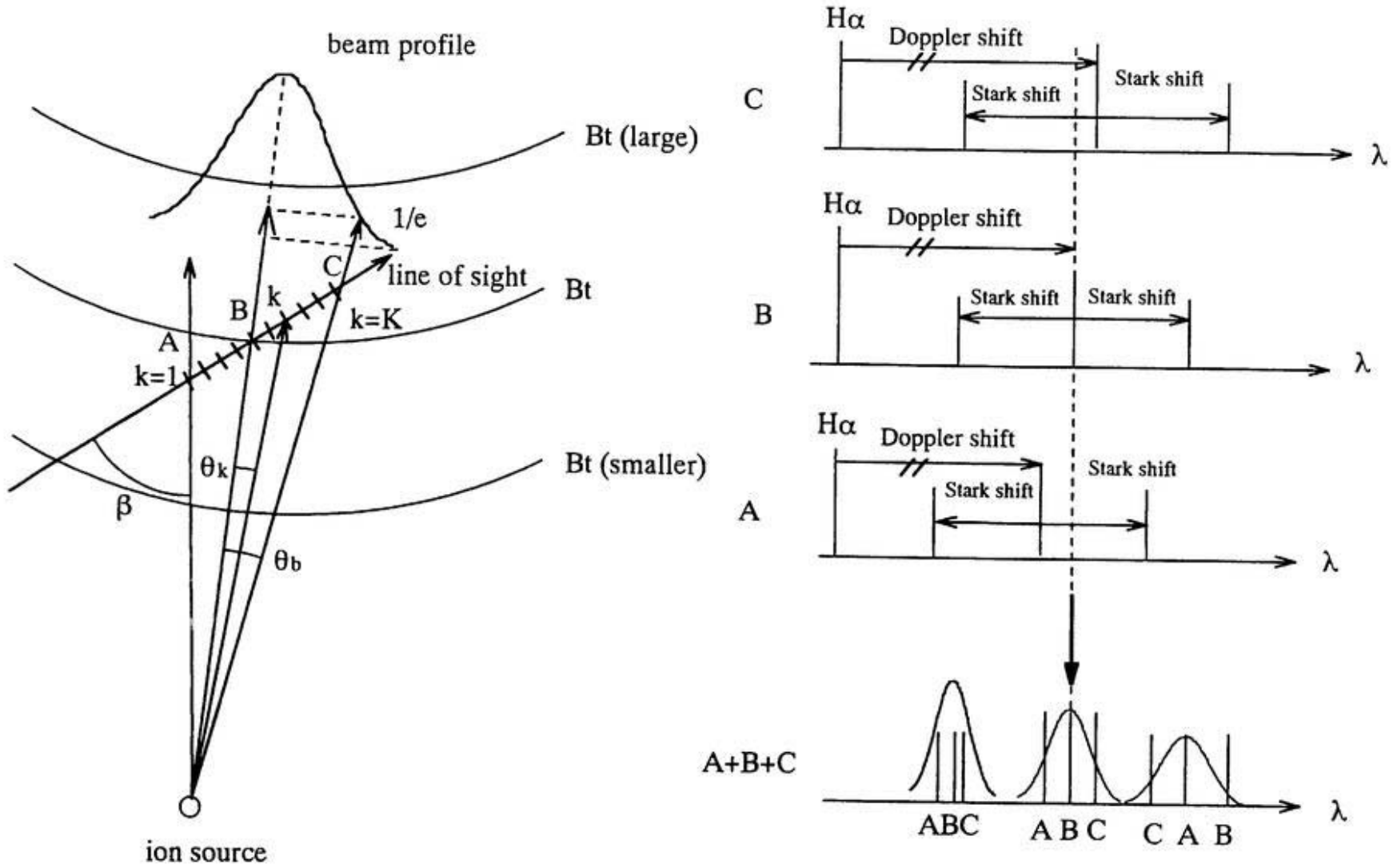

Fig. 2.3 Calculation code of MSE spectra

$$I_{\pi l} = \frac{1}{2} I_{ijk} \sin^2 \zeta, \tag{2-13}$$

$$I_{\sigma l} = \frac{1}{2} I_{ijk} \sin^2 \zeta, \tag{2-14}$$

$$I_{\sigma c} = I_{ijk} \cos^2 \zeta, \tag{2-17}$$

and ζ is the intersection angle between the Lorentz electric field and the line of sight.

2.3 Necessity of DNB for MSE Spectroscopy

To examine the beam divergence angle and the instrumental width of the spectrometer which are both required for the MSE spectroscopy, the spectra with the various beam divergence angles and the various instrumental widths are calculated by using the code.

Figure 2.4 shows the calculated MSE spectra for the instrumental width: dw, which is substituted for 0.01, 0.064, and 0.11 nm with zero beam divergence angle. When the instrumental width is small, each components of 0σ, $\pm 1\sigma$, $\pm 2\pi$, $\pm 3\pi$, and $\pm 4\pi$ is separated from each other. The motional Stark splitting is largest for the full energy component of the beam as indicated in Figure 2.4. As the instrumental width becomes larger, there are no separation of each components of 0σ, $\pm 1\sigma$, $\pm 2\pi$, $\pm 3\pi$, and $\pm 4\pi$, but still clear separation is seen between the π and the σ components. When the instrumental width is 0.11 nm, there is a overlap between the spectra of the σ and the π components.

Figure 2.5 shows the calculated MSE spectra for the beam divergence angle, which is substituted for 1.3, 0.65, and 0 degrees with the instrumental width of 0.064 nm. As shown in Figure 2.5(a), when the beam divergence angle is zero, the

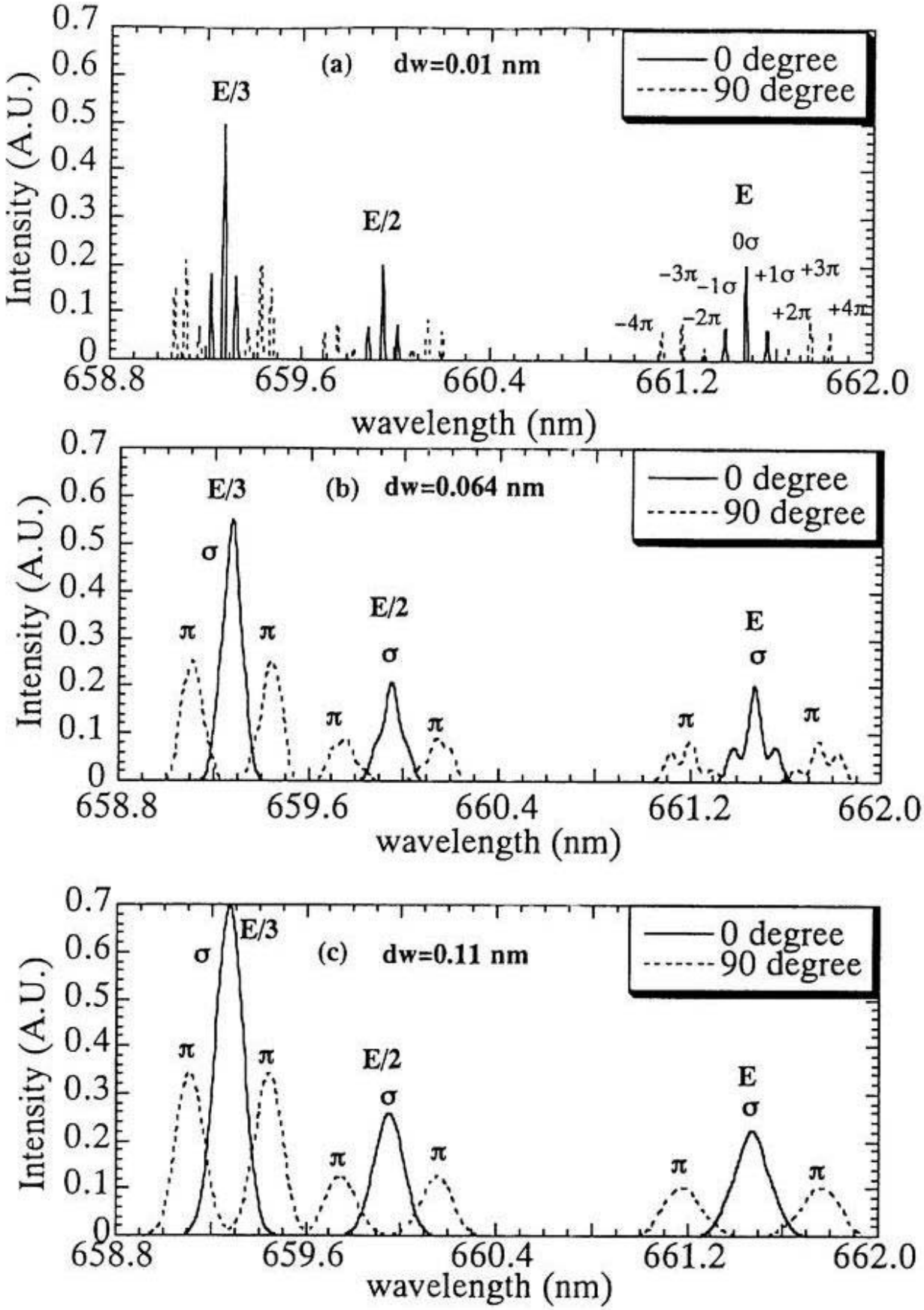

Fig. 2.4 Calculated MSE spectra for dw=0.01,0.064,0.11 nm with Vb=45kV, β=36 degrees

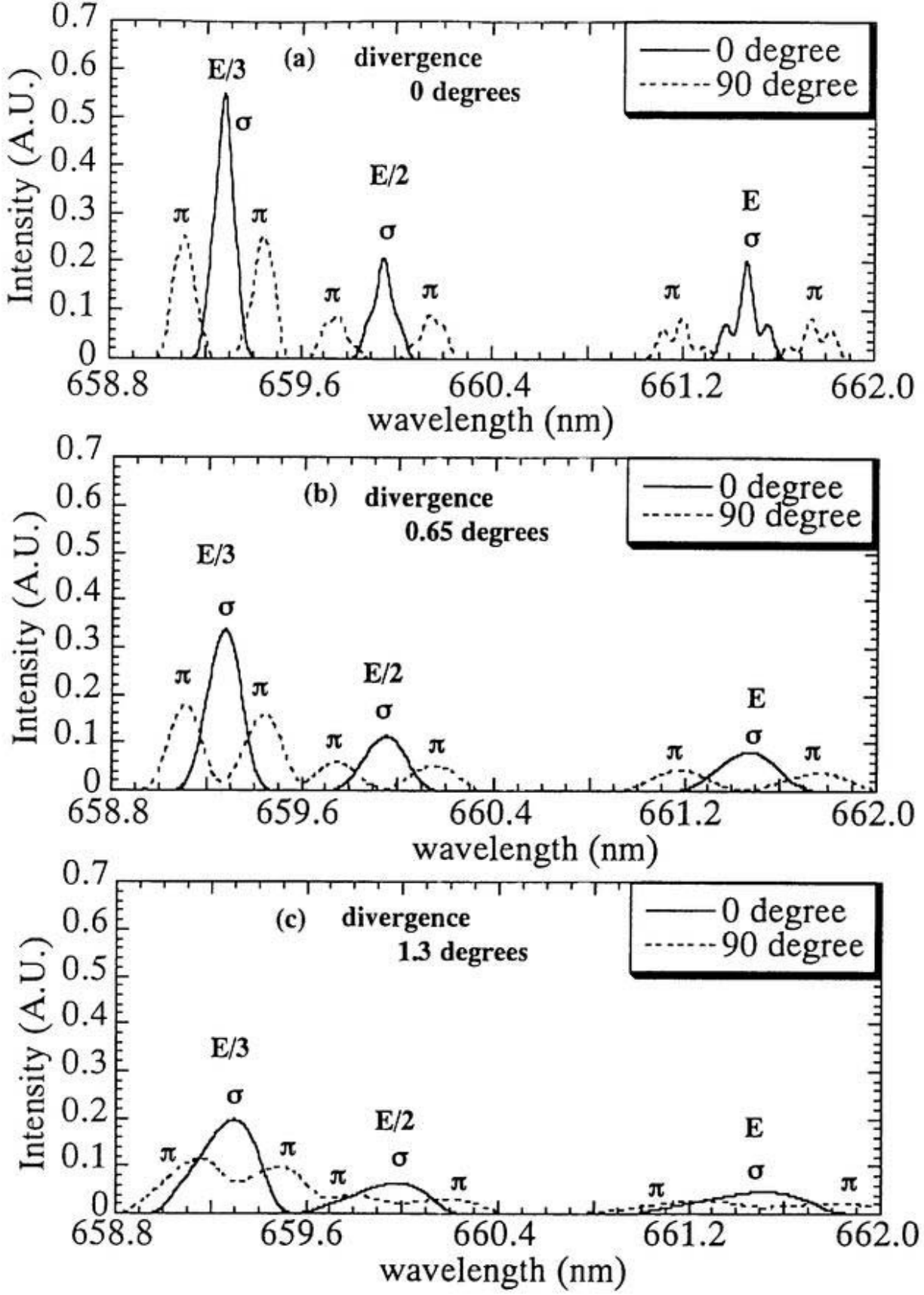

Fig. 2.5 Calculated MSE spectra for divergence=0,0.65,1.3 degree with Vb=45kV, β=36 degrees

spectra of the π component separate from the σ component. When the beam divergence angle is a little bit larger (θ_b = 0.65), the separation is seen between the σ and the π components. However, when the beam divergence angle is as large as the standard heating beam (θ_b = 1.3), the π component is overlapping on the σ component. The spectra of the σ component becomes asymmetry. This asymmetry is due to the nonlinear Doppler shift by the "viewing angle".

Figure 2.6 shows the result that the FWHM of 0σ line of the one-third energy component for the various beam divergence angle with the instrumental width of 0.01, 0.064, and 0.11 nm are calculated. The two width of the motional Stark shift with the magnetic field strength of 0.9 T and 1.8 T are also illustrated. If the beam divergence angle becomes below 0.5 degrees, the instrumental width of the spectrometer changes the calculated FWHM, greatly. Therefore, the instrumental width brings good results only at the small beam divergence angle below 0.5 degrees. The FWHM of spectra doesn't depend on the instrumental width so much at the large beam divergence angle above 0.6 degrees. Therefore, for the pitch angle of the magnetic field, the beam divergence angle required for the MSE measurement is 0.65 degrees at the magnetic field of 0.9 T and 1.4 degrees for the magnetic field of 1.8 T, respectively.

2.4 Schematic View of Experimental Arrangement

Figure 2.7 shows the schematic view of the experimental arrangement of the MSE spectroscopy. The DNB is injected into the horizontal elongated cross section onto the mid-plane.

Each set of optics has a 24 optical fiber-array viewing the plasma from R=0.72 to 1.13 m along the beam line. When the "viewing angle" is small, the larger Doppler shift gives the larger motional Stark splitting, while the spatial resolution

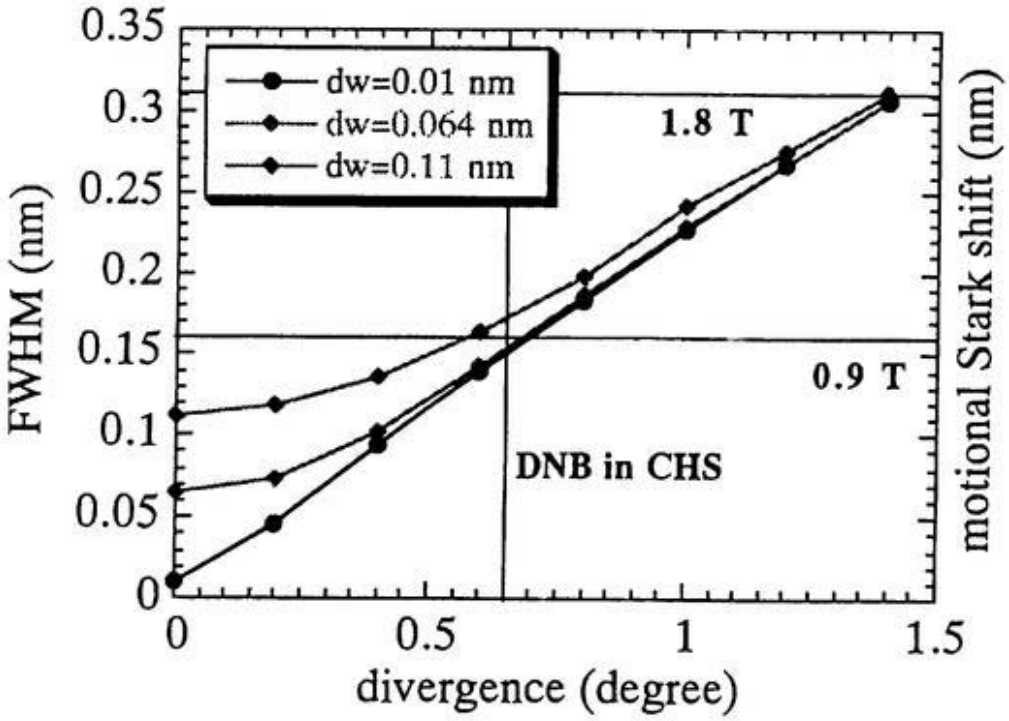

Fig. 2.6 FMHM of σ component as a function of beam divergence angle and the motional Stark shift for the magnetic field strength of 0.9 and 1.8 (T)

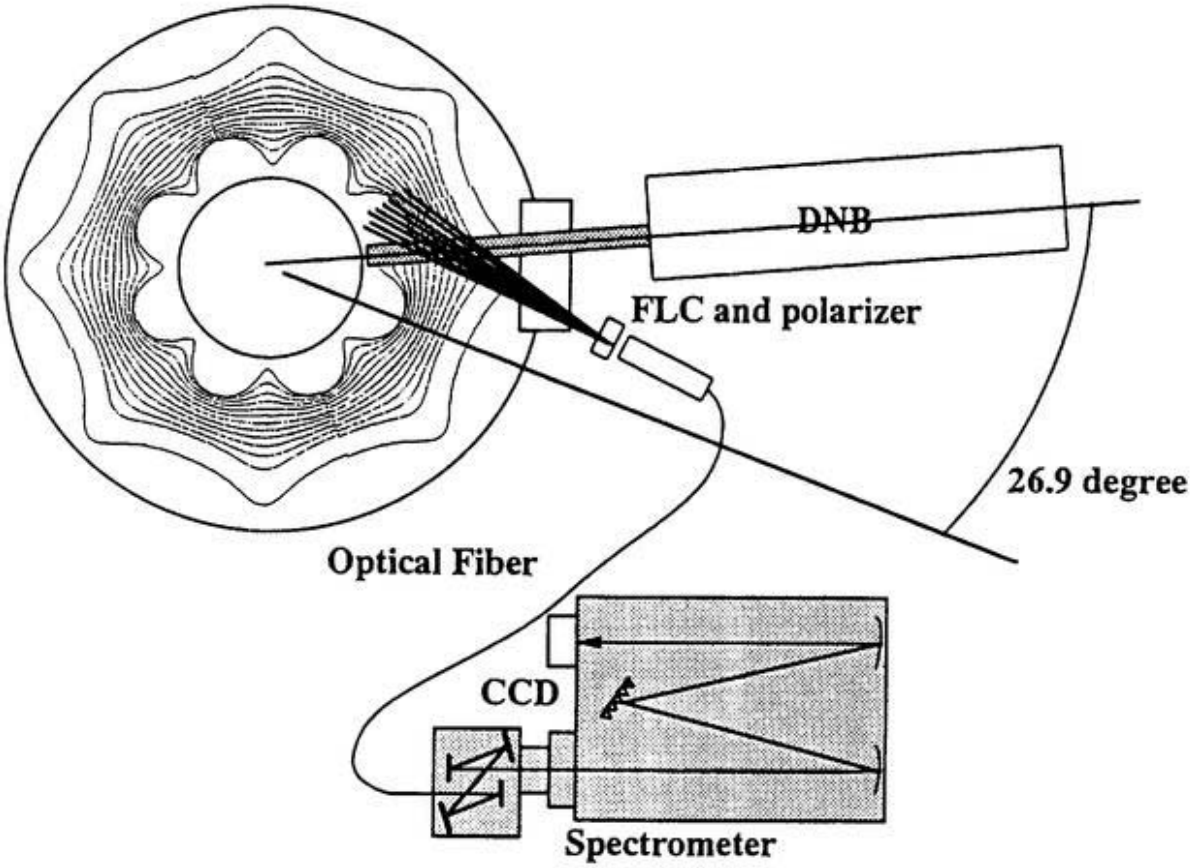

Fig. 2.7 The schematic arrangement of the experimental system

becomes worse. There is a tradeoff between the larger motional Stark splitting and the spatial resolution, and the intermediate "viewing angle" is taken in CHS. Therefore, the line of sight has "viewing angle" of 37.05 ± 21.55 degrees to produce enough Doppler shift and spatial resolution. The light from the fibers is simultaneously led to the entrance slit of the 0.5 m spectrometer and the spectra for each fiber are detected with a two-dimensional (384 X 576 pixel) cooled charge-coupled device (CCD) located at the exit slit of the spectrometer.

Chapter 3

Performance of Diagnostic Neutral Beam (DNB)

3.1 Measurement of DNB Performance

The beam divergence angle of the DNB is measured with the calorimeter inside the beam. Figure 3.1 shows the arrangement for the measurement of the beam divergence angle. The calorimeter is made of the copper with the slits of the 5 mm depth for restraining transition of heat. On the calorimeter, the seven thermoelectric couples are arranged horizontally and the nine thermoelectric couples are arranged vertically which have both the space of 13.5 mm. The thermoelectric couples are fixed into the 2 mm depth in the calorimeter. The shape of the ion source consists of 48 holes (five holes horizontally and ten holes vertically) to reduce the steering angle in horizontally. The calorimeter is located 1.87 m away from the ion source in the best position for the designed focal point (~3 m).

3.2 Estimation of Beam Divergence

Figure 3.2 shows the time evolution of increasing the temperature on the calorimeter for V_b=45 (kV) and I_b=3.5 (A). The number represents the thermocouple number illustrated in Figure 3.1. The output of the #4 thermocouple located at the center in Figure 3.1 has the highest value. The center of the beam line is adjusted to the center of the calorimeter. The time evolution of the thermocouple shows symmetric feature for the position : the time evolution of the #3 thermocouple has almost the same feature as that of the #5 thermocouple.

The calorimeter is located in 1.87 m from the ion source, while the focal length of the beam is ~3 m. Since the ion source is elongated vertically, the ΔT distribution in the vertical direction is sensitive to the focal point, while the

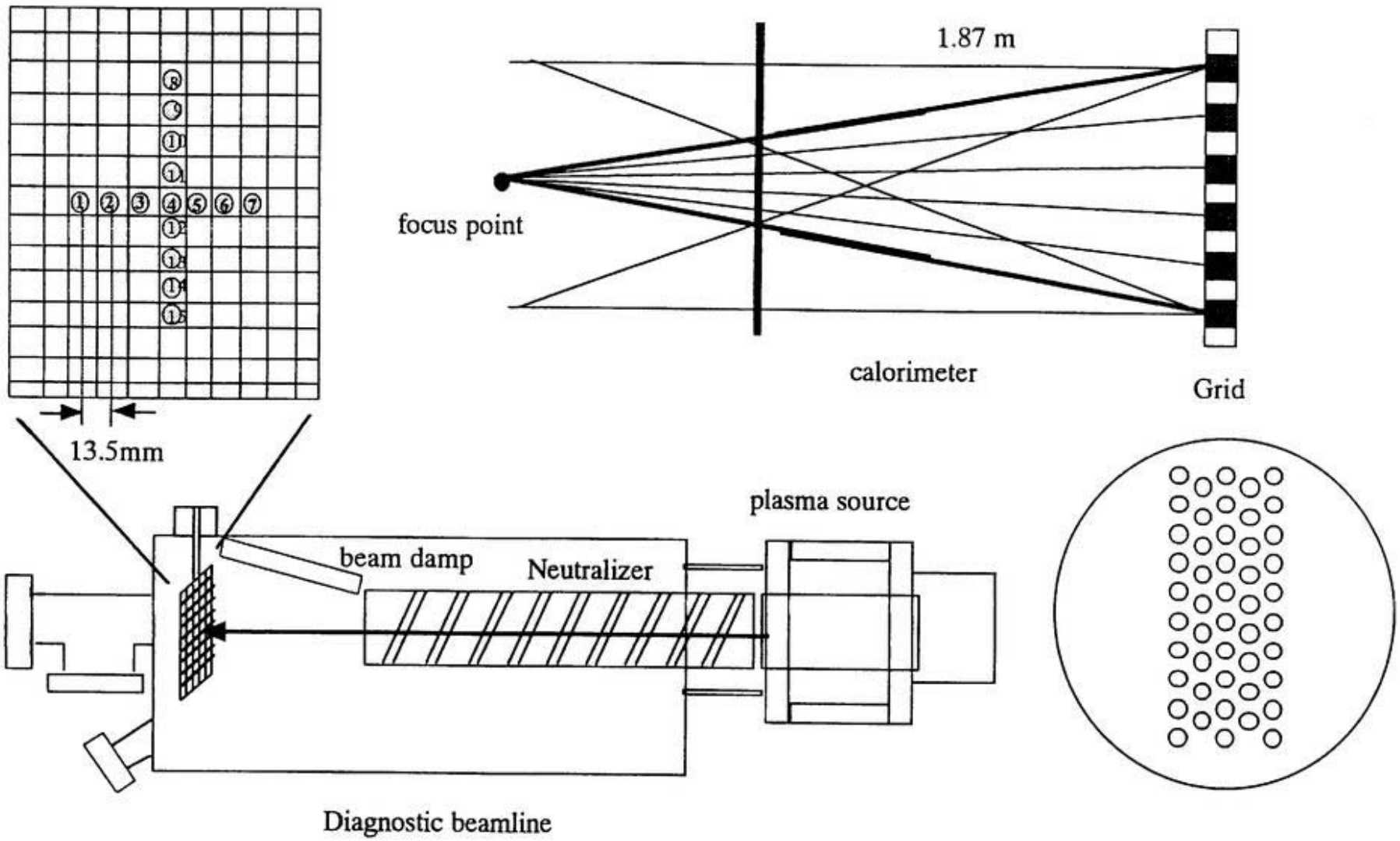

Flg. 3.1 Arrangment for measuring the divergence

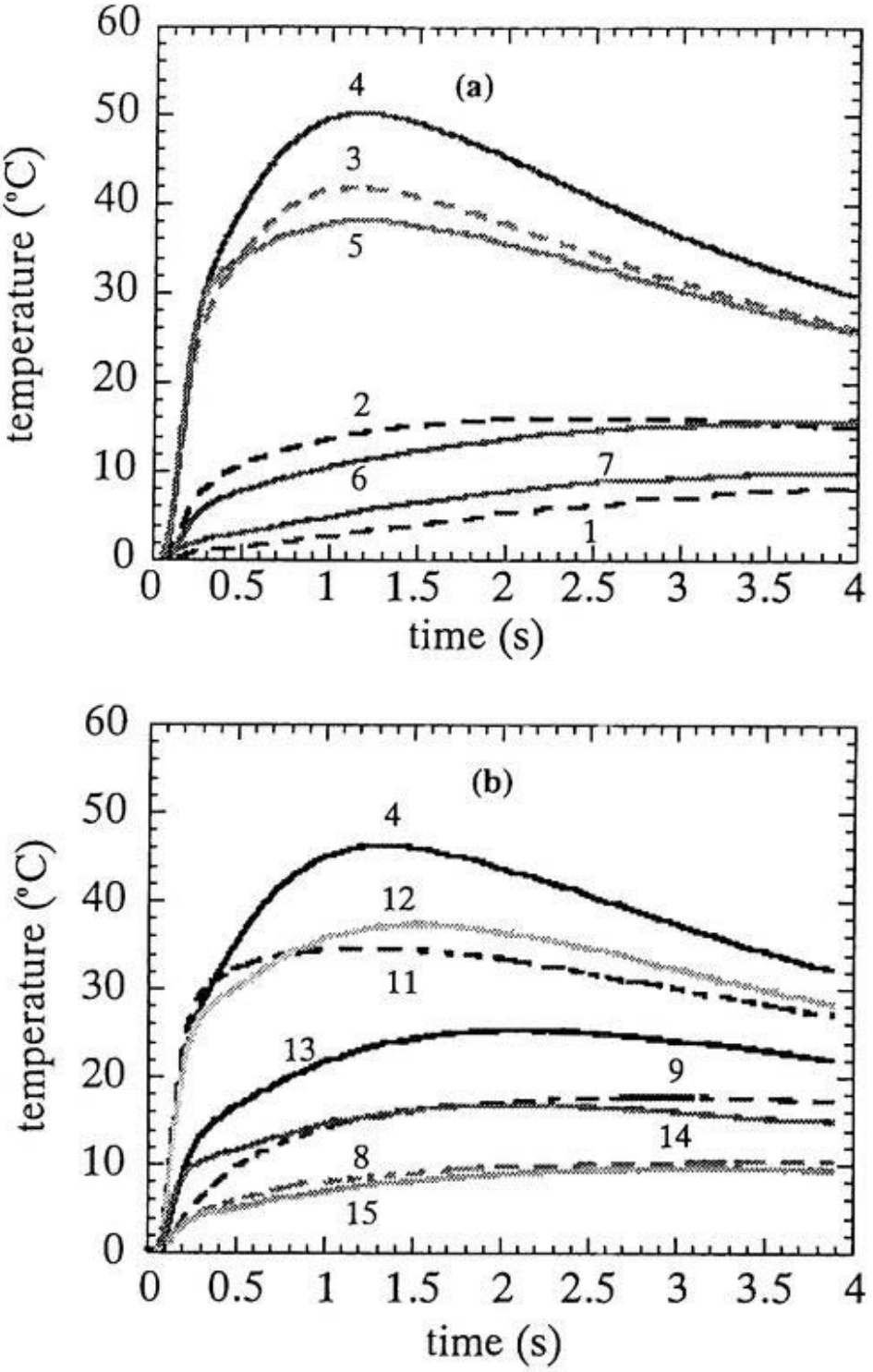

Fig. 3.2 (a) Output of the calorimeter as a function of the time from the shot at Vb 45kV, Ib=3.5A at horizontal
(b) Output of the calorimeter as a function of the time from the shot at Vb 45kV, Ib=3.5A at vertical

horizontal ΔT distribution is sensitive to the beam divergence angle. Therefore, the consistent beam divergence angle and the focal length can be derived from the vertical and the horizontal ΔT distribution. Figure 3.3(a) shows the comparison of the calculated profile at the various divergence angles at the horizontal ΔT profile. The beam profile calculated with the beam divergence angle of 0.6 degrees shows good agreement with the measured ΔT distribution. The averaged ΔT profiles which are calculated in Figure 3.3(a) and (c) are normalized to the measured average of the ΔT profile. Figure 3.3 (b) shows χ^2 value, which means the square of difference between the experimental points of ΔT and the calculated ΔT. The minimum χ^2 value gives the angle of the divergence angle by using the best fit and the divergence angle for $\chi^2 < \chi^2_{min}+1$ gives the allowed range of divergence angle. The result is that the beam divergence angle is measured to be 0.61 ± 1.0 degrees.

Figure 3.3(c) shows the comparison of the measured ΔT to the calculated profile for various focal lengths. The calculated ΔT profile with the focal length of 2.7 m shows good agreement with the measurements. Figure 3.3 (d) shows the χ^2 value as a function of the focal length. These data give the focal length of 2.68 ± 0.3 m.

One of the simplest method is that the beam divergence angle is derived from the full width of half maximum (FWHM) of the ΔT profile measured on the calorimeter. As shown in Figure 3.4(a), the FWHM of the ΔT distribution is 41.2 mm. The beam divergence angle corresponding to the FWHM of 41.2 mm is 0.64 degrees. This value has the same feature as the value (0.61 degrees) derived from the χ^2 method. Figure 3.4(b) shows the FWHM of the calculated ΔT profile with various beam divergence angles, taking into account the actual shape of ion source.

Figure 3.5(a) shows the horizontal ΔT distribution at one, four, and seven second from the time when the beam is injected. The ΔT profile at the center of

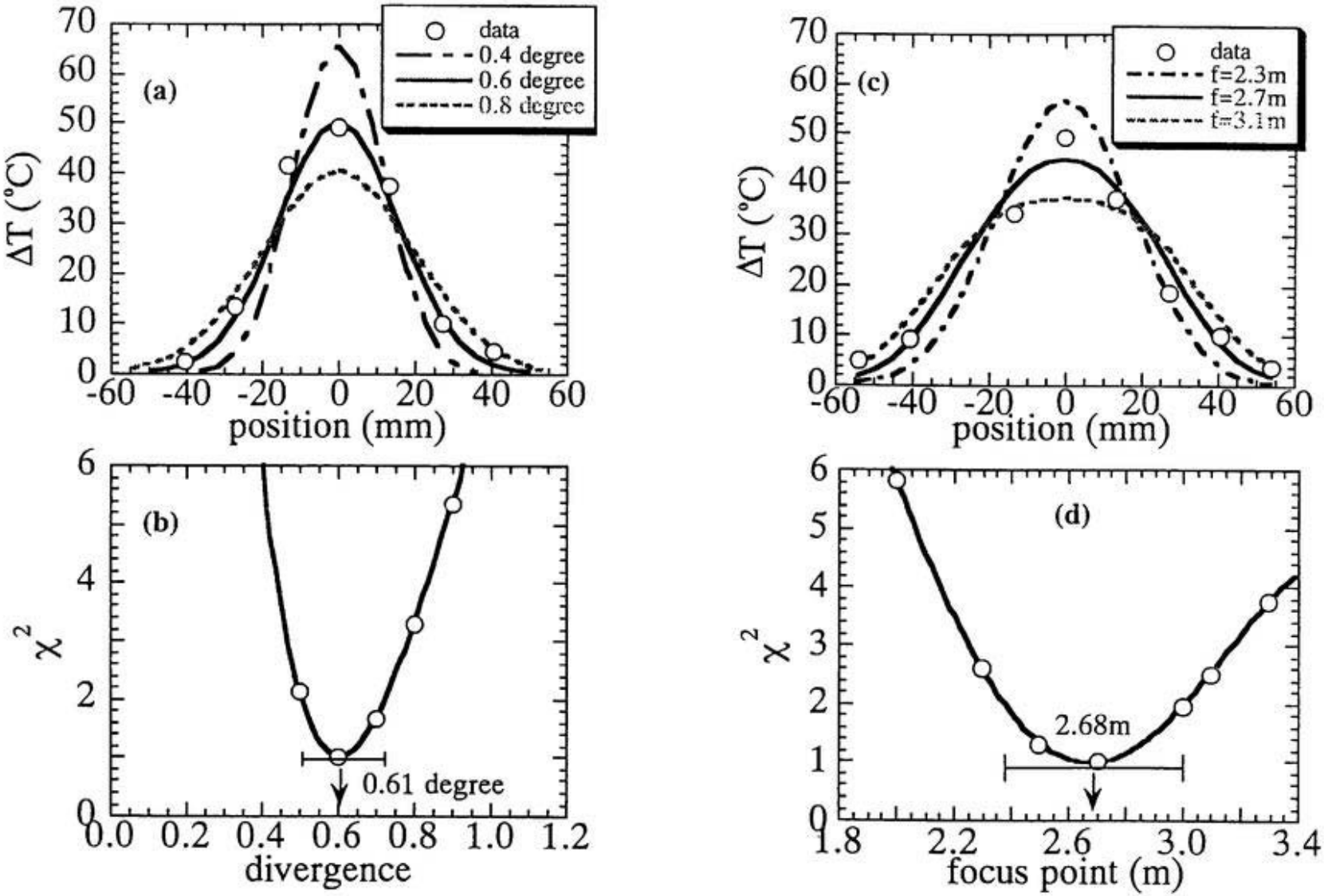

Fig. 3.3 (a) Comparsion of various divergence angle at horizontal (b) Solid lines is the least-squares weighted fit to the experimental points (c) Comparsion of various focus point at vertical (d) Solid line is the least-squares weighted fit to the experimental points

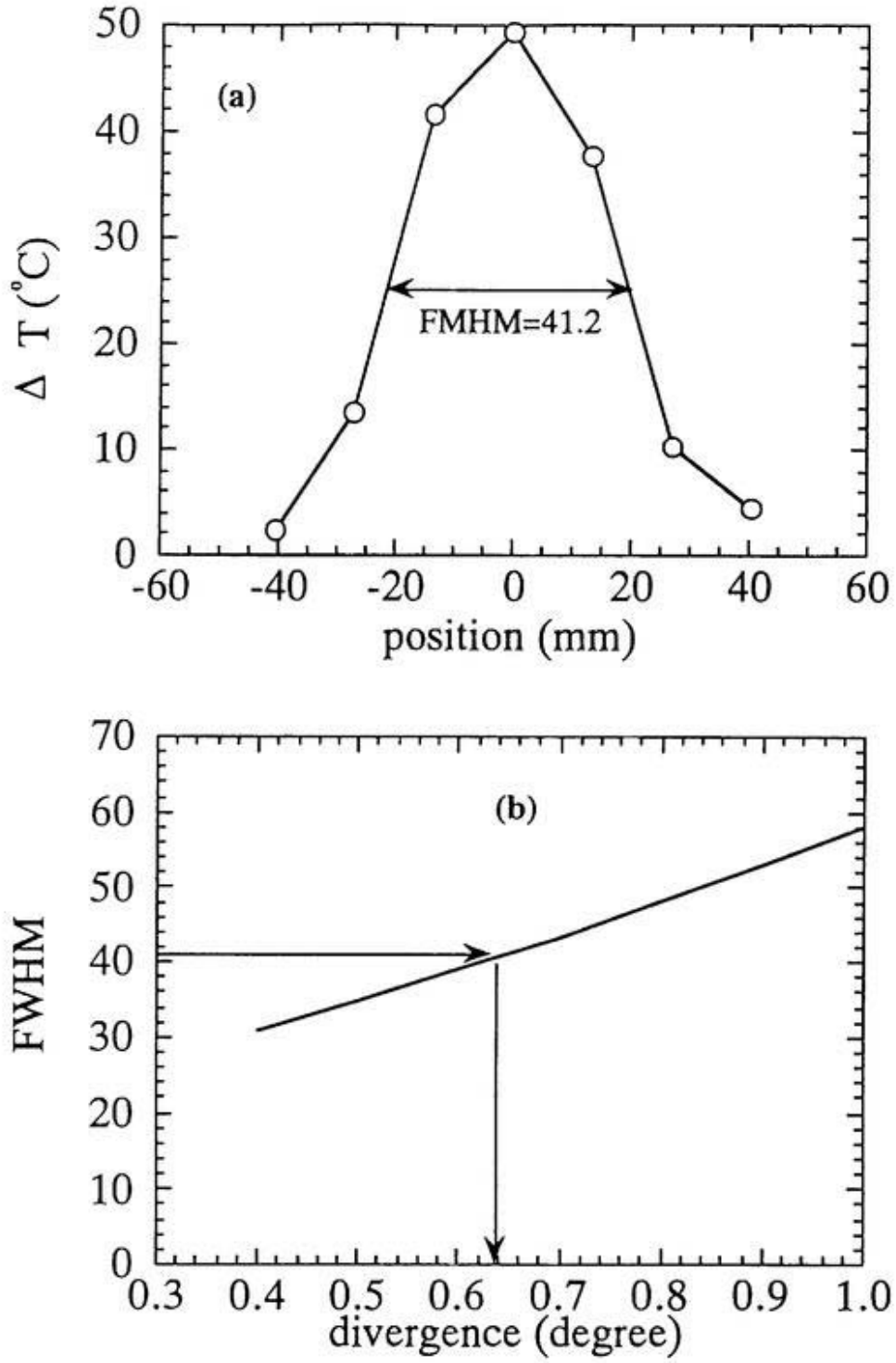

Fig. 3.4 (a) Divergence estimated from FWHM
(b) FWHM as a function of divergence

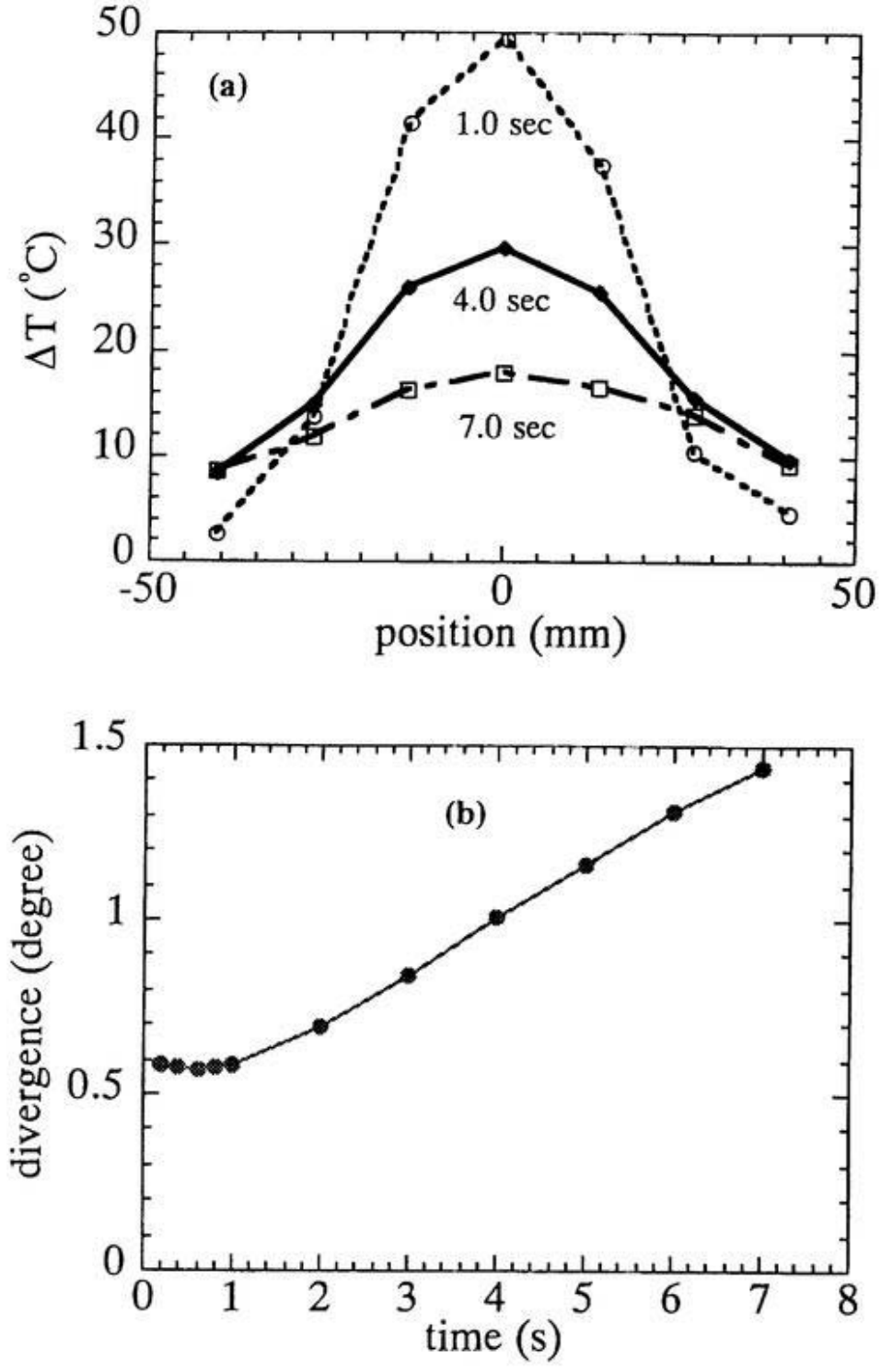

Fig. 3.5 (a) Comparsion of output from a calorimeter
(b) Beam divergence angle estimated from the output of a calorimeter

the calorimeter decreases as time passes, while ΔT at the edge increases after one second. The ΔT profile becomes flatter as time goes on. This is because the heat deposited at the center is transferred to the edge. Therefore, when the beam divergence angle is calculated from the ΔT profile measured after one second, it should be overestimated due to heat transport from the center to the edge. Figure 3.5(b) shows that the beam divergence angle is derived from the FWHM of ΔT profile distribution measured and it works as a function of the time. As shown in Figure 3.5(b), the trouble is that the beam divergence angle is overestimated after one second. On the other hand, there is no effect for the heat transport measured before one second . Therefore, we estimated from the ΔT profile measured before one second.

The beam divergence angle is also derived from the width of the σ component of the measured MSE spectra. Figure 3.6(a) shows the comparison of the calculated spectra at the various divergence angles and the measured spectra with the Stark splitting. Figure 3.6(b) shows the least square of deviation of the experimental points of the MSE profile from the calculated MSE profile. The best fit for the calculated profile to the measured ΔT give the divergence angle of 0.67 ± 0.25 degrees. It is estimated that the large error bar is due to the large photon statistics of emission. Although the larger error bar of the beam divergence angle by using the MSE spectroscopy is seen more than one by using the calorimeter which prevents the beam injecting into the plasma, the MSE spectroscopy can measure the beam divergence angle as well as the pitch angle of the magnetic field line, simultaneously.

3.3 Optimization of Operation for MSE Spectroscopy

It is desirable that the DNB has the small divergence angle for the MSE spectroscopy. This divergence angle is varied depending on the acceleration

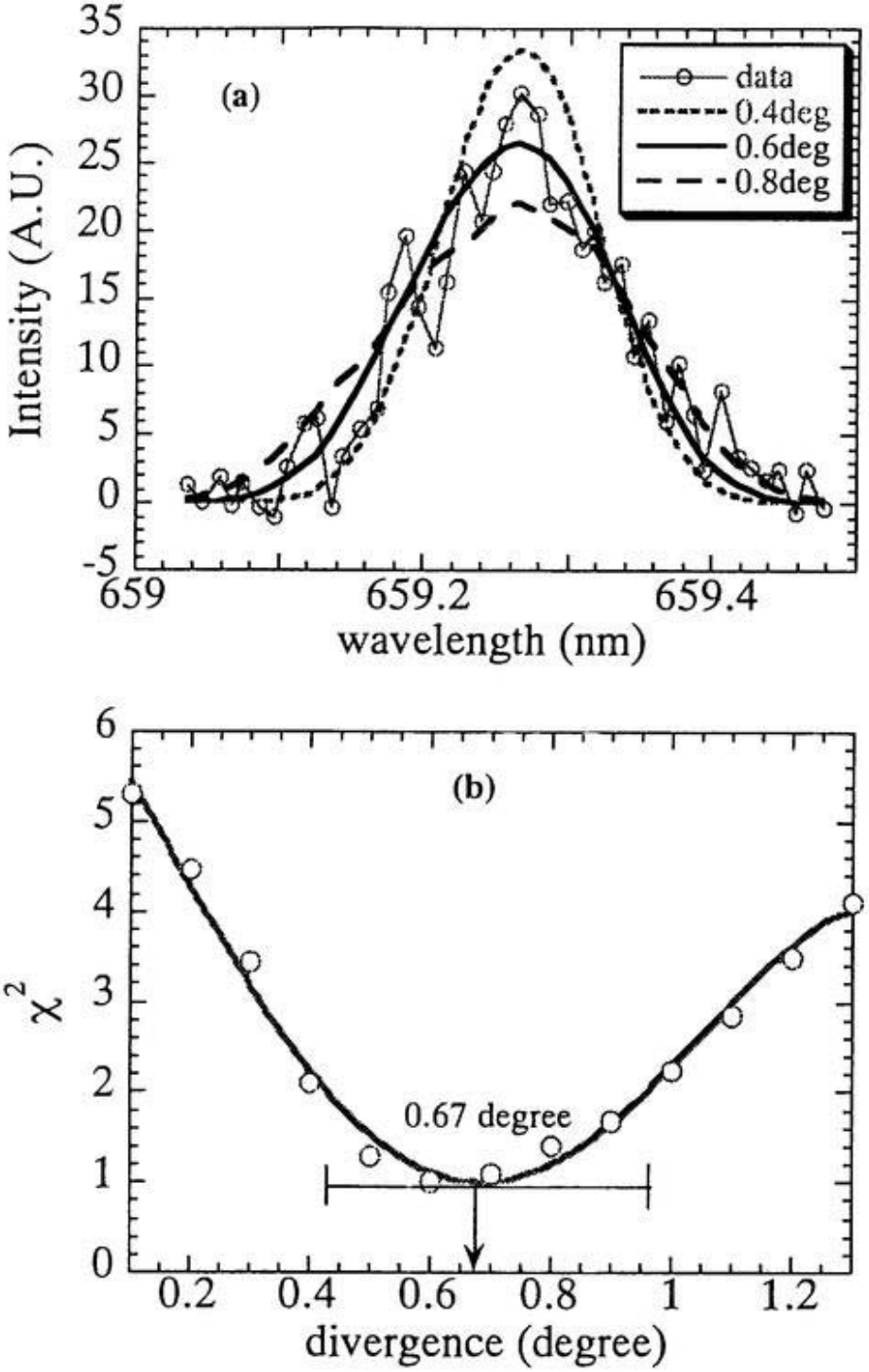

Fig. 3.6 (a) Comparsion of various divergence angle
(b) Solid line is the least-squares weighted fit to the experimental points

voltage and the beam current. At the given acceleration voltage, the beam divergence angle decreases with the increase of the beam current up to a critical value, but it increases rapidly when the beam current is over the critical point. So it is desirable that the DNB is operated with the beam current for the minimum divergence or a little bit than the beam current. In order to know the various conditions for the operation which will take the minimum beam divergence angle, the beam divergence angles are measured for various beam currents and the various acceleration voltages. Figure 3.7(a) shows the beam divergence angle as a function of the beam current for the various acceleration voltages. Figure 3.7(b) shows that the beam current for the minimum divergence angle depends on the acceleration voltage. The optimized beam current, I_b, for the minimum divergence angle depends on the acceleration voltage, V_b, as,

$$I_b = V_b^{1.57} \qquad (3\text{-}1)$$

The minimum divergence angle of ~0.65 degrees is observed in the wide range of the beam voltage. Figure 3.7(b) gives the guideline for the DNB operation with the minimum divergence angle for the MSE measurement.

The energy ratio is measured from the intensity of H_α spectrum. There are H^+, H_2^+, and H_3^+ ions in the ion source, and they are accelerated by the acceleration voltage, E. When H^+, H_2^+, and H_3^+ travel through the neutralizer, they capture one electron and become hydrogen atoms as

$$H^+ \rightarrow H,$$
$$H_2^+ \rightarrow 2H,$$
$$H_3^+ \rightarrow 3H,$$
$$H_2O^+ \rightarrow 2H.$$

The intensity of each beam components, I_i, is given by

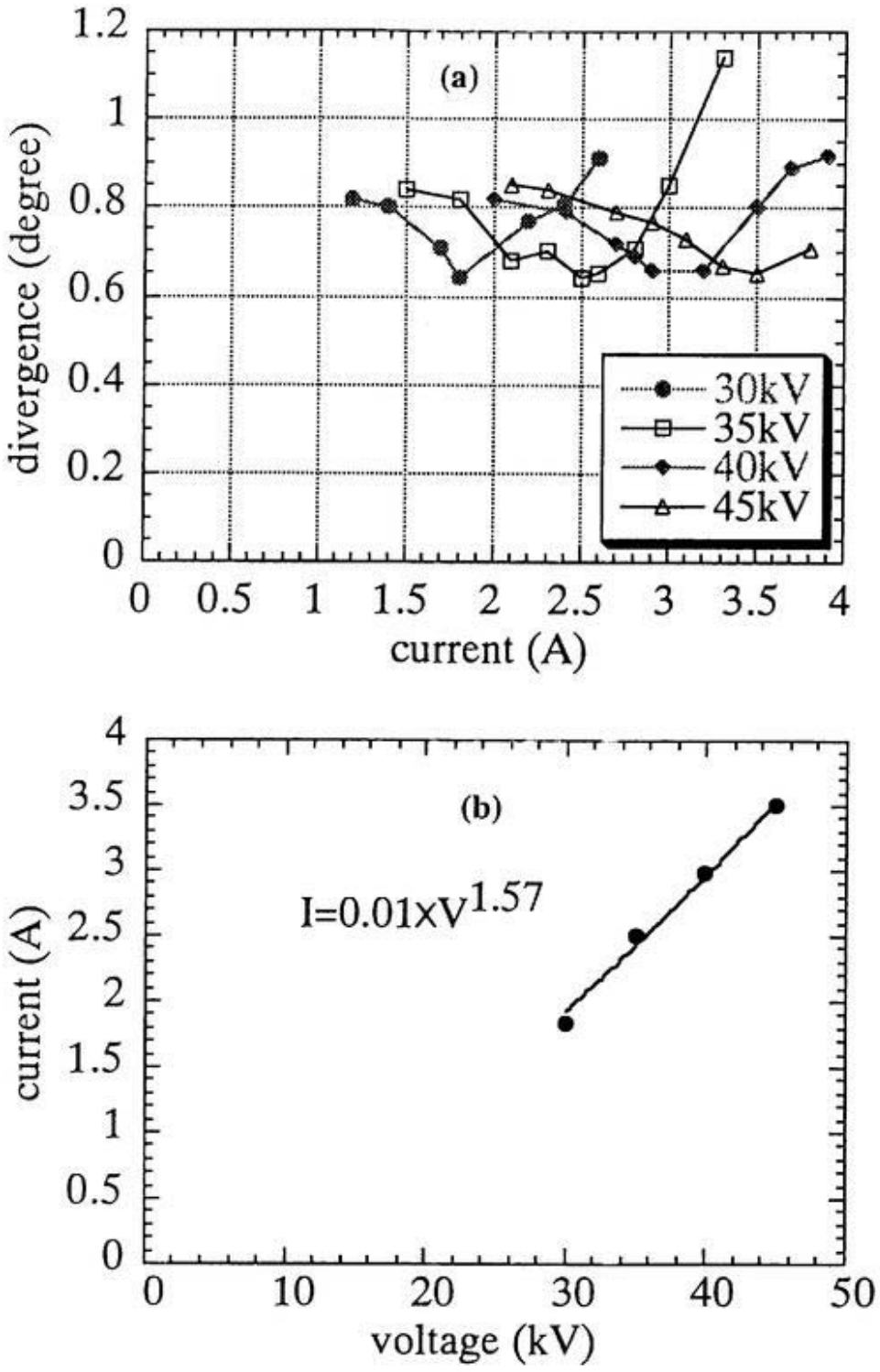

Fig. 3.7 (a) Beam divergence angle as a function of the beam current for various the acceleration voltage (b) Beam current as a function of the acceleration voltage at the minimum divergence angle

$$I_i \propto \frac{N_i j_i \{1-\exp(-\sigma_i nl)\}}{ev_i}, \qquad (3\text{-}2)$$

$$V_i = \sqrt{\frac{2eE}{M_i}}, \qquad (3\text{-}3)$$

where the current of H^+, H_2^+, and H_3^+ are expressed j_1, j_2, and j_3, respectively, the neutralize cross section of H^+, H_2^+, and H_3^+ are expressed σ_1, σ_2, and σ_3, respectively, l is the length of the neutralizer, n is the density of the neutralizer, V_i is the velocity of the hydrogen, and i is the number of the energy component. N_i is the number of the hydrogen atom arising from one ion (N_1=1, N_2=2, N_3=3, and N_{18}=2). M_i is the mass of ions (H^+, H_2^+, H_3^+, H_2O^+)=(M_1=m, M_2=2m, M_3=3m, M_{18}=18m), where m is the mass of the hydrogen atom. The power ratio consumed by each energy components is given by

$$\begin{aligned} &P(E) : P(E/2) : P(E/3) : P(E/18) \\ &= Ej_1 : Ej_2 : Ej_3 : Ej_{18} \\ &= \frac{I_1}{1-\exp(-\sigma_1 nl)} e\sqrt{\frac{2eE}{m}} : \frac{I_2}{2\{1-\exp(-\sigma_2 nl)\}} e\sqrt{\frac{2eE}{2m}} : \frac{I_3}{3\{1-\exp(-\sigma_3 nl)\}} e\sqrt{\frac{2eE}{3m}} : \frac{I_{18}}{2\{1-\exp(-\sigma_{18} nl)\}} e\sqrt{\frac{2eE}{18m}} \\ &= \frac{I_1}{1-\exp(-\sigma_1 nl)} : \frac{I_2}{2\sqrt{2}\{1-\exp(-\sigma_2 nl)\}} : \frac{I_3}{3\sqrt{3}\{1-\exp(-\sigma_3 nl)\}} : \frac{I_{18}}{6\sqrt{2}\{1-\exp(-\sigma_{18} nl)\}} \end{aligned} \qquad (3\text{-}4)$$

for $\sigma_1 = 1.3\times10^{-16}$ cm^2, $\sigma_2 = 3.0\times10^{-16}$ cm^2, $\sigma_3 = 5.0\times10^{-16}$ cm^2, $\sigma_{18} = 9.0\times10^{-16}$ cm^2, $n = 2\times10^{14}$ cm^{-3}, and l=70 cm. The power ratio are calculated from the intensity ratio as

$P(E) : P(E/2) : P(E/3) : P(E/18) = I_1 : 0.301\ I_2 : 0.161\ I_3 : 0.099\ I_{18}$

Figure 3.8 shows the arrangement for the measurement of the power ratio. The spectra is measured by using 0.25 m scanning mirror spectrometer with 13.6 degrees angle which is the intersection angle between the beam path and the line of

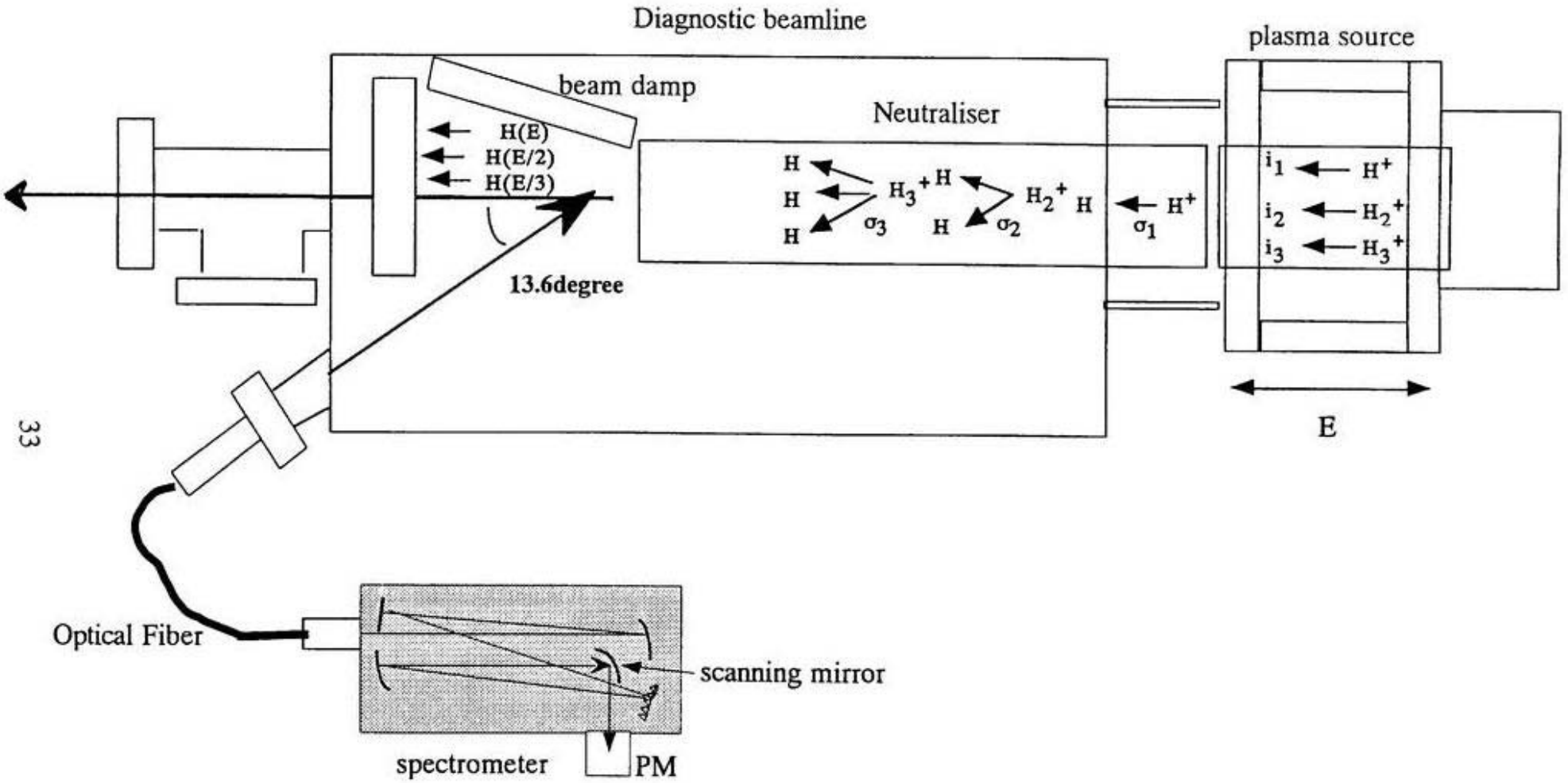

Flg. 3.8 Arrangment for measuring the energy ratio

sight.

Figure 3.9(a) shows the controlled voltage for scanning the mirror of spectrometer with the frequency of 50 Hz. Figure 3.9(b) shows the output of the photomultiplier at the exit slit of the spectrometer. The peak with the highest intensity is the H_α line. Figure 3.9(c) shows the spectra for the full energy, the half energy, the one-third energy, and the 1/18 energy components at t=40~50 (msec). The intensity ratio can be derived only from the peak intensity of each spectra, because the width of the spectra is determined by the instrumental width.

Figure 3.10(a) shows the time evolution of the peak intensity ratio of each component. Figure 3.10(b)(c) shows both the fraction of the intensity ratio of the spectra and the beam power ratio for various currents for the acceleration voltage of 45 kV. The power ratio of E/3 increases with the beam current. However, it is more important to operate the DNB with the minimum beam divergence angle than to operate it with the highest power ratio.

The four power ratios of the full energy, the half energy, the one-third energy, and the 1/18 energy components are 0.57, 0.08, 0.23, and 0.12, respectively, for the acceleration voltage of 45 kV and the beam current of 3.5 A. The spectra of the full energy component has the largest motional Stark shift, but the intensity of the full energy is smaller than that of the one-third energy component. Therefore, when the magnetic field is large enough to give reasonable separation between the σ and the π components, the spectra of the one-third component would be better for the measurement than the full energy component.

As shown in Figure 3.11, the alignment of beam line is checked by measuring the ΔT profile of carbon which is arranged inside the tours by using the IR camera with the frame rate of 80 msec. The target carbon plate is divided into 21 sections to prevent the heat from flowing on the surface. If the carbon plate is just made

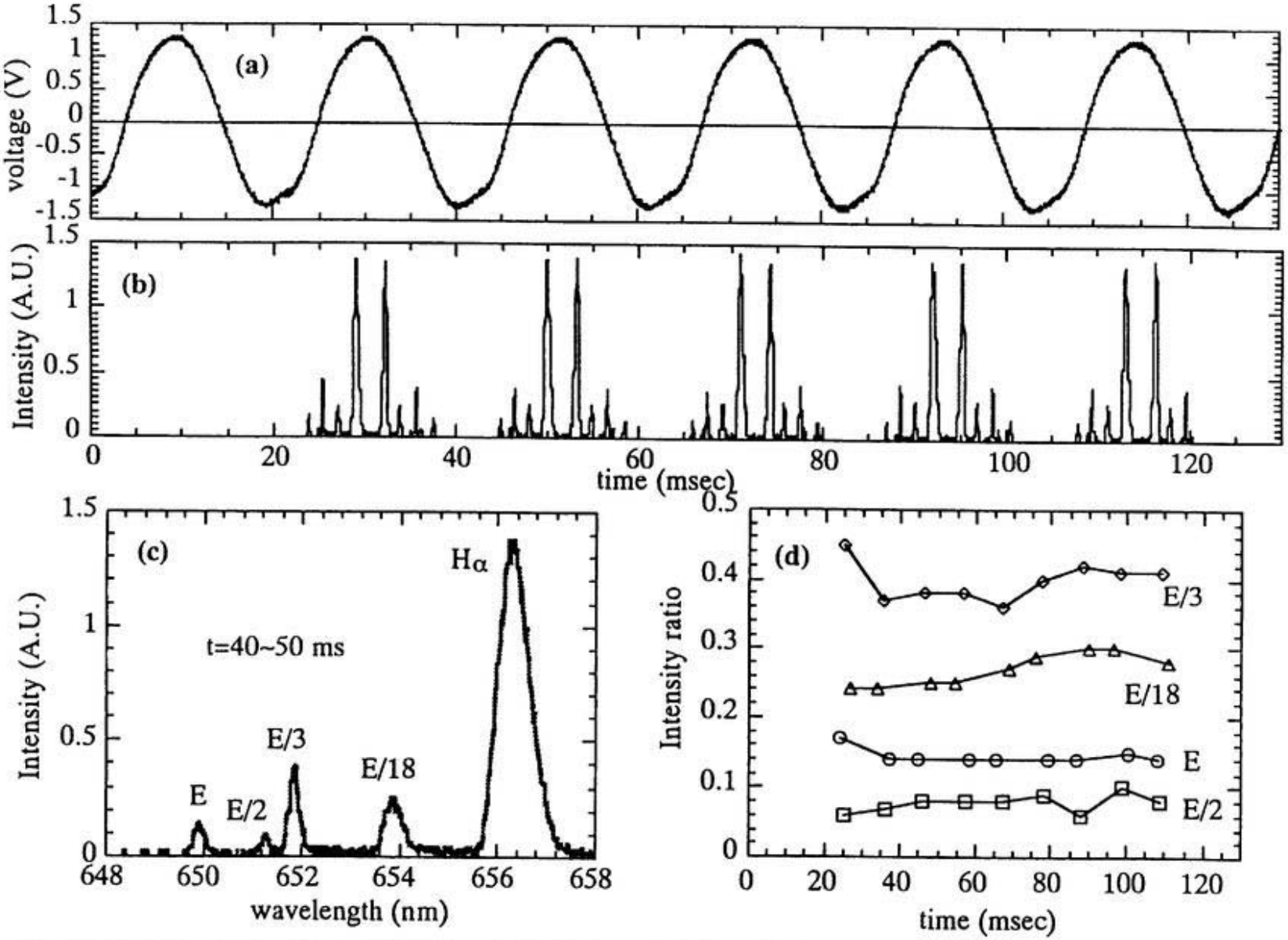

Fig. 3.9 (a) Control voltage (b) Output of photomultiplier (c) Spectra from 40 to 50 msec (d) Intensity ratio as a function of time

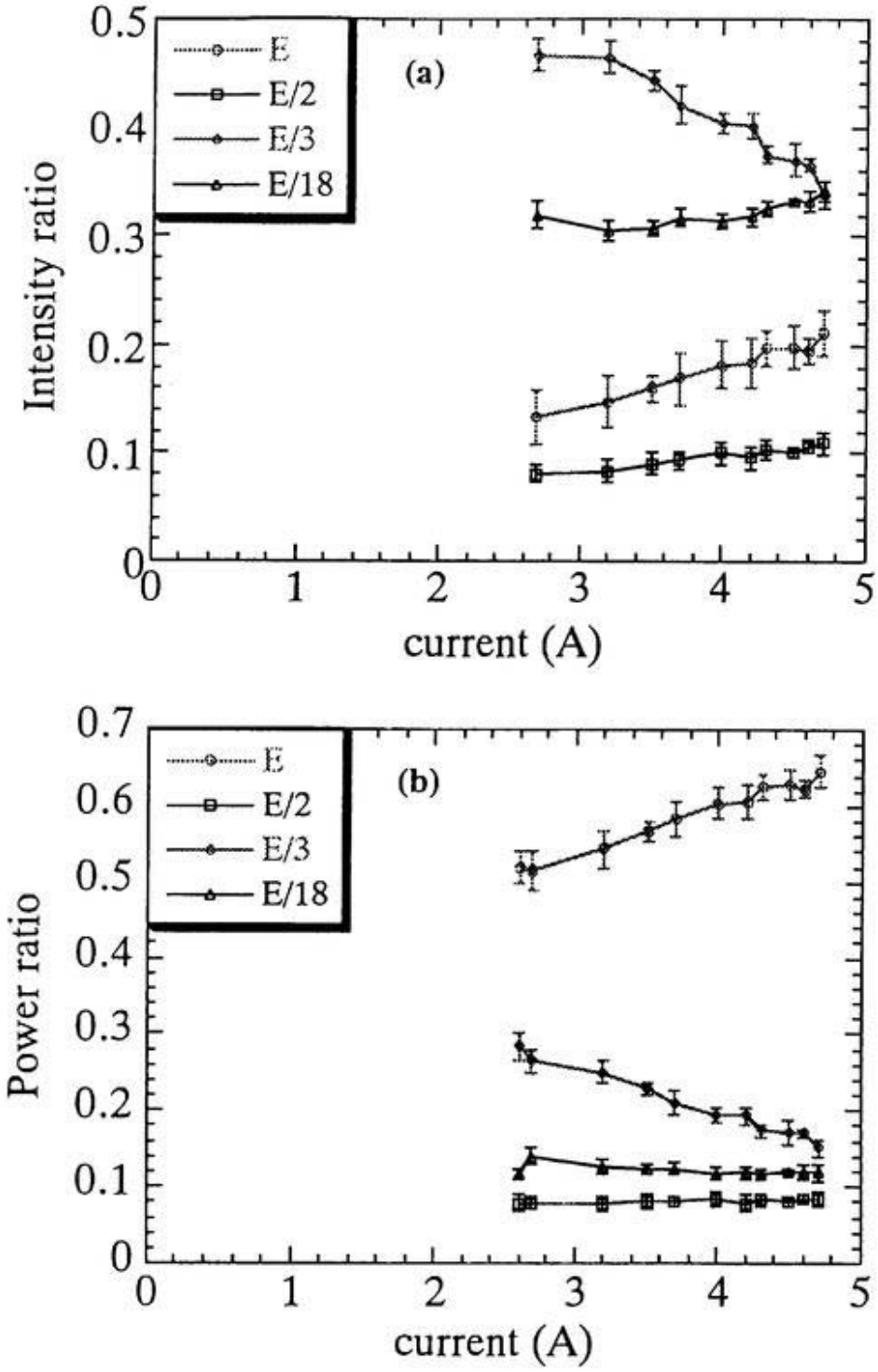

Fig. 3.10 (a)(b) Intensity ratio of spectra and power ratio at Vb=45kV

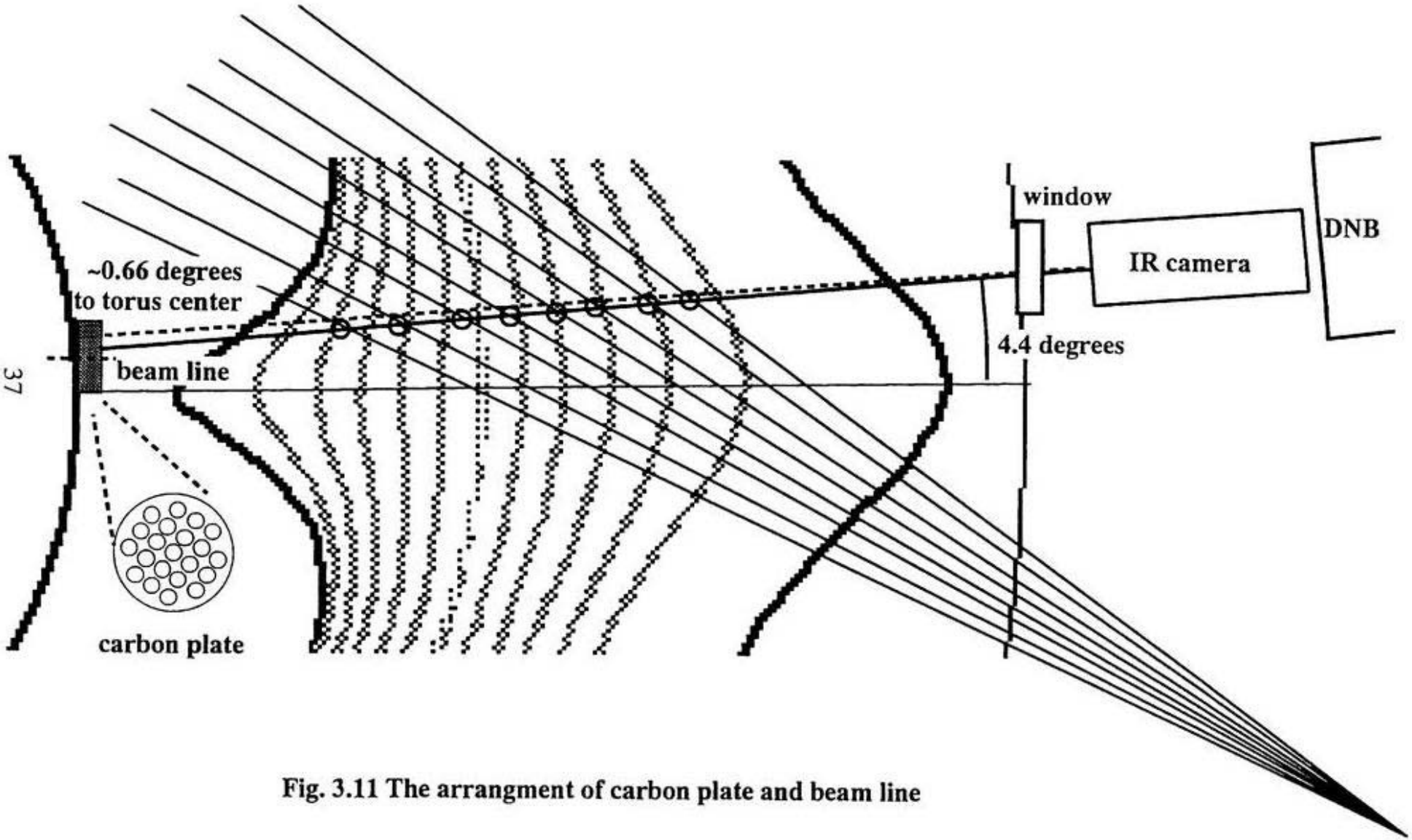

Fig. 3.11 The arrangment of carbon plate and beam line

of one plate, the deposited heat spreads out very quickly, and there is no sign of the deposition profile obtained. Figure 3.12 shows the profile of increasing the temperature on the carbon plate measured with the IR camera. This frame is measured at every 80 msec. The #2 frame arises just after the DNB is injected. Figure 3.13(b) shows the ΔT profile with the minimum divergence angle of the DNB on the carbon. This fit shows the center of the beam line is 8 mm away from the line toward the torus center. The beam is slightly off perpendicular by 0.66 degrees at the nearly horizontally elongated cross section with the offset of the toroidal angle of 4.4 degrees. By the accurate measurement of the beam line, the observed points are given precisely. The pitch angle of the magnetic field has been measured by the MSE spectroscopy on this observed points.

Fig.3.12 Temperture profile of carbon plate

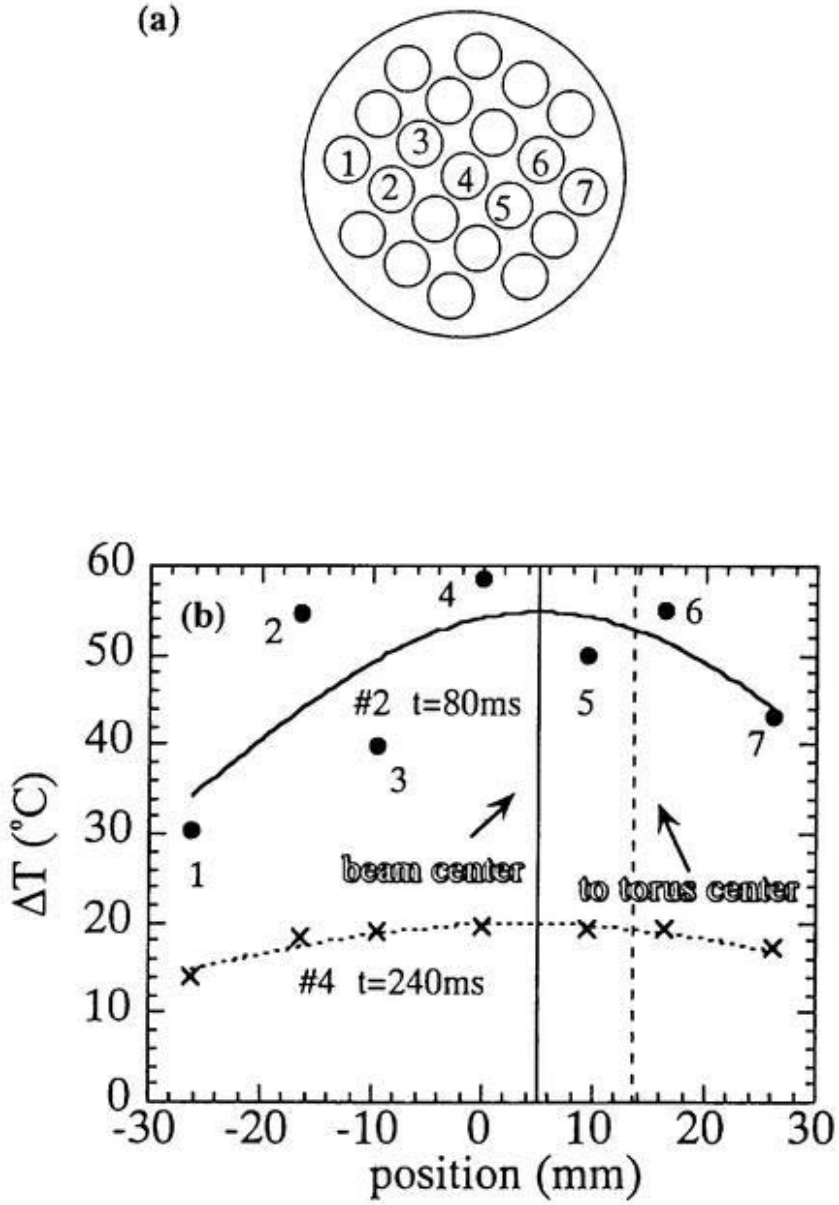

Fig. 3.13 (a) Mesured position
(b) Center of beam profile given by ΔT profile

Chapter 4

Performance of Polarization Sensitive Spectroscopy

4.1 Performance of DigDagCCD

4.1.1 Design of DigDagCCD

In order to get rid of the offset due to the difference of the transmission of each optical fiber, the polarization sensitive spectroscopy should have only one polarizer to measure two polarization components perpendicular to each other. In general, the charge ofthe CCD should be read out after exposing one polarization component before it exposes the next polarization component. The time response of the FLC is faster than the time for the readout (frame rate) of the CCD. Therefore, the new CCD, in which the charge of the CCD is shifted up and down as being synchronized with the FLC modulation has been developed. This CCD is called Dig Dag CCD. By using the Dig Dag CCD and the modulated FLC, the two polarization components perpendicular to each other can be detected in two strips nearby with one optical fiber.

The CCD control system has the function for the on-charge binning. The binning of the CCD pixel should correspond to the optical fiber. The open circle in Figure 4.1 shows the optical fiber, and the closed circle shows the dummy fiber. The dummy fiber gives the space for the Dig Dag CCD. And the upper strips are exposed to 0 or 90 degrees polarization components, and the under strip are exposed to 45 or -45 degrees polarization ones. Besides the horizontal pixels of the CCD are in the wavelength. When +5V (-5V) is applied to the FLC, the light with 0 or -45 degrees polarization components is focused onto stripe A (stripe B) as shown in Figure 4.1. By synchronizing the pixel shift with the FLC modulation,

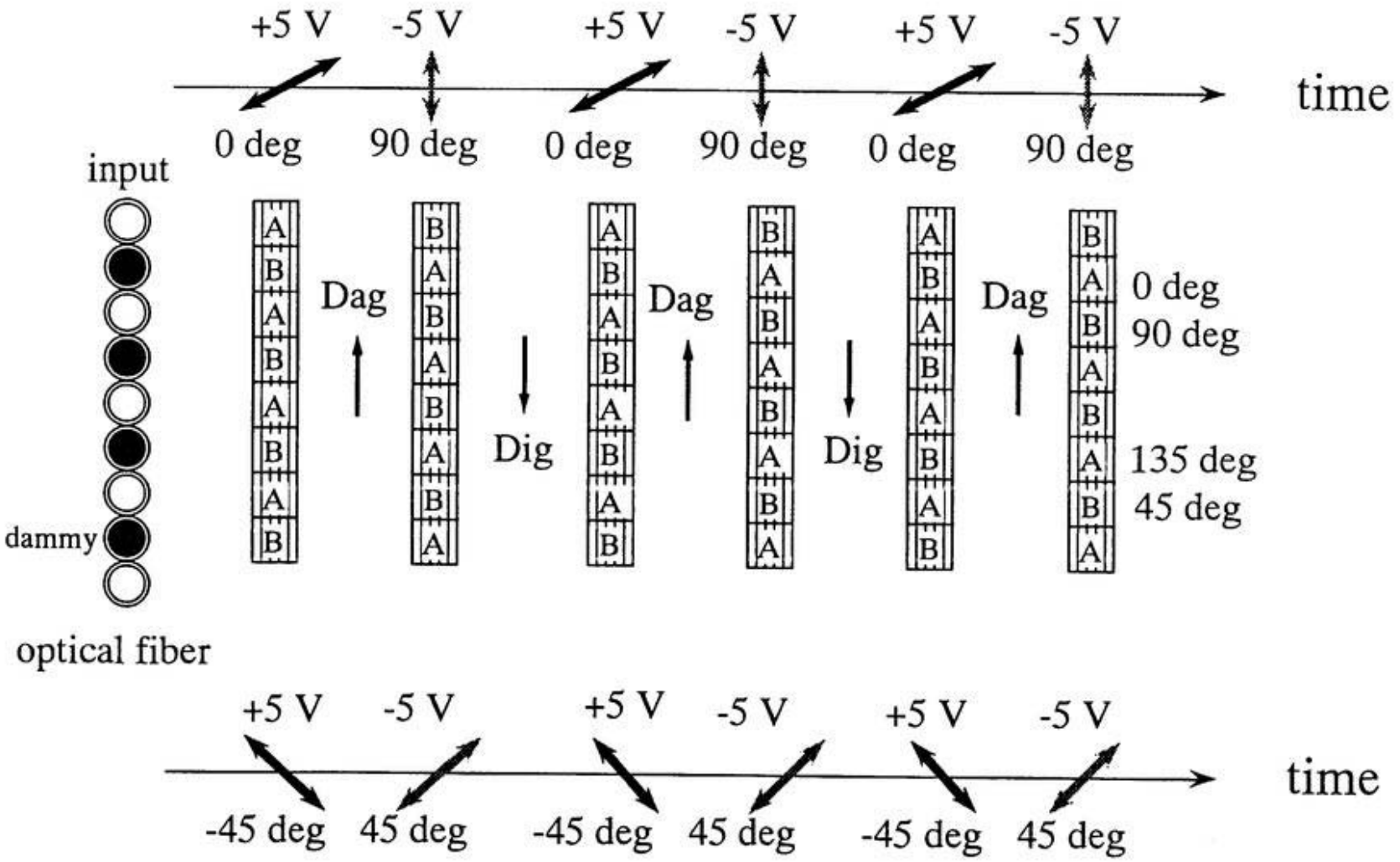

Fig. 4.1 Pixel of CCD is shifted up and down (Dig Dag) when the CCD is applied 5 V and 0 V. Syncronized with the FLC modulation, the charge of each CCD pixel can be shifted.

stripe A accumulates the light with 0 or -45 degrees polarizers, while stripe B accumulates the light with 90 or 45 degrees polarizers.

4.1.2 Estimation of Performance for DigDagCCD

Because the beam diameter is designed to be only 6 cm (the diameter of the heating beam is ~20 cm) for achieving good spatial resolution, the beam current of DNB is one order of magnitude smaller than that of the heating neutral beam. The S/N of the MSE spectra radiated from the DNB is not as good as that from the heating beam like in other experiments[9]. There are several sources of the noise in the system, such as the dark charge, the readout noise, the smear, and the photon noise which are explained later. The dark charge is the electron accumulated from the CCD without exposing, while the readout noise is the amplifier noise of the CCD controller. The smear is the exposure for the CCD during Dig Dag operation. In this section, the dark charge, the read out noise, and the smear of the CCD are evaluated.

Because the dark charge of the CCD arrays decreases significantly (roughly 1/4 every 10 degrees) by lowering the temperature, the dark charge is measured at various temperatures of the cooled CCD.

Figure 4.2(a) shows the intensity as a function of the exposure time for various temperatures of the cooled CCD, when there is no light on the CCD. The dark charge of the CCD is evaluated from the slope, because it is proportional to the exposure time. As shown in Figure 4.2(b), the dark charge is proportional to the binning number. Therefore, the dark charge is defined as the number charge per second and per pixel. Figure 4.2(c) shows the result of the dark charge as a function of the cooled temperature. The dark charge decreases from 5601 electron/pixel/sec to 43 electron/pixel/sec by lowering the temperature of the CCD

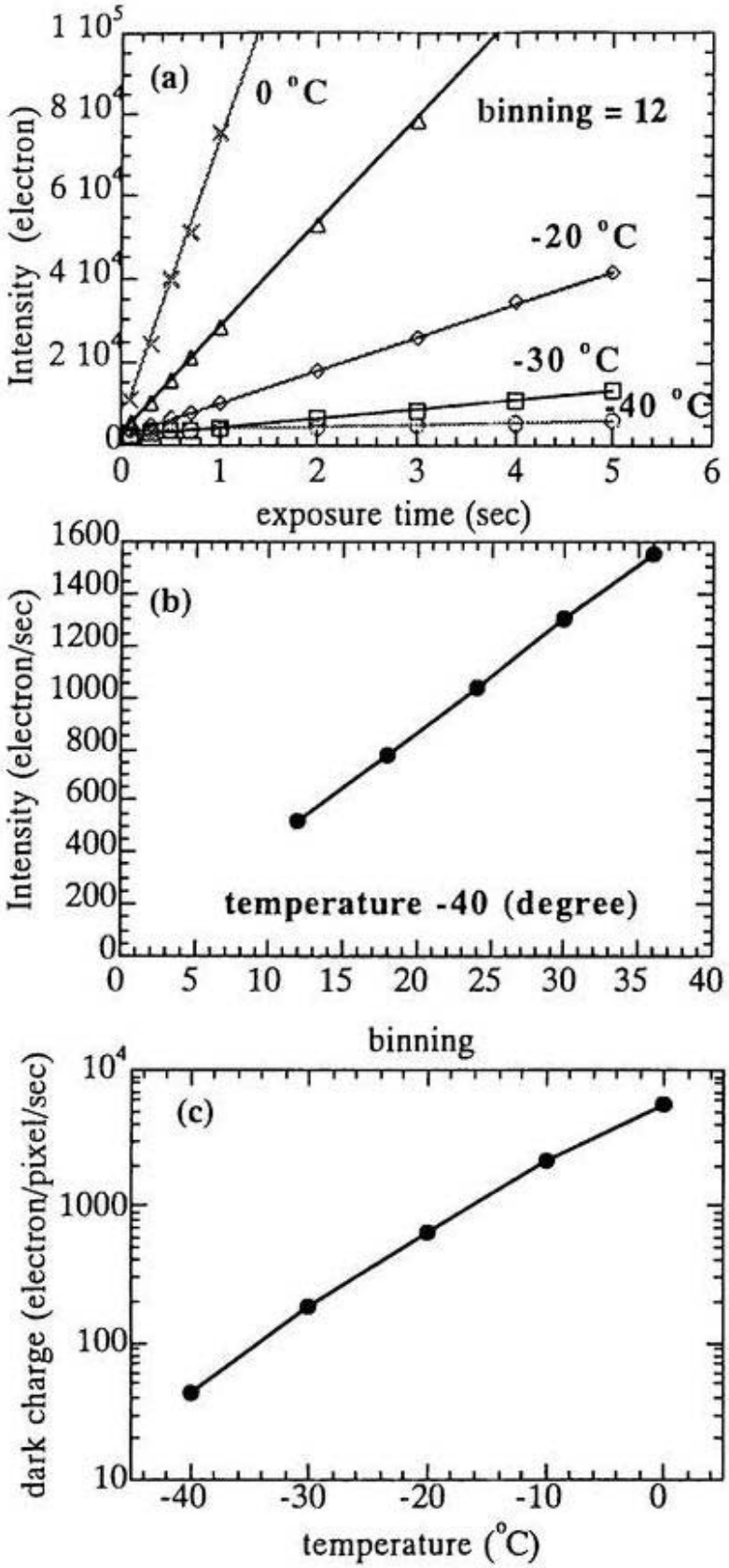

Fig. 4.2 (a) Intensity as a function of the exposure time for various temperature cooled the CCD (b) Intensity as a function of the binning (c) Dark charge of the CCD as a function of the temperature

from 0 to -40 degrees (normal operation). Because the CCD pixels are binned by 12 pixels that one stripe can correspond to one input optical fiber, the noise level in the MSE measurement is 516 electron/sec (12 binnig). When the exposure time is 100 ms, the dark charge becomes 51.6 electron : about 0.01% of the dynamic range which is 551200 electron (65000 count). The peak intensity of the measured MSE spectra is about 300 electron, and the signal to the noise ratio in the measurement is about 17%.

There are two amplifier "fast" and "slow" in the CCD controller depending on the A/D converter rate. The "fast" amplifier is used for the A/D rate of 430 kHz, while the "slow" one is used for the A/D rate from 50 to 150 kHz. The readout noise is evaluated by the root mean square (RMS) of the noise in the intensity at zero exposure time, while the dark charge is evaluated from the intensity itself.

The RMS noise for various A/D rates is evaluated. Figure 4.3(a) shows the noise as a function of the exposure time for various A/D converters rates for the CCD which is cooled to -40 degrees. The readout noise is defined as the y-intercept in Figure 4.3(a). The increase of the noise for the longer exposure time is due to the deviation from the dark charge itself, not from the increase of the readout noise. Figure 4.3(b) shows the readout noise as a function of the binnig number. The readout noise depends on the binning number a little. Then, the relationship between the readout noise and the A/D converter rate is evaluated. Figure 4.3(c) shows the readout noise as a function of the A/D converter rate, which has the "slow" amplifier used for the 100 kHz and the 150 kHz A/D converters, and the "fast" amplifier for the 430 kHz A/D converter. This readout noise depends on the "fast" or the "slow" amplifier, not on the A/D rate directly. The readout noise for the "fast" A/D converter is 35 electron, while the readout noise for the "slow" A/D converter is 20 electron. The readout noise for the "fast"

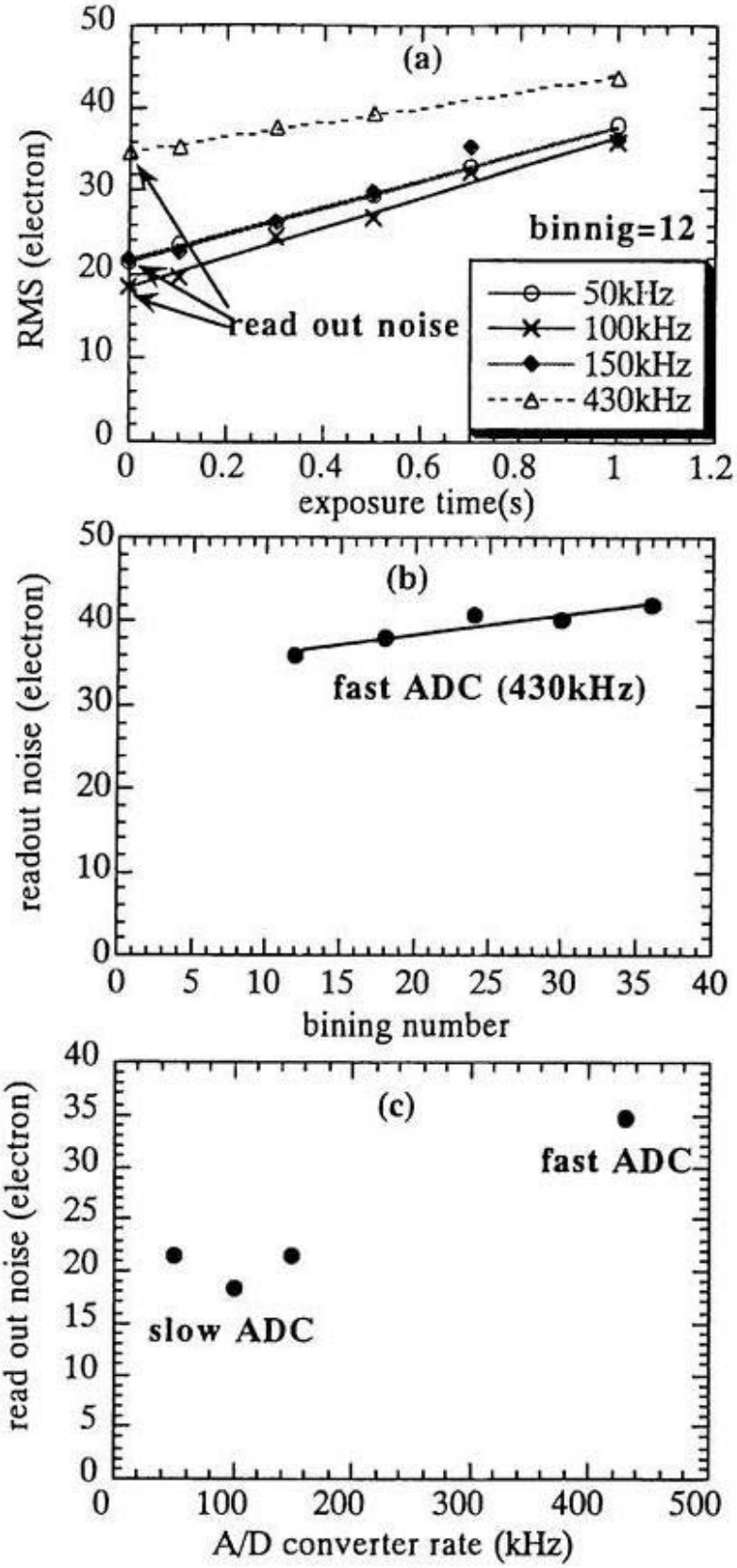

Fig. 4.3 (a) RMS as a function of the exposure time for A/D converter rate. (b) Readout noise as a function of the binning (c) read out noise of the slow and fast ADC

is about 11% to the peak intensity (300 electron) of the MSE spectra for the one-third energy component, while the readout noise for the "slow" A/D converter is only 6% to the peak intensity of the MSE spectra.

When the CCD pixels are shifted up and down, there is the finite time of the exposure on the CCD while shifting, because the shutter of the CCD is kept open. This is called "smear". This smear depends on the exposure time. Therefore, the smear is measured with the various exposure times, then the shift speed is evaluated.

Figure 4.4(a) shows the intensity of the each stripe with the shift lines (N_s) of 120 (10 strips with 12 binnigs) and Δt=20 (msec). I_1 is the intensity due to the exposure during the shift, and I_2 is the average of the Dig and the Dag peak intensities. The smear is given by

$$\text{smear} = \frac{I_1}{I_1 + I_2} = \frac{\Delta t_1}{\Delta t_0 + \Delta t_1} = \frac{N_s \Delta t_s}{\Delta t_0 + N_s \Delta t_s}, \qquad (4\text{-}1)$$

where Δt_0 shows time when the pixels remain stationary, while Δt_1 shows the time the pixels shift. Figure 4.4(b) shows the measured smear as a function of $\Delta t/N_s$. When the smear becomes one, the time for exposing (Δt_0=0), then $\Delta t = N_s \Delta t_s$. The Δt_s is evaluated to be three μsec from Figure 4.4(b). For example, the smear is 0.7% when the FLC modulation is 50 Hz and the N_s is twenty four.

4.1.3 MSE spectra by using DigDag Scheme on CCD

The MSE spectra is measured by using the Dig Dag CCD. Figure 4.5 shows the spectra of the σ and the π components of the H_α spectrum at the major radius of 92.9 cm and 100.7 cm with the motional Stark effect measured by synchronizing

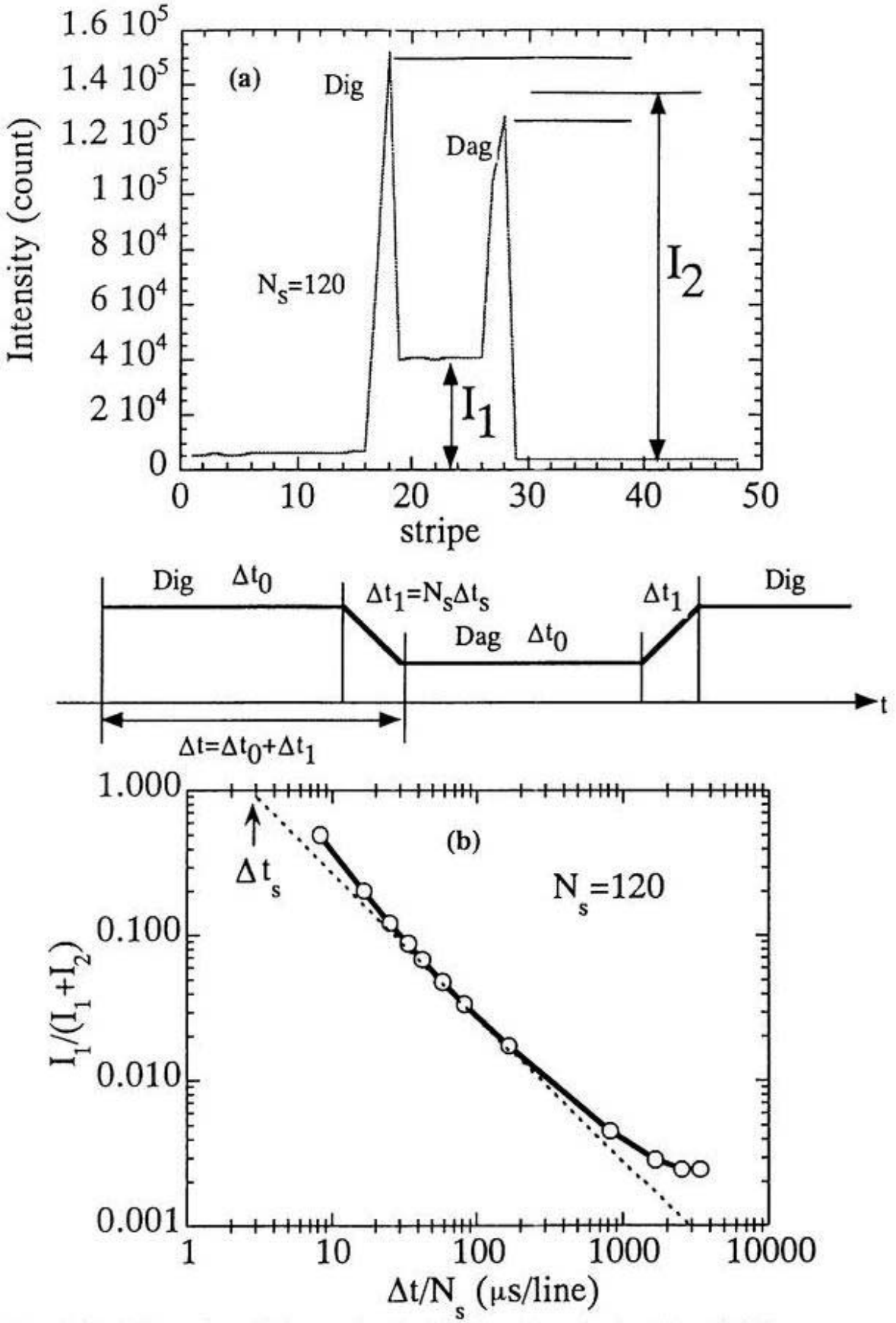

Fig. 4.4 (a) Intesity of the each pixel when the pixel of the CCD is shifted Dig Dag. (b) Smear estimated for various modulation of the Dig Dag scheme.

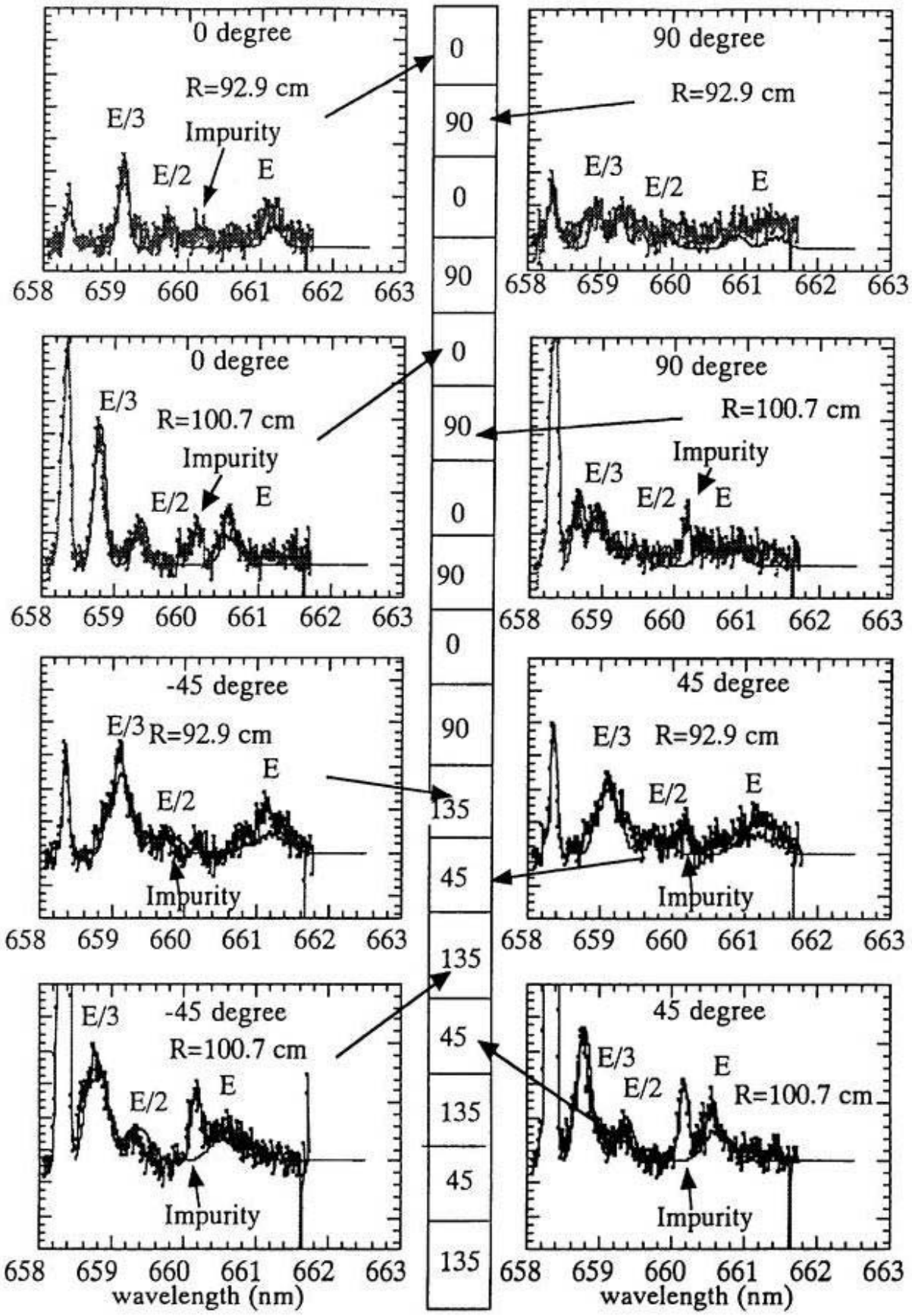

Fig. 4.5 MSE spectra measured by using Dig Dag sheme

the Dig Dag operation with the modulation of the two FLC. The three peaks of spectra correspond to the emission from the atomic hydrogen beam with the full energy, the half energy, and the one-third energy beam components. The solid line is the MSE spectra calculated from the vacuum magnetic field line. The acceleration voltage is 45 kV and the beam current is 3 A. The ratio of the injected neutral beam density are represented as n(E) : n(E/2) : n(E/3), the calculated $I(0,\lambda)$ and $I(-45,\lambda)$ adjusted to get the best fit to the measured $I(0,\lambda)$ and $I(-45,\lambda)$, respectively. The spectra through 0 degree polarizer represent the σ component of the H_α spectrum, and the spectra through the 90 degrees polarizer represent the π components of the H_α spectrum. The spectra through 45 and -45 degrees polarizers represent the spectra mixture of the σ and the π components, and they are sensitive to the pitch angle. At the magnetic axis (R=92.9 cm), the spectra for -45 degrees should be identical to that of 45 degrees. The discrepancy between the calculated MSE spectra and the measured MSE spectra, as seen in the R=92.9 cm, -45 degrees of Figure 4.5, is due to the offset angle of the retardance and the optical axis of the FLC. The lines observed at 658.3 nm and 660.1 nm show the impurity lines of C II and Ti I, respectively. Because the noise in the MSE spectra is mainly due to the photon noise of emission, the shot of plasma discharge must be accumulated for evaluating the pitch angle of the local magnetic field line.

4.2 Performance of Ferroelectric Liquid Crystal

The FLC has a function that the half-wave plate with 180 degrees retardance can be used in two switchable states electrically. The FLC is composed of a thin layer (< 2 μm) of the ferroelectric liquid crystal material sandwiches between two glass plates. The optical axis of the FLC has two proper orientations which are separated from each other by approximately 45 degrees. However, the retardance

of the FLC varies with temperature. The retardance of the FLC at the temperature in the experimental room should be evaluated.

As shown in Figure 4.6(a), the ellipticity of circularly polarized light through the FLC is measured to evaluate the retardance. The retardance, δ, of the FLC is derived from using the two measured intensities express I_{-45} and I_{45} or I_0 and I_{90} as

$$\frac{I_{45}(I_0)}{I_{-45}(I_{90})} = \frac{1+\cos(\delta+90)}{1-\cos(\delta+90)}. \qquad (4\text{-}2)$$

The measured intensity rations are I_{45}/I_{-45} = 0.69 and I_0/I_{90} = 0.75. The retardances are $\delta_{-45,45}$ = 190.6 and $\delta_{0,90}$ = 188.2 degrees. Figure 4.6 illustrates a theoretical plot of the retardance with respect to temperature.

This FLC is optimized at the temperature of 35 degrees : the retardance of the FLC becomes 180 degrees. Therefore, the retardance of FLC at the temperature in the experimental room, in which temperature is 23 degrees, is about 190 degrees. The measured retardance almost agree with this theoretical curve.

The rotating angle of the optical axis of the FLC layer is evaluated by measuring the polarization angle of linearly polarized light through FLC as seen in Figure 4.7(a) when -5 V or +5 V are applied to the FLC. The intensity of light after FLC is given by

$$I = E_x^2 + \acute{E}_y^2 = \sin^2(\omega+\phi) + \sin^2(\omega+\phi+\delta). \qquad (4\text{-}3)$$

Where δ is the retardance and ϕ is the rotating angle of FLC with the voltage of +5 V respect to the optical axis of FLC with the voltage of -5 V.

Figure 4.7(b) shows the intensity as a function of the polarization angle of input light. The offset angle, $\Delta\theta_{-45,45}$, of the FLC is 8.2 degrees. This offset angle arise from the retardance offset and the rotating angle offset. As seen in

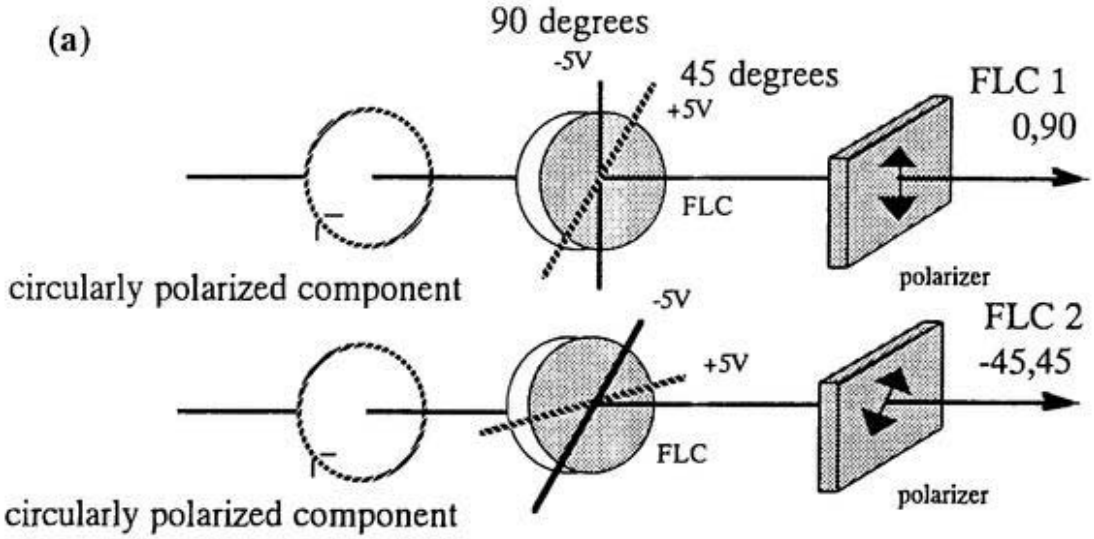

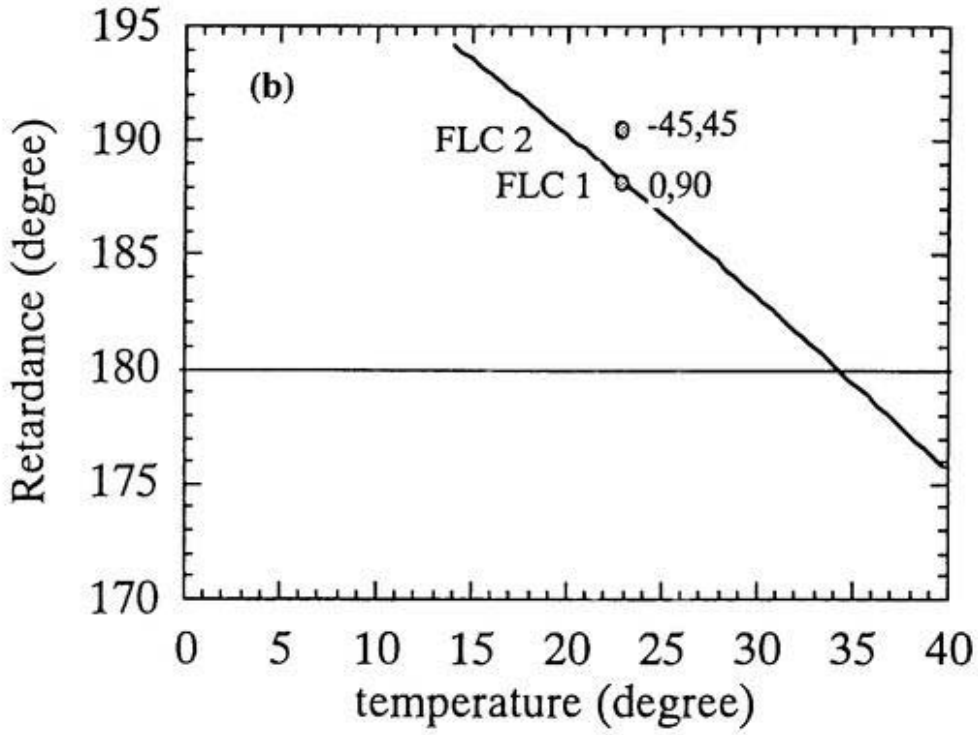

Fig. 4.6 (a) Measurement of the intensity of the final transmitted light. (b) Retardance as a fuction of temperature

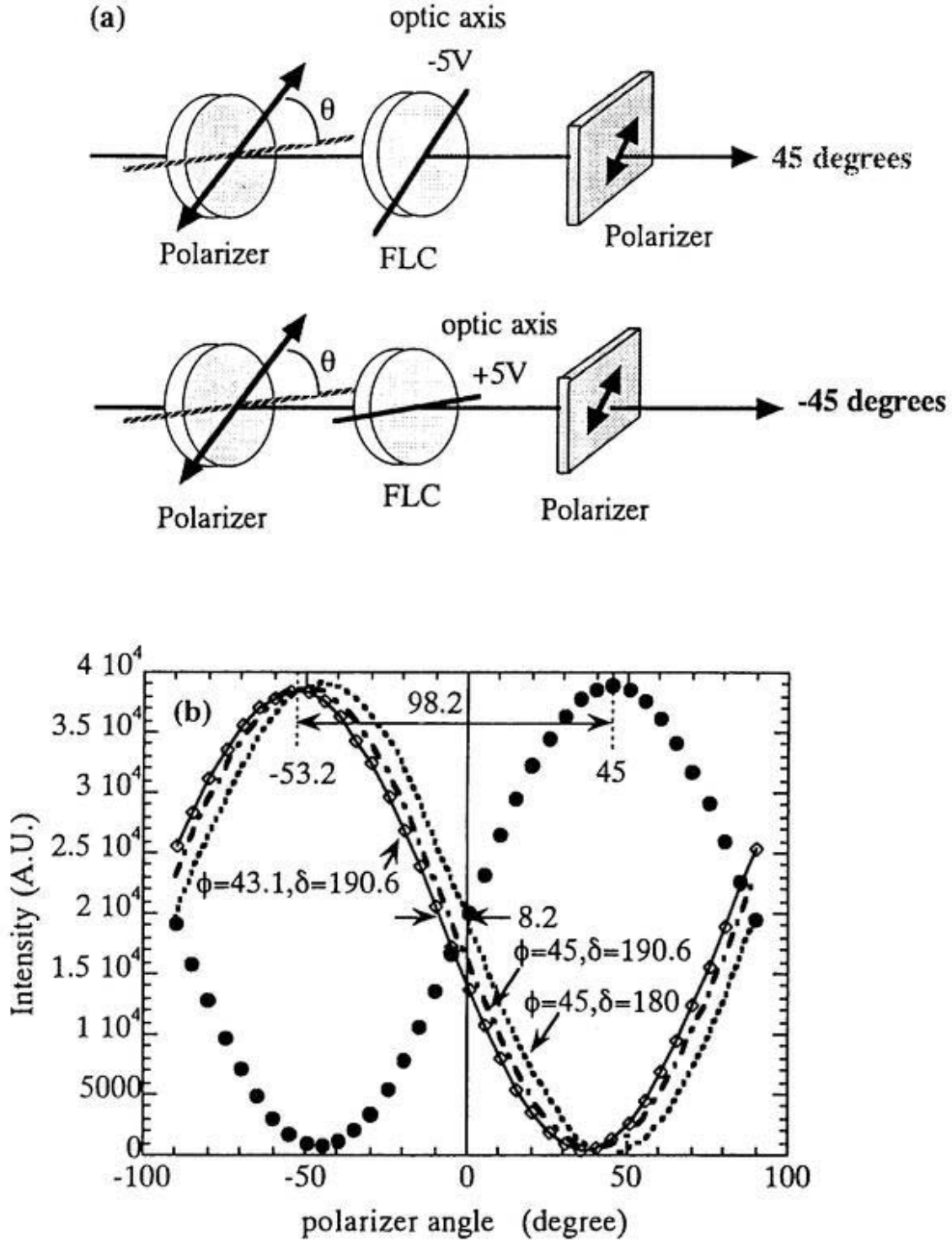

Fig. 4.7 (a) Measurement of the intensity of the final transmitted light. (b) Intensity as a function of angle oriented transmission axis

Figure 4.7(b), the intensity with the retardance of 190.6 degrees doesn't agree with the experimental point. The best fit of the curve to the experimental data gives the rotating angle ϕ= 43.1 (degrees) with δ=190.6 (degrees).

The offset of the retardance and the rotating optical axis cause the offset in the measured polarization angle. The polarization angle α_σ is given by

$$\tan(2\alpha_\sigma) = \frac{I(-45,\lambda) - I(45,\lambda)}{I(90,\lambda) - I(0,\lambda)}. \qquad (4\text{-}4)$$

This formula (4-4) is only valid when the polarizer angle is exactly 0, 90, +45, and -45 degrees. When there are offsets of angle, $\Delta\theta_{-45,45}$, or, $\Delta\theta_{0,90}$, in the -45/45 FLC or 0/90 FLC, respectively, the formula (4-4) gives the only apparent polarization angle, α_σ', and the offset angle, $\Delta\alpha$, too. This offset angle in the measurement can be calculated as

$$\Delta\alpha_\sigma = \alpha_\sigma' - \alpha_\sigma$$
$$= \frac{1}{2}\tan^{-1}\left\{\frac{I(-45+\Delta\theta_{-45,45},\lambda) - I(45,\lambda)}{I(90,\lambda) - I(0+\Delta\theta_{0,90},\lambda)}\right\} - \frac{1}{2}\tan^{-1}\left\{\frac{I(-45,\lambda) - I(45,\lambda)}{I(90,\lambda) - I(0,\lambda)}\right\}. \qquad (4\text{-}5)$$

Alternatively, the offset angle, $\Delta\alpha_\sigma$ derived from the measured intensities by Equation (4-4). Figure 4.8(a) shows the measured polarization angle after the FLC as a function of the polarization angle of incident light using Formula (4-4). If there is no offset, the data should be on the straight line as indicated in Figure 4.8(a). Figure 4.8(b) shows the measured offset angle and the offset angle calculated by Equation (4-5) from the measured $\Delta\theta_{0,90}$ and $\Delta\theta_{-45,45}$, discussed before. The calculated offset angle by Equation (4-5) agrees with the measured

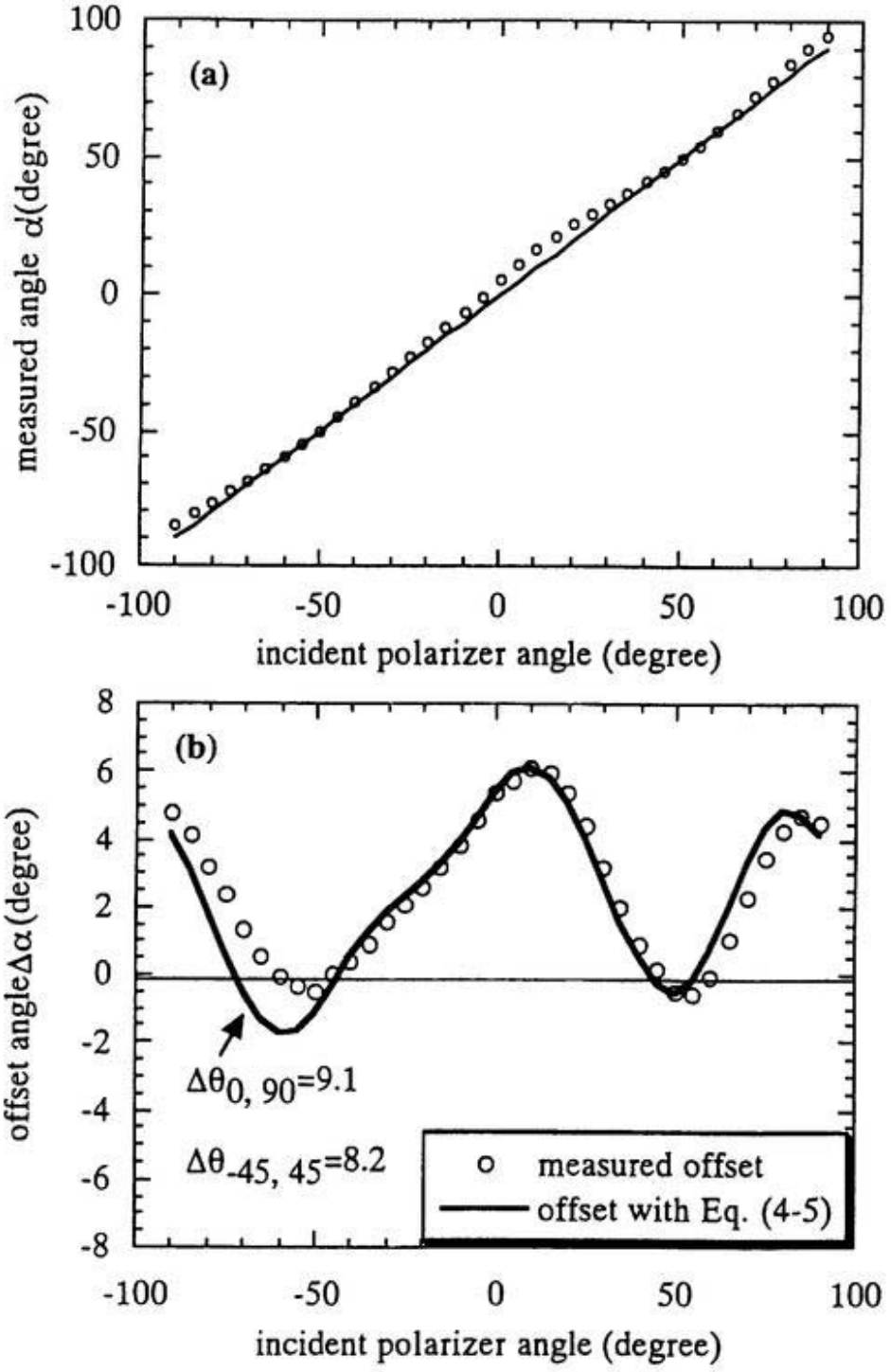

Fig. 4.8 (a) Measureing angle as a function of an angle oriented transmission axis (b) Comparison between the angle with Equation (4-5) and the measured offset angle

offset angle between -40 and 40 degrees. The measured offset angle is well explained by the offset of the retardance (δ=190) and the rotating optical axis angle (ϕ=43). These measured offsets are taken into account in the measurement of the polarization angle derived from formula (4-4).

In order to check the time response of FLC, the FLC is used as the shutter. A pair of polarizer whose transmission axis is parallel is arranged in front of and behind the FLC, as shown in Figure 4.9(a). When -5 V is applied to the FLC, the optic axis of the FLC layer becomes parallel to the transmission axis of the first polarizer. Light passes through the FLC layer without any change : the shutter remains open.

When +5 V applied to the FLC, the optic axis of the FLC layer is oriented at about 45 degrees angle with respect to the transmission axis of the first polarizer. After passing through the FLC layer, the orientation of the polarization axis of the transmitted light will be rotated by the half-wave retardance of the cell, and the rotated angle is nearly 90 degrees : the shutter remains closed. The intensity of transmission light was measured by the photomalutplier for the FLC modulation of 2 kHz, as shown in Figure 4.9(b). The delay time is about 50 μsec and the rise time to open is about 75 μsec, so the time response of the FLC is less than 130 μsec. The response time is only 1.3% of the flat top when the FLC is modulated with the FLC modulation of 50 Hz.

The offset angle depends on the magnetic field in the PEM strongly due to Faraday rotation effect. For example, the offset angle is about -12 degrees when the magnetic field is 1.8 T on DIII-D. However, there may be little offset angle due to Faraday rotation effect, because a thin layer of the ferroelectric liquid crystal material inside the FLC is < 2 μm.

Figure 4.10(a) shows the polarization angle for each optical fiber when the

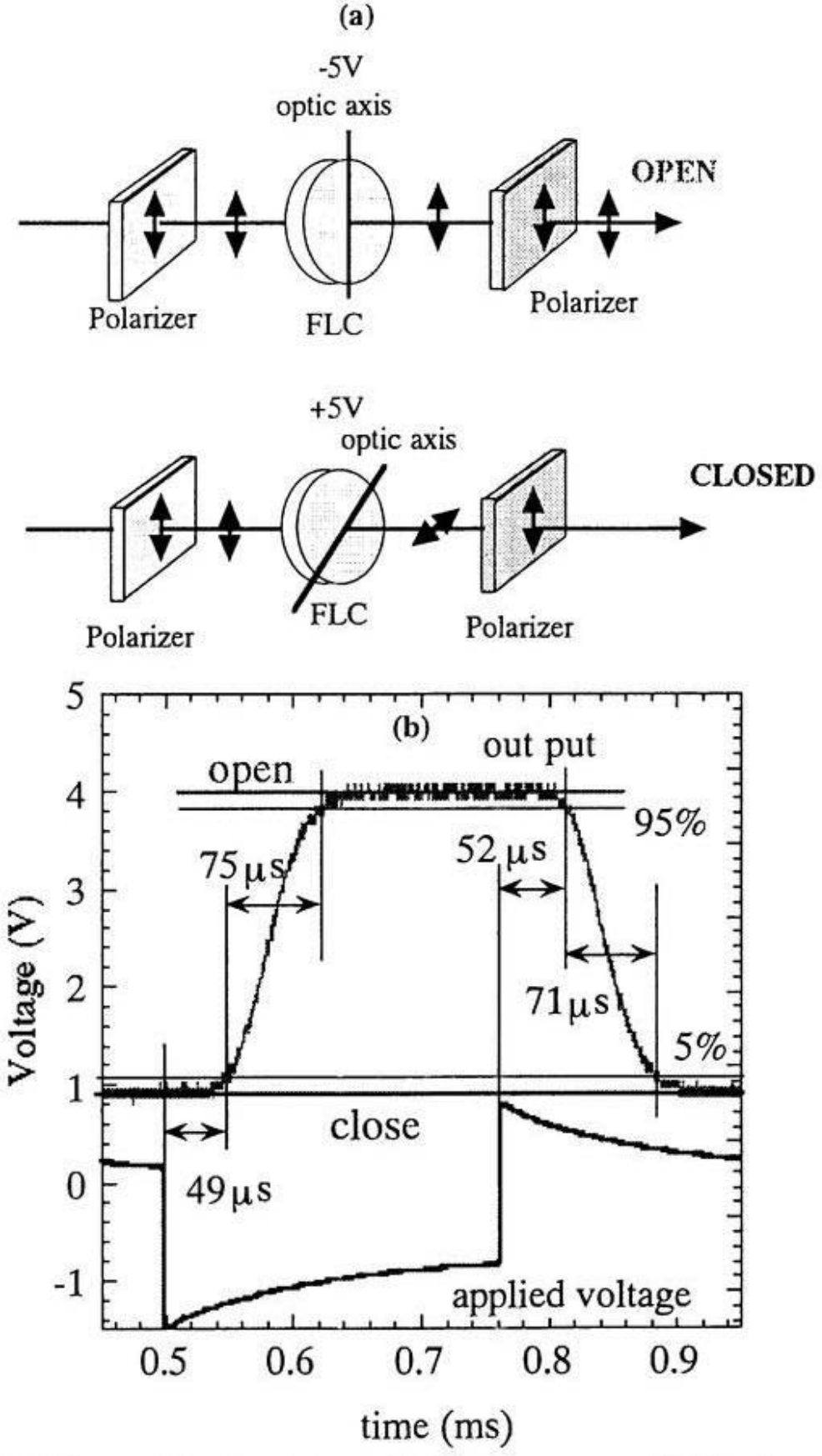

Fig. 4.9 (a) FLC is used for the shutter. (b) Time responce of FLCcell.

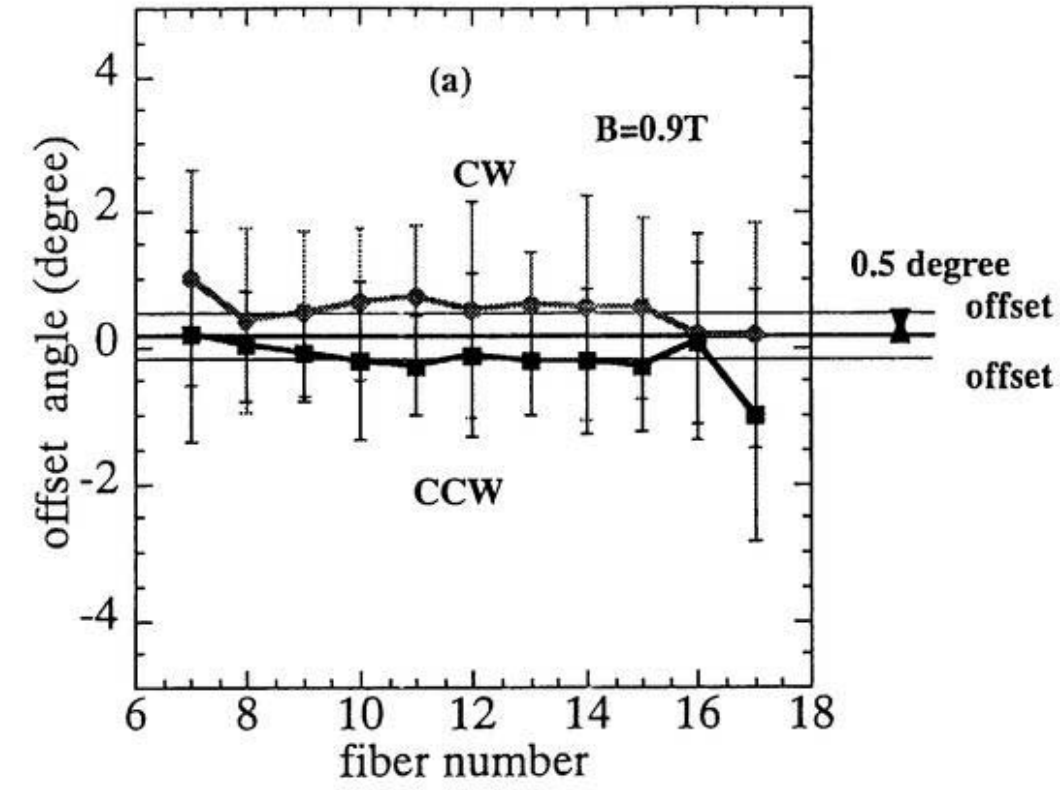

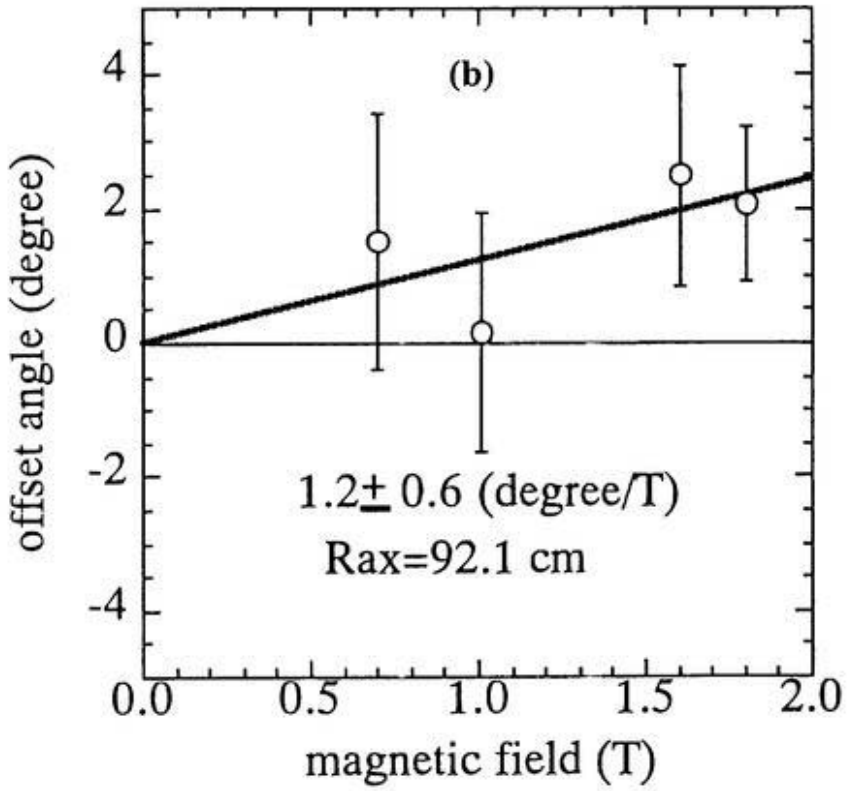

Fig. 4.10 (a) Offset angle owing to magnetic field at magnetic axis of 94.9 cm (b) Offset angle as a function of the magnetic field

magnetic axis and the magnetic field strength are 92.1 cm and 0.9 T, respectively. The averaged offset angle due to the magnetic field is 0.5 ± 1 degrees. Figure 4.10(b) shows that the offset angle depends on the magnetic field strength with the magnetic axis of 92.1 cm, and it is only 1.2 ± 0.6 degree/T. The small offset due to the magnetic field is considered to be a big advantage in the MSE measurement, because it is not necessary to calibrate the offset angle by injecting the neutral beam into the gas target under the magnetic field in our system.

4.3 Spectrometer

The dispersion of the spectrometer used for the MSE measurement is evaluated. The diffraction is given by

$$d(\sin\alpha + \sin\theta) = \lambda , \qquad (4\text{-}5)$$

where α is the incident angle, θ is the angle of diffraction, $\theta - \alpha = 2\gamma$ as shown in Figure 4.11(a), d is the space of grating, and λ is the wavelength.

The dispersion of the spectrometer is given by

$$\frac{\Delta\lambda}{\Delta x} = \frac{d\cos\theta}{f} = \left\{ \sqrt{\left((d\cos(\gamma))^2 - \left(\frac{\lambda}{2}\right)^2 \right)} - \frac{\lambda}{2} \times \tan(\gamma) \right\} / f \qquad (4\text{-}6)$$

where x is the detector and f is the focus length.

The grating is 2160 lines/mm ($d = 1/2160 \times 10^{-6}$ nm^{-1}) and the focal length of the spectrometer is 0.5 m. Figure 4.11(b) shows the dispersion which is evaluated from the doublet lines of H_g summarized in Table I. The solid line is the dispersion curve given by Formula(4-6). This data gives the angle, γ, of 13.5 degrees and the focal length, f, of 498 mm. The evaluated dispersion at the wavelength of H_α is 0.46 (nm/mm).

(a)

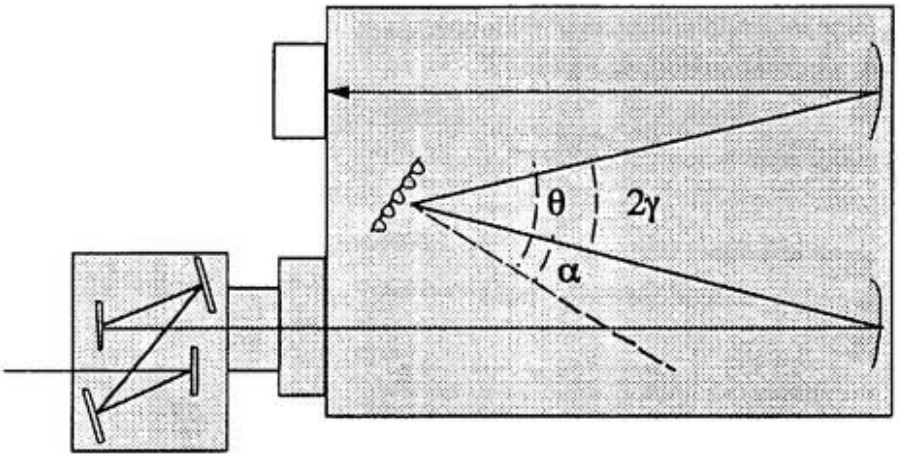

Spectrometer

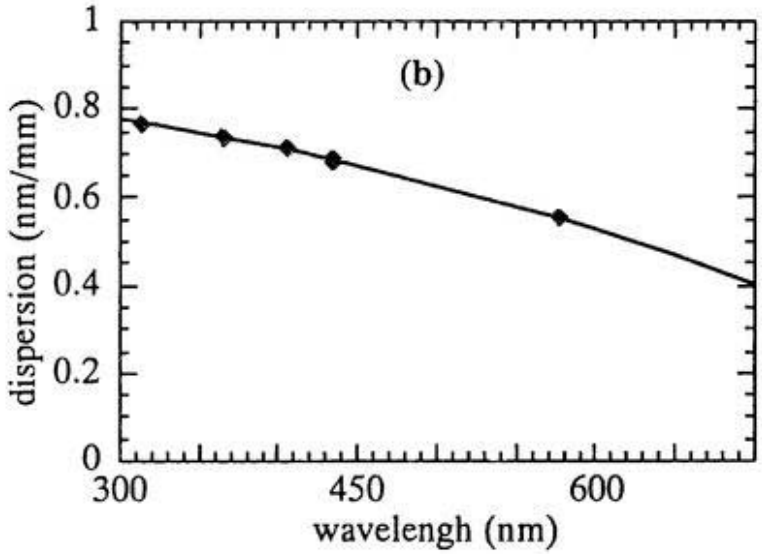

Fig. 4.11 (a) Spectrometer
(b) Dispersion of spectrometer

Table 1 wavelength of Hg

	wavelength (nm)	wavelength (nm)	middle (nm)	pixel (stripe=25)	pixel (stripe=25)	(nm/pixel)	(nm/mm)
0	296.7283	302.1500	299.4391	24.000	339.00	0.017212	0.78235
1	312.5670	313.1551	312.8610	159.00	194.00	0.016803	0.76377
2	365.0157	365.4839	365.2498	155.00	184.00	0.016146	0.73390
3	404.6572	407.7838	406.2205	100.00	300.00	0.015633	0.71059
4	433.9224	434.7496	434.3360	147.00	202.00	0.015040	0.68362
5	434.7496	435.8377	435.2936	202.00	274.00	0.015113	0.68693
6	576.9598	579.0663	578.0131	107.00	280.00	0.012176	0.55345

The distortion of spectrometer is given by

$$X = \frac{\tan\theta\cos\gamma}{f} Z^2. \qquad (4\text{-}7)$$

Figure 4.12(a) shows the distortion measured at H_g : 671.6 nm and the calculated distortion for H_g : 671.6 nm (θ=61.75 degrees) and H_α : 656.28 nm (θ=60.27 degrees).

Full width of half maximum (FWHM) of the spectra is measured at H_g : 671.6 nm. As shown in Figure 4.12(b), the measured FWHM is 0.076 nm with the equivalent H_g : 671.6 nm and slit width of 106 μm (fiber diameter).

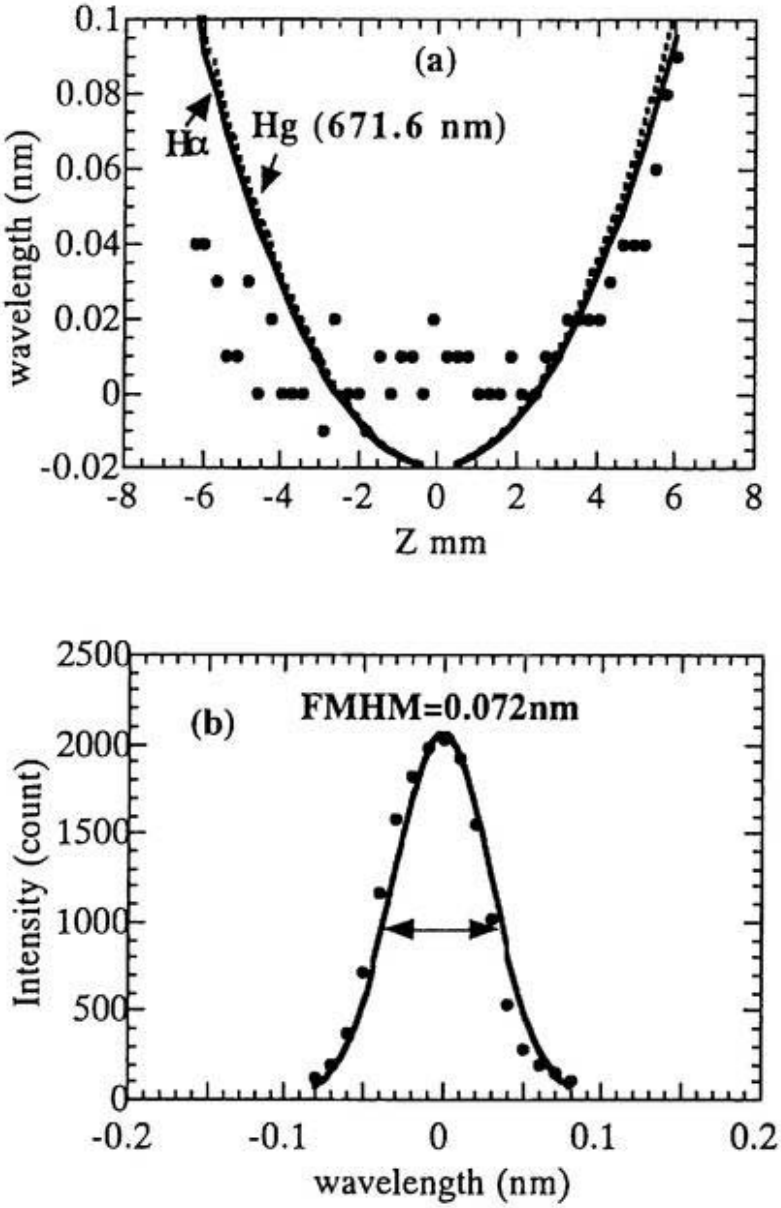

Fig. 4.12 (a) Aberration of spectrometer
(b) FMHM of spectrometer

Chapter 5

Experimental Results of MSE Spectroscopy

5.1 Measurements of MSE Spectra

The radial profile of the pitch angle of the local magnetic field line is measured for CHS plasma with the magnetic field of 0.88 T and the magnetic axis of 92.1 cm. As shown in Figure 5.1, the ECH with 53 GHz injected from 12 msec to 32 msec to produce the target plasma, and the NBI is injected from 30 msec to 130 msec to sustain the plasma. The line averaged density measured with FIR interferometer is increasing after the neutral beam is injected, and reaches the study state value. The averaged electron density and the beta value are 3×10^{13} cm^{-3} and 0.4 %, respectively. The DNB is injected to the plasma at the steady state phase from 60 msec to 120 msec. The radiation increases to 300 kW and reaches 300 kW at 110 msec. As seen in magnetic probe signal, there is no significant MHD activity observed.

Figure 5.2, 5.3, and 5.4 show the measured MSE spectra at the major radius of 93, 110, and 78 cm. At R=93 cm, the Doppler shift is 5.2 nm for the full energy component, and it is 3 nm for the one-third energy component. The motional Stark splitting for the full energy component and the one-third energy component are 0.5 nm and 0.3 nm, respectively. At R=110 cm, the Doppler shift becomes smaller to be 4.5 nm, while the Doppler shift becomes larger (5.5 nm) at R=78 cm.

Figure 5.2 shows the comparison of the measured four spectra (with 0, 90, 45, and -45 degrees polarizer angle) for the full energy, the half energy, and the one-third energy beam components at the major radius of 93 cm with the calculated ones with the vacuum magnetic field, where the pitch angle of the local magnet field line is almost zero. The intensity ratio I(E), I(E/2), and I(E/3) in the calculated spectra for $I(0,\lambda)$, $I(90,\lambda)$ and $I(45,\lambda)$, $I(-45,\lambda)$ are normalized to fit the

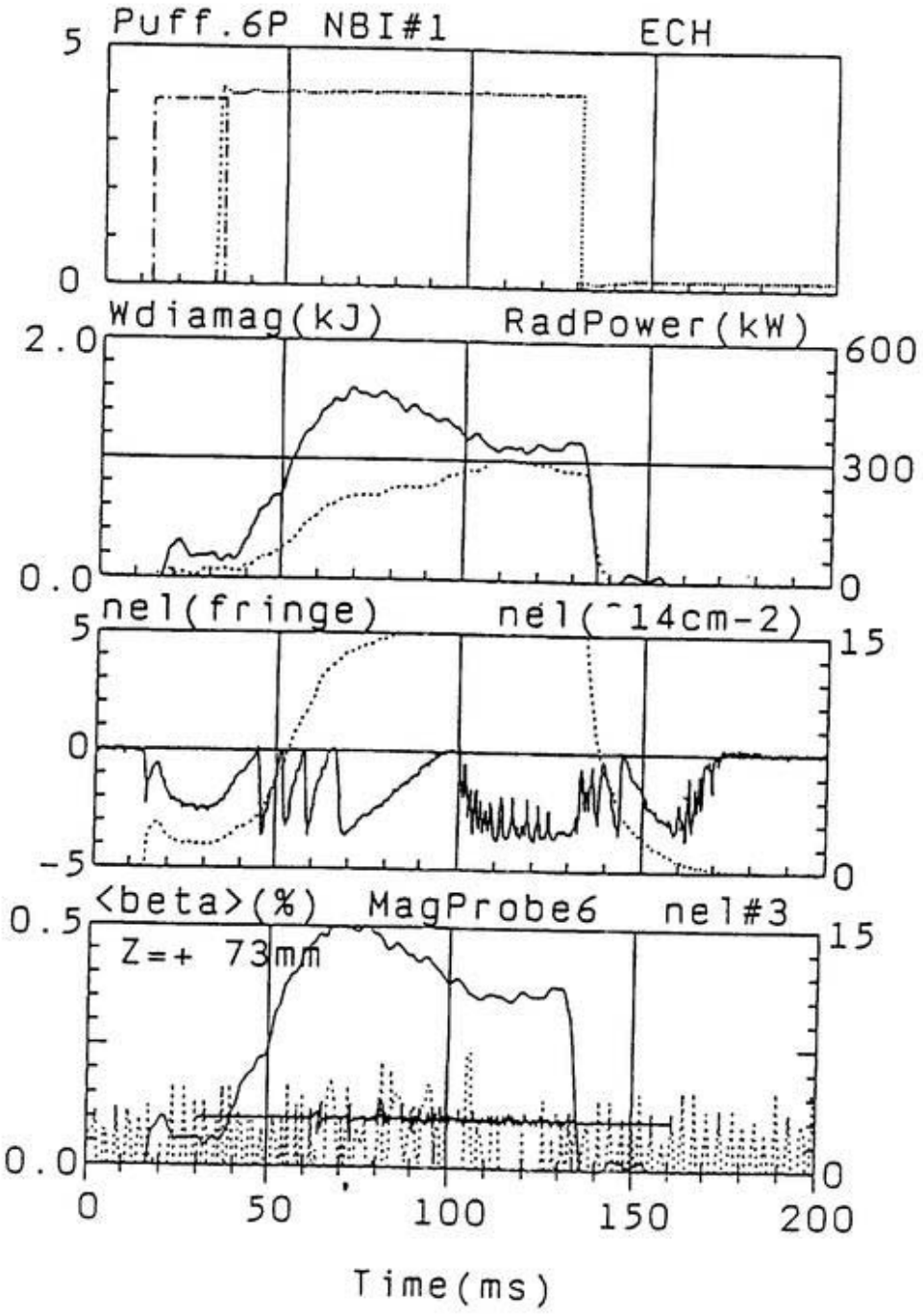

Fig. 5.1 Time evolution of radiation , density and beta

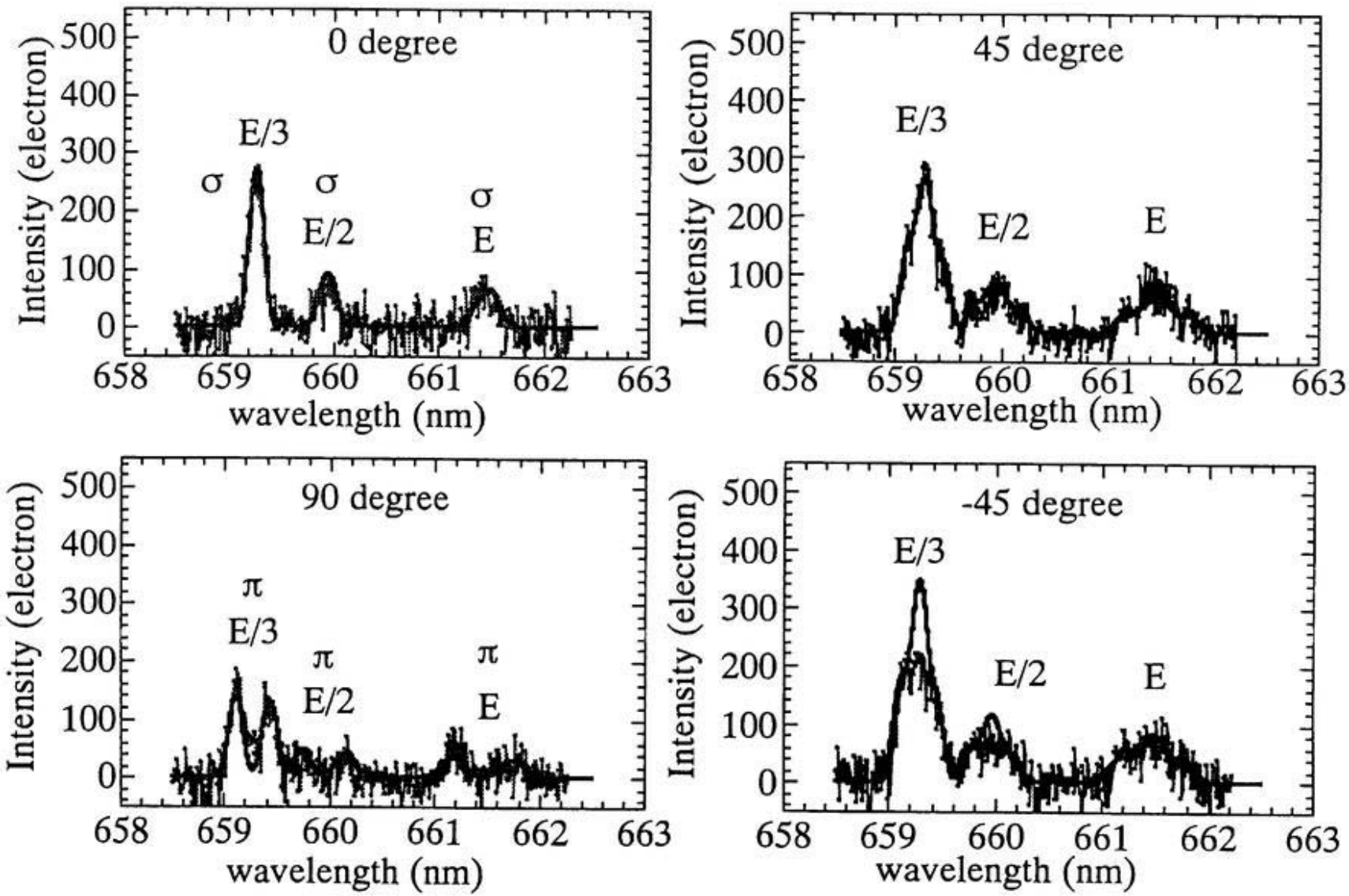

Fig. 5.2 Comparsion of the measured and calculated MSE spectra with 0 degree, 90 degrees, 45 degrees, 135 degrees at the major radius of 93 cm.

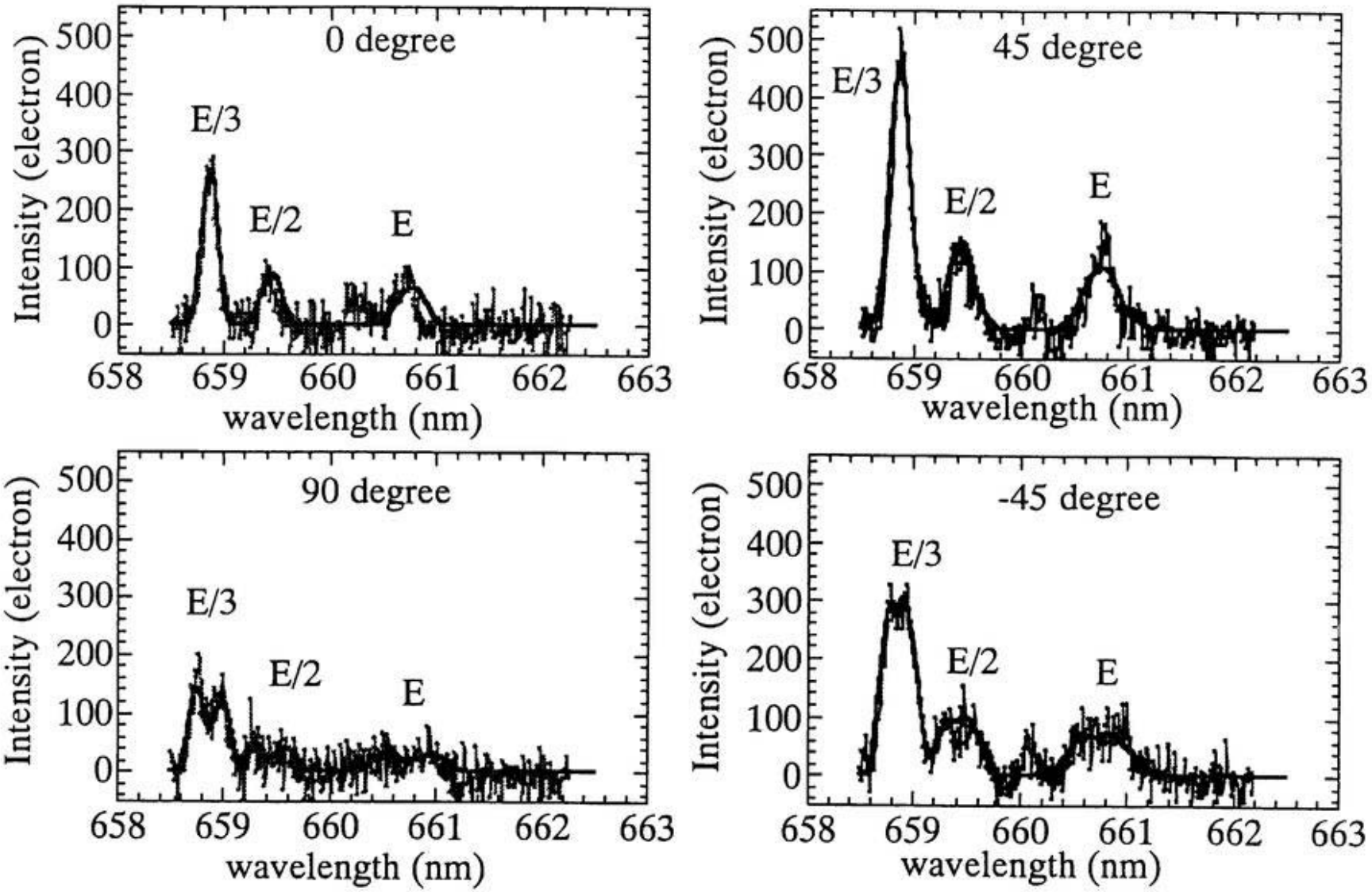

Fig. 5.3 Comparsion of the measured and calculated MSE spectra with 0 degree, 90 degrees, 45 degrees, 135 degrees at the major radius of 110 cm.

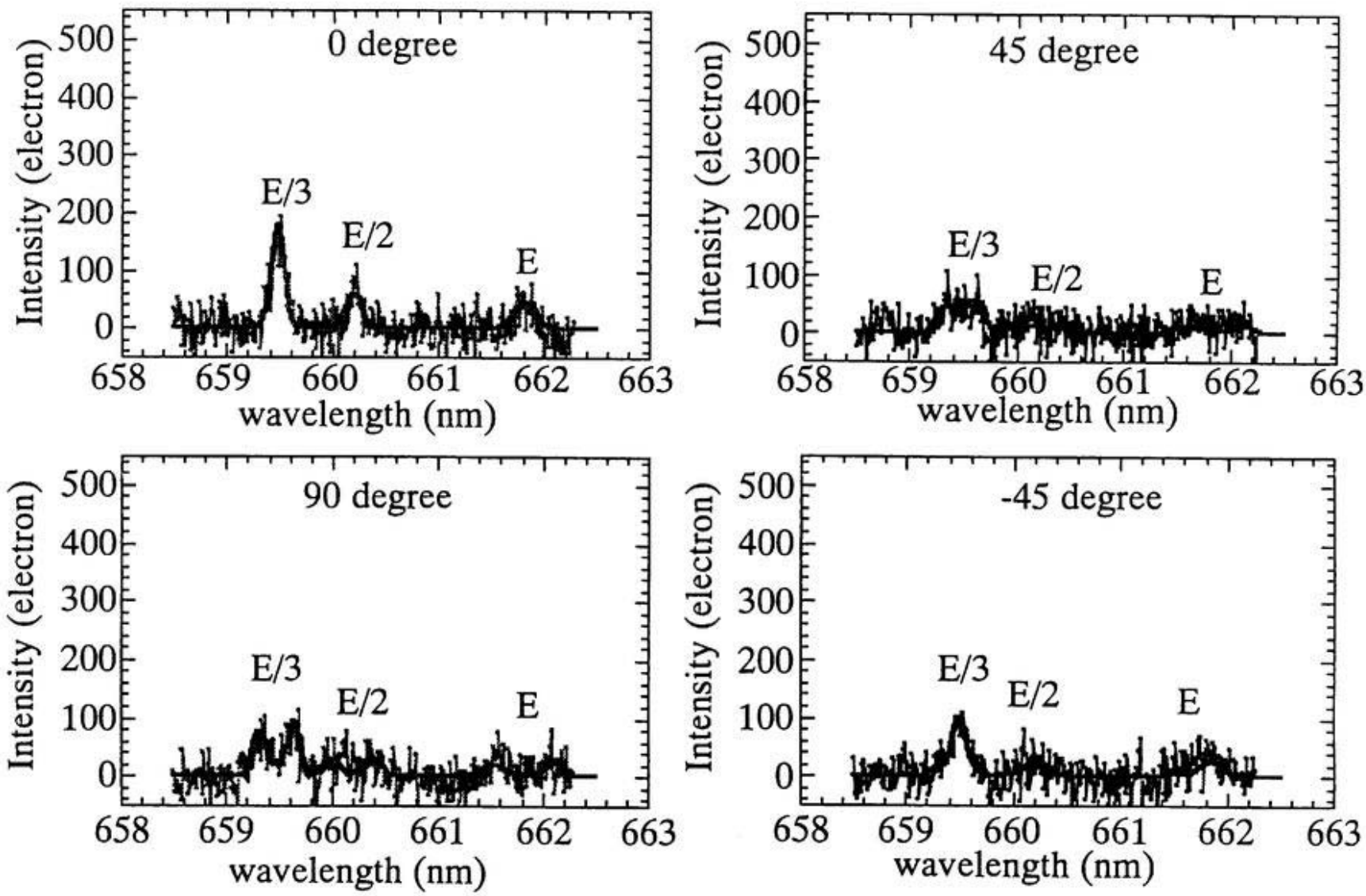

Fig. 5.4 Comparsion of the measured and calculated MSE spectra with 0 degree, 90 degrees, 45 degrees, 135 degrees at the major radius of 78.2 cm.

measured $I(0,\lambda)$ and $I(45,\lambda)$ spectra for each energy components, respectively. The spectra with -45 degrees polarizer in Figure 5.2 shows the difference between the calculated spectra and the measured MSE spectra. This is because of the offset angle in the system and the shift due to the finite beta. Although the full energy component has the largest motional Stark splitting and the separation in the wavelength between the σ and the π components, the intensity of the full energy component is not sufficient to determine the pitch angle. Therefore, the one-third energy component which has the largest intensity is used to derive the pitch angle. The shape of the measured spectra described reasonable agreement with the calculated ones.

As shown in Figure 5.3, the spectra with 45 degrees polarizer is narrower than that of -45 degrees polarizer. This is because the polarization angle of the π component is in between 0 degree and 90 degrees, and the spectra of +45 degrees polarization component is more contributed by the σ component than the π component. The asymmetry of the π component is observed in the spectra with 90 degrees polarizer. The peak of the $-\pi$ component (in the shorter wavelength) is higher than the peak of the $+\pi$ component (in the longer wavelength). This is because the Doppler shift and the motional Stark shift is in the opposite direction for $-\pi$ component, while they are in the same direction for the $+\pi$ component. The Doppler shift and motional Stark shift becomes smaller (because of lower magnetic field strength) as the major radius increase. The line at 660.1 nm shows the impurity line of Ti I.

Figure 5.4 shows that the spectra of -45 degrees polarizer is the narrower than that of 45 degrees polarizer at R=78 cm. This is because the polarization angle of the σ component is in between 0 degree and 90 degrees, and the spectra of -45 degrees polarizer is more contributed by the σ component. As seen in spectra with the 90 degrees polarizer, the peak of the π component in the shorter wavelength is

stronger than the peak in the longer wavelength. This is because the magnetic field : the motional Stark shift, and the Doppler shift depend on the "viewing angle" between the beam path and the line of sight. In the smaller major radius beyond the magnetic axis, the Doppler shift becomes larger but the motional Stark shift becomes smaller.

5.2 Estimation of Pitch Angle from MSE Spectra

5.1.2 Intensity Difference of MSE Spectra

The wavelength averaged polarization angle, $\overline{\alpha_i}$, is given by

$$\overline{\alpha_i} = \frac{1}{2}\tan^{-1}\left\{\frac{1}{2\Delta\lambda}\int_{\lambda-\Delta\lambda}^{\lambda+\Delta\lambda}\left[\frac{I_{\pm 45}}{I_{0,90}}\right]d\lambda\right\} + \delta_i - \Delta\alpha_i , \qquad (5\text{-}1)$$

where

$$\Delta I_{-45,+45} = \frac{I(-45+\Delta\theta_{-45,45},\lambda) - I(45,\lambda)}{I(-45+\Delta\theta_{-45,45},\lambda) + I(45,\lambda)}, \qquad (5\text{-}2)$$

$$\Delta I_{0,90} = \frac{I(90,\lambda) - I(0+\Delta\theta_{0,90},\lambda)}{I(90,\lambda) + I(0+\Delta\theta_{0,90},\lambda)}, \qquad (5\text{-}3)$$

$i=\pi-$, σ, $\pi+$ and $\delta_\sigma=0$, $\delta_{\pi-}=\delta_{\pi+}=90$, $\Delta\theta_{-45,45}=8.2$, $\Delta\theta_{0,90}=9.1$, and $\Delta\alpha_i$ depends on polarization angle [seen in Figure 4.8(b)]. The polarization ratio, $\Delta I_{0,90}$, becomes 1 for only π component, and -1 for only σ component. The data in which the polarization ratio, $\Delta I_{0,90}$, is smaller than the noise level are masked. The wavelength in which the polarization ratio is more than the noise level shows the region, $\Delta\lambda$. Here, the noise level is defined as RMS noise level where there is no σ or π lines.

Figure 5.5 shows the values of $\Delta I_{-45,+45}$, $\Delta I_{0,90}$, and $\Delta I_{-45,+45}/\Delta I_{0,90}$. The data in the region, $\Delta\lambda$, are averaged by using Equation (5-1). As shown in Figure

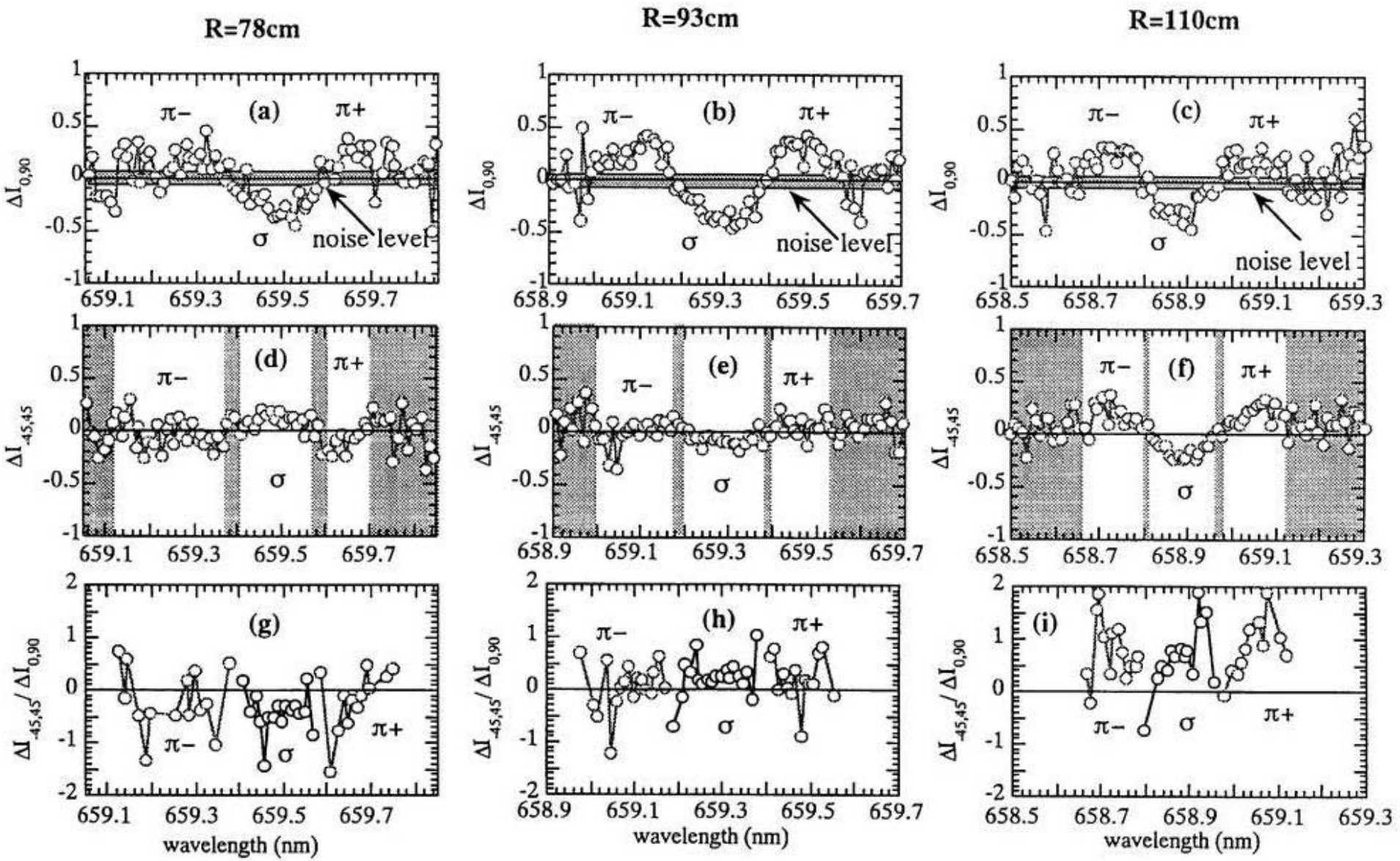

Fig. 5.5 (a)(b)(c) Value of $\Delta I_{0,90}$ (d)(e)(f) Value of $\Delta I_{-45,45}$ (g)(h)(i) Value of $\Delta I_{-45,45} / \Delta I_{0,90}$

5.5(b), the $\Delta I_{-45,+45}$ is almost zero in each range of wavelength, because the pitch angle of the local magnetic field line is almost zero near the plasma center (R=93 cm). However, $\Delta I_{-45,+45}$ is negative for the σ component and positive for the π component outside of the tours (R=110 cm). This is because the polarization angle of the σ component is in between 0 degree and 90 degrees, while the polarization angle of the π component is in between 90 degrees and 135 degrees. The sign of $\Delta I_{-45,+45}$ is reversed in the spectra observed at R=78 cm. When each polarization ratio is larger than about 0.2, the value of $\Delta I_{-45,+45}/\Delta I_{0,90}$ is almost constant in the wavelength. Therefore, the pitch angle of the local magnetic field line can be derived from the intensity ratio in the wavelength region where the polarization ratio is over 0.2.

5.2.2 Radial Profile of Pitch Angle

When there is no difference in the transmission between two sets of optical fibers, FLC, and polarizer, $I(90,\lambda)+I(0,\lambda)$ is equal to $I(135,\lambda)+I(45,\lambda)$. Figure 5.6(a) shows the radial profile of the averaged value of $\{I(90,\lambda)+I(0,\lambda)\}/\{I(135,\lambda)+I(45,\lambda)\}$ in the wavelength range for the $-\pi$, the σ, and the $+\pi$ components. The three ratios of $(I(90,\lambda)+I(0,\lambda))/(I(135,\lambda)+I(45,\lambda))$ for the $-\pi$, the σ, and the $+\pi$ components are almost identical, although they are scattered greatly depending on the fiber. The scatter of the ratio from unity is due to the difference of the transmission of each optical fiber, FLC, and polarizer. Therefore, the values of I(45)-I(-45) and I(90)-I(0) have to be normalized by the values of I(45)+I(-45) and I(90)+I(0). Then, in the experiment, the averaged values of $\{I(90,\lambda)+I(0,\lambda)\}/\{I(135,\lambda)+I(45,\lambda)\}$ for the $-\pi$, the σ, and the $+\pi$ components are used through put each fiber. Figure 5.6(b) shows the effect of the normalization. By normalization, the ratio are changed factor of two at most (seen

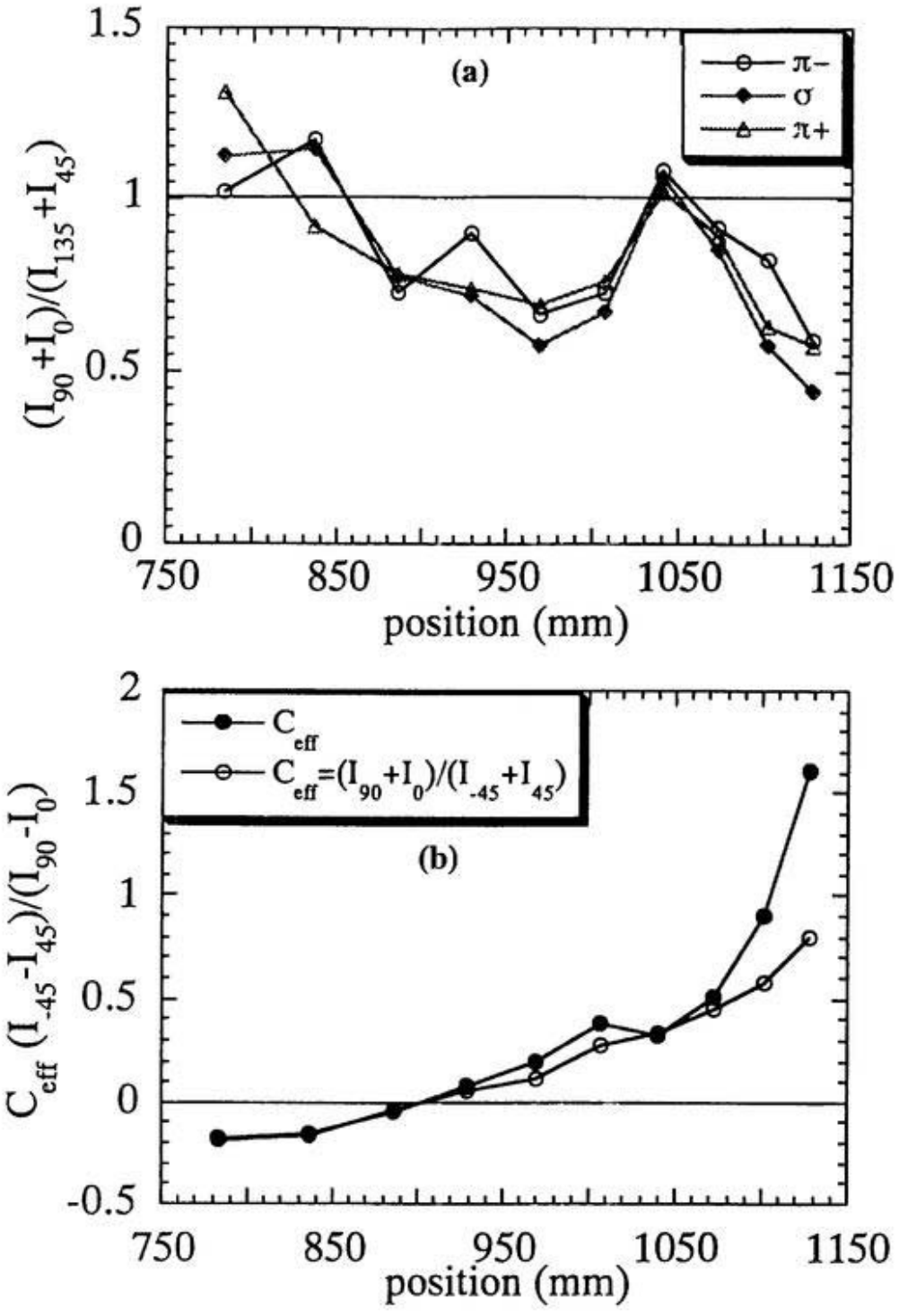

Fig. 5.6 (a) Difference in each optics fiber
(b) Revised data of difference in each optics fiber

the data at R=1130 mm).

Figure 5.7 shows how to correct the offset angle of the α and the π components, respectively. The real polarization angle, α_σ, and, α_π, are plotted as a function of apparent polarization angle of α_σ' and α_π'. The offset angle, $\alpha_\sigma'-\alpha_\sigma$, and, $\alpha_\pi'-\alpha_\pi$, are taken into account in measuring the pitch angle of the magnetic field line.

Figure 5.8(a) shows that the radial profile of the polarization angle is derived from Equation (5-1) and (2-4) with the spectra of the $-\pi$, the σ, and the $+\pi$ components of the one-third energy component. These error bars are derived from the standard deviation of $\Delta I_{-45,+45}/\Delta I_{0,90}$ in Figure 5.5 that should be constant in the wavelength. The dotted line shows the vacuum magnetic field calculated from the external coil current. The magnetic axis for the both beta of 0.5 and 0.8 % show by the arrow.

The dots in Figure 5.8(b) shows the pitch angle averaged from the three pitch angle which had been measured before, and the solid line in Figure 5.8(b) shows polynomial curve fitting. The shift of the Bz=0 position measured is 28 ± 16 mm. Figure 5.9 shows the shift of the magnetic axis and the Bz=0 position as a function of the beta values. The Bz=0 position shifts as much as the magnetic axis for the plasma with small beta below 0.2%. However, the difference between the Bz=0 shift and the magnetic axis shift becomes larger as the beta values increases. At the high beta of 1 %, the shift of the Bz=0 position is only 37% of the magnetic axis shift. The beta measured with the diamagnetic loop is 0.42%. However, the parallel component of the beam pressure is not included in this beta, because the parallel pressure has no diamagnetic loop. As seen in Table 2, the anisotropy of the beam, $\beta_{\parallel}^{b}/\beta_{\perp}^{b}$, has been evaluated to be from one to four at the plasma center in CHS[2]. The value of $\beta_{\perp}^{beam}$ is the same value at that of $\beta_{\parallel}^{beam}$ for $\beta_{\parallel}^{b}/\beta_{\perp}^{b}=1$.

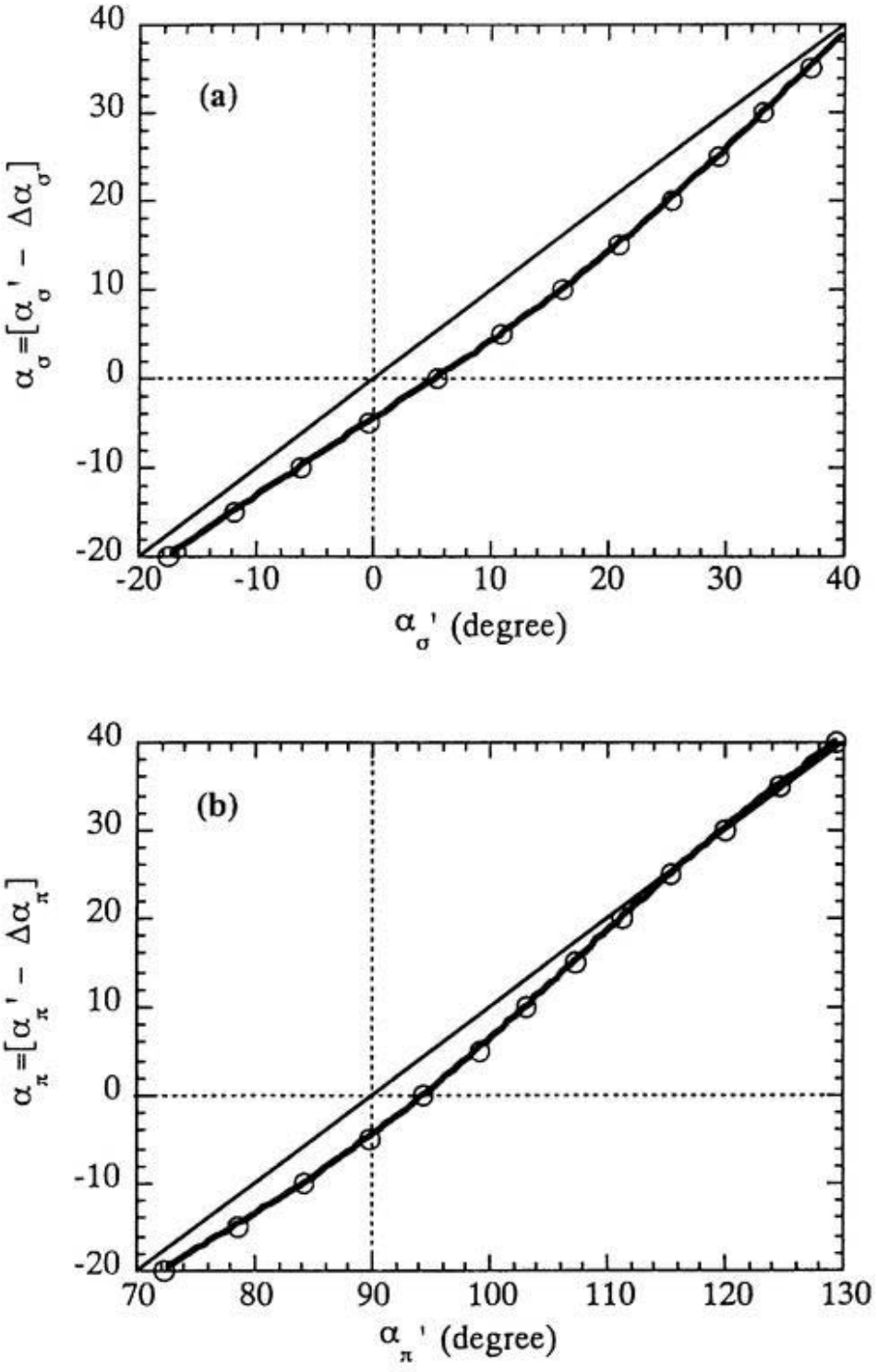

Fig. 5.7 (a) The fitting function of σ component for revising offset angle (b) The fitting function of π component for revising offset angle

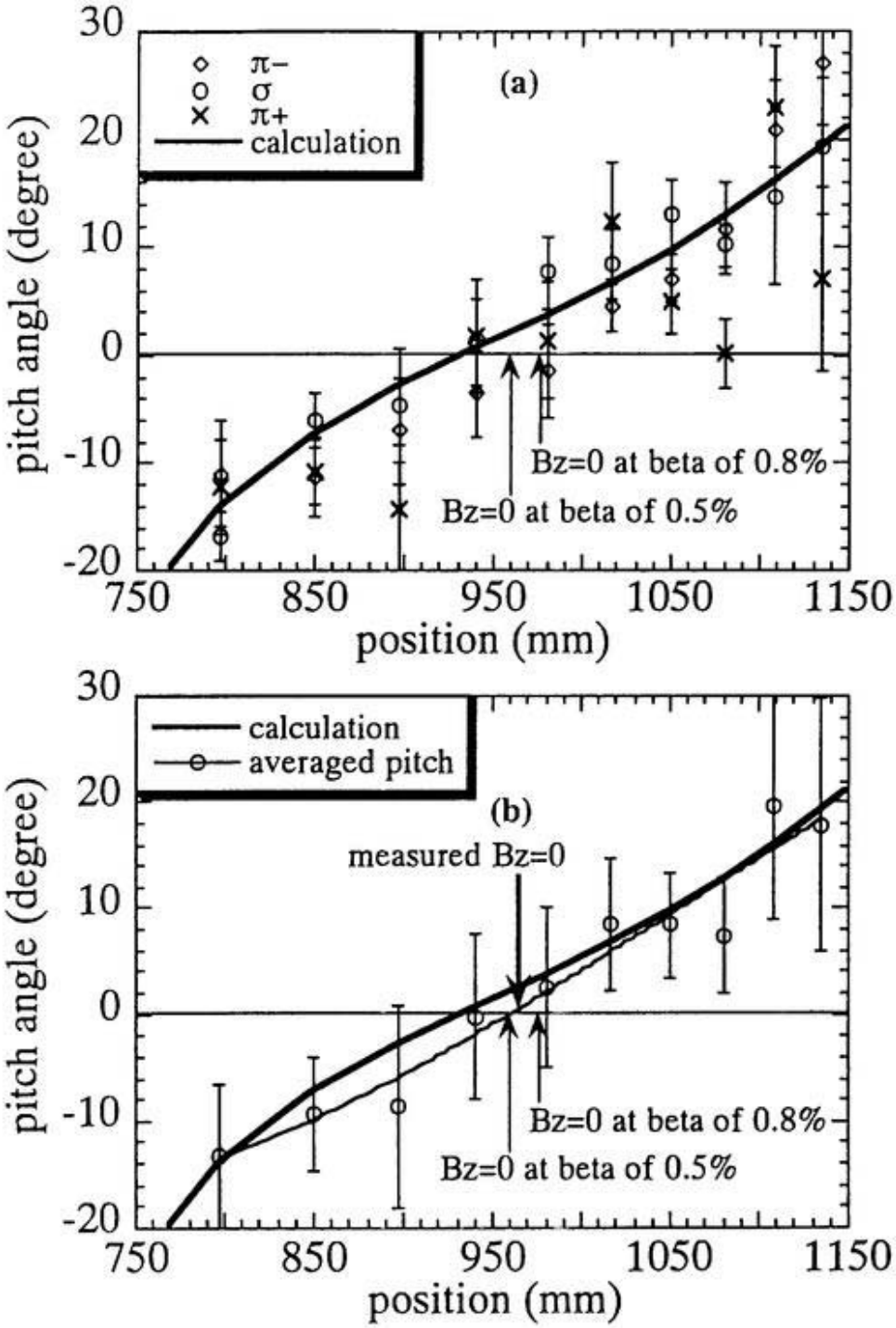

Fig. 5.8 (a) Radial profile of the pitch angle are given by 1/3 energy. (b) Shift of the Bz=0 due to the beta.

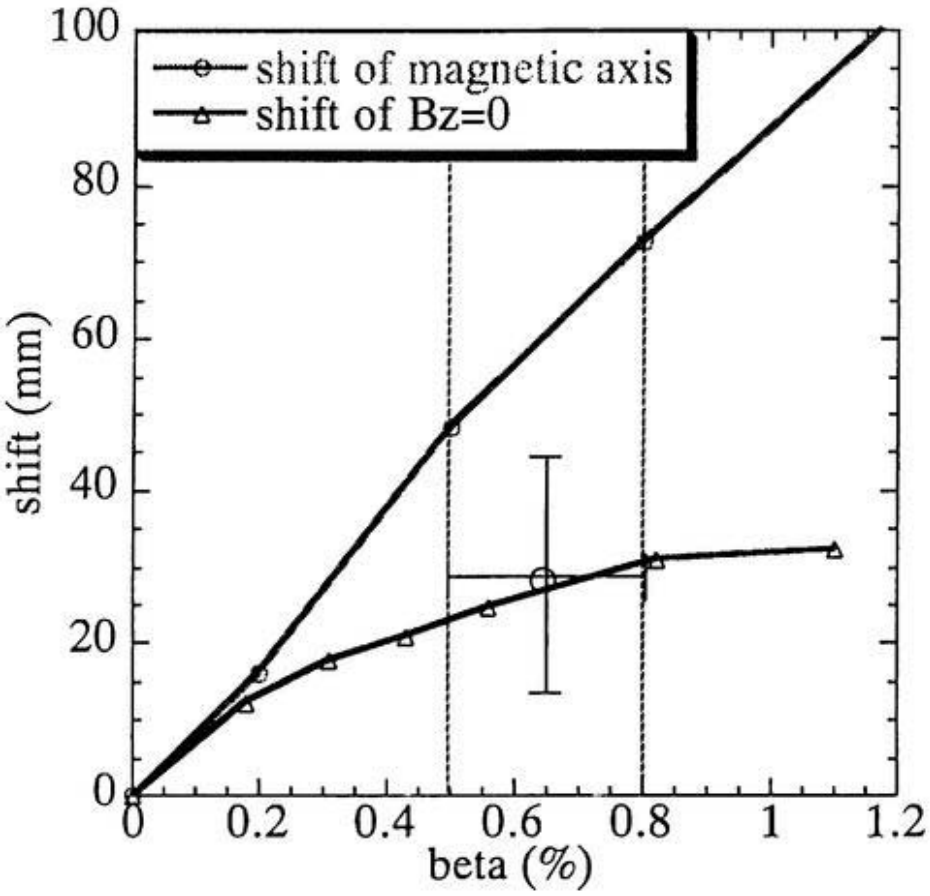

Fig.5.9 The shift of magnetic axis and Bz=0 depend on beta

Table 2 Comparsion measurement and beta shift with beam pressure

	measurement	$\beta_{\parallel}^{b}/\beta_{\perp}^{b}=1$	$\beta_{\parallel}^{b}/\beta_{\perp}^{b}=4$
$\beta_{thermal}$	0.42%	0.3%	0.3%
$\beta_{\perp}^{beam}$		0.1%	0.1%
$\beta_{\parallel}^{beam}$		0.1%	0.4%
β(total)		0.5%	0.8%
shift of magnetic axis		48mm	73mm
shift of Bz=0	28 ± 16mm	23mm	31mm

On the other hand, the value of $\beta_{\parallel}^{beam}$ is as four times big as that of $\beta_{\perp}^{beam}$ for $\beta_{\parallel}^{b}/\beta_{\perp}^{b}=4$. The value in $\beta_{thermal}$, $\beta_{\perp}^{beam}$, and $\beta_{\parallel}^{beam}$ added is β(total). Then, the total beta for this plasma should be in the rang of 0.5~0.8%. The shift of the magnetic axis predicted is from 48 to 73 mm, and that of the Bz=0 is predicted to be from 23 to 31 mm. Therefore, the measured shift (28 ± 16 mm) is consistent with the shift calculated with the finite beta equilibrium code which takes into account both the bulk and the beam pressure into account.

Chapter 6
Discussion and Summary

The new polarization sensitive spectroscopy, which consists of the polarizer the and FLC cell, has been developed to measure the polarization angle with good accuracy. The spectra with the polarizer angle of 0 and 90 degrees or -45 and 45 degrees can be measured with the fast modulation of 50 Hz, because the FLC has fast response. New CCD detector, where the charge of each pixel is shifted up and down (Dig Dag) with the shift rate of 3 μsec/pixel synchronized with the two sets of FLC modulation, has been developed for the MSE spectroscopy. The main noises of this measurement are the readout noise (11% at the fast ADC and 6% at the slow ADC) and the photon noise (5.7%). On the other hand, the noise of the dark charge (1.4%) and the smear (0.7%) are smaller than the readout noise and the photon noise. The two offsets of retardance existed in the FLC are $\Delta\delta = 10.6$ and $\Delta\delta = 8.2$ (degrees), and the offset of rotating angle $\Delta\phi = 1.9$, produces the offset angle in the system measuring the pitch angle of the magnetic field line up to 6 degrees.

New developed polarization sensitive spectroscopy has the character that the dependence of the offset angle due to the magnetic field strength is only 1.2 ± 0.6 degree/T, and this value is one order of magnitude smaller than that in the MSE spectroscopy using the PEM. The negligible offset in the FLC due to the magnetic field is considered to be a big advantage in the MSE measurement, because the calibration with injection of neutral beam to the gas target under the magnetic field is not necessary.

On the other hand, the offset angle becomes up to 6 degrees in the FLC system. This is because the offset of the retardance and that of rotating angle of optical axis have about 10 degrees and 2 degrees, respectively. However, this

offset in the FLC system can be easily calibrated before the experiment. Therefore, the FLC system will be better for the experiment. The beam divergence angle and the focal length measured with the calorimeter are 0.61 ± 1.0 degrees and 2.68 ± 0.3 m, respectively. This small beam divergence angle gives the enough separation between the measured σ and the π components in the MSE spectroscopy. The alignment of the beam line is checked by measuring the profile of increase of temperature with the IR camera at the carbon target plate located inside the tours. The beam line is found to be almost perpendicular with only 0.66 degrees at the nearly horizontally elongated cross section with the offset of the toroidal angle of 4.4 degrees. The pitch angle of magnetic field line is measured by the MSE spectroscopy along beam line. The observation points is precisely determined by the "viewing angle" between the beam path and the line of sight measured.

The pitch angles of the magnetic field line are derived from the polarization angles of the measured σ component and the measured π component. The MSE measurements give the Bz=0 position but it cannot give the magnetic axis, because of the helicity of the magnetic field. The Bz=0 shift is measured to be 28 ± 16 mm for the plasma with the diamagnetic beta of 0.42% (total beta is in the range of 0.5~0.8%). This measured shift is consistent with the predicted one (23 ~ 31 mm) with the finite beta equilibrium code including both the bulk and the beam pressure.

This error bar is mainly due to the insufficient intensity of H_α emission. If the pitch angle of magnetic field line is measured by using neutral beam with large beam current, this error bar may become smaller. And the offset angle with FLC will be smaller by controlling of the temperature because the retardance depends on the temperature.

Appendix A
Principle of MSE Spectroscopy

The spectral intensity through the optics transmitting at ϕ degree with respect to the mid-plane at the wavelength, λ, is given by

$$I(\phi,\lambda) = I_{\pi l}(\lambda)\cos^2(\alpha_\pi - \phi) + I_{\sigma l}(\lambda)\cos^2(\alpha_\sigma - \phi) + \frac{1}{2} I_{\sigma c}(\lambda) , \qquad \text{(A-1)}$$

where $\alpha_\pi = \alpha_\sigma + 90$, $I_{\pi l}(\lambda)$ and $I_{\sigma l}(\lambda)$ are the linearly polarized π component and the σ component, respectively, while $I_{\sigma c}(\lambda)$ is the circularly polarized σ component. The intensity of the spectra with the polarization angle of 0, 45, 90, and 135 polarization angle by Equation (A-1) substituting ϕ=0, 45, 90, and 135 is given by

$$I_0(\lambda) = \frac{1}{2} I_{\sigma c}(\lambda) + I_{\sigma l}(\lambda) + \left\{ I_{\pi l}(\lambda) - I_{\sigma l}(\lambda) \right\} \sin^2\left(\alpha_\sigma\right) \qquad \text{(A-2)}$$

$$I_{45}(\lambda) = \frac{1}{2} I_{\sigma c}(\lambda) + I_{\sigma l}(\lambda) + \left\{ I_{\pi l}(\lambda) - I_{\sigma l}(\lambda) \right\} \sin^2\left(\alpha_\sigma - 45\right) \qquad \text{(A-3)}$$

$$I_{90}(\lambda) = \frac{1}{2} I_{\sigma c}(\lambda) + I_{\sigma l}(\lambda) + \left\{ I_{\pi l}(\lambda) - I_{\sigma l}(\lambda) \right\} \cos^2\left(\alpha_\sigma\right) \qquad \text{(A-4)}$$

$$I_{135}(\lambda) = \frac{1}{2} I_{\sigma c}(\lambda) + I_{\sigma l}(\lambda) + \left\{ I_{\pi l}(\lambda) - I_{\sigma l}(\lambda) \right\} \cos^2\left(\alpha_\sigma - 45\right) \qquad \text{(A-5)}$$

The spectra with the motional Stark splitting have the circularly polarized σ component. Therefore, to estimate the pitch angle of the local magnetic field line from the MSE spectra, the four spectra of 0, 45, 90, and 135 degrees polarization angle must be measured. The polarization angle of the σ component, α_σ, is given by

$$\tan(2\alpha_\sigma) = \frac{I(135,\lambda) - I(45,\lambda)}{I(90,\lambda) - I(0,\lambda)}, \qquad \text{(A-6)}$$

using the four sets of intensity, $I(\phi,\lambda)$, with the different ϕ [=0, 45, 90, and 135]. The pitch angle, γ, defined as $\tan^{-1}(B_p/B_t)$ (B_p : the poloidal magnetic field, B_t : the toroidal magnetic field), is derived from the polarization angle, α_σ, or, α_π, as

$$\tan\gamma = \tan\alpha_\sigma / \cos\beta = \cot\alpha_\pi / \cos\beta, \qquad \text{(A-7)}$$

where β is the "viewing angle" between the beam path and the sight of line.

Appendix B

Dispersion of Spectrometer

When the incident plane light wave is inclined to the grating by the angle of incidence, α, the angle of diffraction, θ, relates to the angle of incidence by

$$d(\sin\alpha + \sin\theta) = \lambda , \tag{B-1}$$

where d is the space of the grating and λ is the wavelength.

By Equation (B-1) substituting $\alpha=\theta-2\gamma$, we have

$$d\{\sin(\theta-2\gamma) + \sin\theta\} = \lambda , \tag{B-2}$$

where γ is the half angle between the incident light and the diffraction light.

Therefore, we obtain

$$2d\cos^2\gamma \sin\theta = \lambda + 2d\sin\gamma \cos\gamma \cos\theta. \tag{B-3}$$

By taking square in both sides of the equation, Equation (B-3) becomes

$$4d^2\cos^4\gamma \sin^2\theta = \lambda^2 + 4\lambda d\sin\gamma \cos\gamma \cos\theta + 4d^2\sin^2\gamma \cos^2\gamma \cos^2\theta. \tag{B-4}$$

By Equation (B-1) substituting $\sin^2\theta = 1 - \cos^2\theta$, we have

$$4\cos^2\gamma(d\cos\theta)^2 + \lambda^2 + 4\lambda\sin\gamma \cos\gamma (d\cos\theta) + \lambda^2 - 4d^2 \cos^2\gamma = 0. \tag{B-5}$$

If we solve the equation for $d\cos\theta$, we obtain

$$d\cos\theta = \sqrt{(d\cos\gamma)^2 - \left(\frac{\lambda}{2}\right)^2} - \frac{\lambda}{2}\tan\gamma . \tag{B-6}$$

Therefore, by Equation (B-6) substituting $d\cos\theta = \frac{1}{f} \times \frac{\Delta\lambda}{\Delta x}$, the dispersion of the spectrometer is given by

$$\frac{\Delta\lambda}{\Delta x} = \left\{\sqrt{\left((d\cos(\gamma))^2 - \left(\frac{\lambda}{2}\right)^2\right)} - \frac{\lambda}{2} \times \tan(\gamma)\right\}/f , \tag{B-7}$$

where x is the detector and f is the focus length.

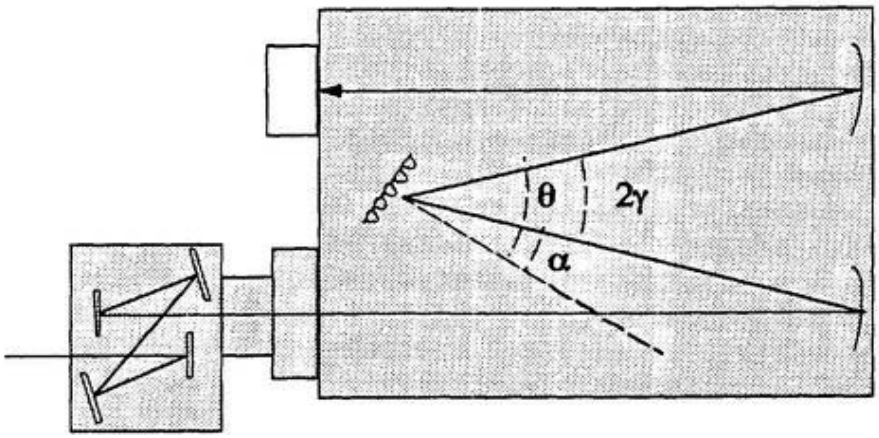

Spectrometer

Figure B.1 Arrangement of spectrometer